TMMOB
ELEKTRİK MÜHENDİSLERİ ODASI
ESKİŞEHİR ŞUBESİ

ESKİŞEHİR OSMANGAZİ
ÜNİVERSİTESİ

ULUSLARARASI

RUSİS 2017

ELEKTRİKLİ RAYLI ULAŞIM SİSTEMLERİ
SEMPOZYUMU

ESKİŞEHİR OSMANGAZİ ÜNİVERSİTESİ KONGRE VE KÜLTÜR MERKEZİ 27-28 Ekim 2017

SYMPOSIUM PROCEEDINGS

1954
The Chamber of Electrical Engineers
Eskişehir Branch

RUSiS 2017
International Symposium on Electrical Railway Transportation Systems
SYMPOSIUM
ESKİŞEHİR OSMANGAZİ UNIVERSITY CONGRESS AND CULTURE CENTER 27-28 OCTOBER 2017

Eskişehir Osmangazi University

INTERNATIONAL SYMPOSIUM on ELECTRICAL RAILWAY TRANSPORTATION SYSTEMS

SYMPOSIUM PROCEEDINGS

First Edition, Eskişehir - October 2017
ISBN: 978-605-01-1072-2
EMO Publication No: SK/2017/691

TMMOB The Camber of Electrical Engineers
Eskişehir Branch
İstiklal Mah. Şair Fuzuli Cad. Özkal İşm. No:36 K:2 D:1 – ESKİŞEHİR
Phone/Fax: 0222 231 94 47
e-mail: eskisehir@emo.org.tr
http://eskisehir.emo.org.tr

Değerli Katılımcılar,

Dördüncüsü gerçekleştirilen Elektrikli Raylı Ulaşım Sistemleri Sempozyumu, bu yıl uluslararası olarak ve çağrılı konuşmalar yerine hakem sürecinden geçen bildirilerin sunulduğu bir sempozyum olarak düzenlenmiştir. Sempozyuma gönderilen 25 bildiriden 15 tanesi sunulmak üzere kabul edilmiştir.

Bugün öğleden sonra Raylı Sistemler konusunda faaliyet gösteren kamu kurumlarının değerli yöneticilerinin katılacağı panelde Raylı Taşımacılık konusunda önemli konular tartışılacaktır. Daha sonra bugün ve yarın 3 farklı oturumda bildiri sunumları gerçekleştirilecektir.

Sempozyumun düzenlenmesi sürecinde desteklerini esirgemeyen üniversitemiz rektörü Prof. Dr. Hasan Gönen'e, Elektrik Mühendisleri Odası Genel Merkez ve Eskişehir Şubesi yönetimlerine ve çalışanlarına, Sempozyum düzenleme kurulu üyelerine, bildirileri değerlendiren hakemlerimize teşekkür ederim. Ayrıca sempozyuma destek veren Savronik AŞ, STM, Piton Yazılım, Çözüm TR, Anot AŞ ve Pentair'e teşekkür ederim.

Verimli bir toplantı olması dileklerimle iyi günler dilerim.

Prof. Dr. Osman Parlaktuna

ERUSİS 2017 Düzenleme Kurulu Başkanı

Değerli Demiryolcular,

2011 yılında başladığımız Elektrikli Raylı Ulaşım Sistemleri Sempozyumu etkinliğimiz, bu yıl 4. Kez düzenlenmektedir. Önceki yıllardan farklı olarak ilk kez bir üniversite ile ortak düzenlediğimiz ERUSİS'te diğer önemli farklılığımız ise sempozyumumuz ilk kez uluslar arası bir etkinlik olarak gerçekleştirilmesidir.

ERUSİS etkinliğinde, Türkiye'de demiryolu taşımacılığının görsel ve anlayış olarak bu kadar etkin değişimine tanık olduğumuz günümüzde teknoloji olarak dünyanın neresindeyiz sorusunun yanıtını bulmayı hedeflemekteyiz. Bu amaçla, dünyadaki demiryolu taşımacılığının hedefleri ve etki alanındaki Türkiye, ülke kaynaklarımız ve teknolojik birikimlerimiz, değişime katkıları ile daha verimli bir taşımacılık hedefi için bundan sonra neler yapılmalı konularında elimizdeki verileri ortaya koymak ve ortak akıl oluşturmayı hedeflemekteyiz. Bu kapsamda ERUSİS 2017 bildirilerimizin ve hazırlanacak sonuç raporunun, ülkemizde yetkili kurumlar tarafından değerlendirileceğine ve halkımıza yararlı olacağına inanmaktayız.

EMO Eskişehir Şubesinin son dönemdeki etkinliklerine katkı sağlayan ESOGÜ'ye Rektörümüz Prof. Dr. Hasan Gönen'e ve Değerli ESOGÜ Yöneticilerine, ERUSİS Düzenleme Kurulunun tüm toplantılarına katılım sağlayan Başkan Prof. Dr. Osman Parlaktuna, Prof. Dr. Hasan Hüseyin Erkaya, Prof. Dr. Rıfat EDİZKAN, Ömür YILDIZ, Oğuz SOYLU, Aykut Kadir KOZANDAĞI ve Şube Müdürümüz Kaan HÜRLER'e, yıllardır sponsor desteğini esirgemeyen SAVRONİK'e, diğer sponsorlarımız STM, Piton Yazılım, Çözüm TR, Anot AŞ ve Pentair'e, kapılarını sürekli EMO'ya açık tutan TÜLOMSAŞ Genel Müdürü Sayın Hayri AVCI'ya ve tüm TÜLOMSAŞ çalışanlarına, TCDD ve TCDD Taşımacılık A.Ş yönetimine, TÜVASAŞ'a, RSK Rayder ve DTD Yönetim Kurullarına, Eskişehir Büyükşehir Belediyesi, Odunpazarı ve Tepebaşı Belediyesine, desteklerinden dolayı EMO Bursa Şube Yönetim Kuruluna, EMO Genel Merkez Yönetim Kurulu ve çalışanlarına, EMO Genç'e gönülden teşekkür ederim.

Saygılarımla

Hakan TUNA

EMO Eskişehir Şube Yönetim Kurulu Başkanı

EXECUTIVE COMMITTEE

Chairman	
Osman Parlaktuna	Eskisehir Osmangazi University
Members	
Aykut Kozandagi	EMO Eskisehir Branch
Ender Kelleci	EMO Eskisehir Branch
Hakan Tuna	EMO Eskisehir Branch
Hasan Huseyin Erkaya	Eskisehir Osmangazi University
Huseyin Yesil	EMO
M. Turan Soylemez	Istanbul Technical University
Oguz Soylu	EMO Eskisehir Branch
Omer Mete Kockar	Anadolu University
Omur Yildiz	EMO Eskisehir Branch
Rifat Edizkan	Eskisehir Osmangazi University

ADVISORY COMMITTEE

Ahmet Sert	EMO Mersin Branch
Akin Eser	EMO Gaziantep Branch
Alaattin Yolcu	EMO Ankara Branch
Alpay Zeybek	STM
Aslihan Vural Cobanoglu	EMO Antalya Branch
Berkcan Gucer	EMO Mersin Branch
Bulent Erkul	IMO Eskisehir Branch
Bulent Pala	EMO Denizli Branch
Cigdem Gundogan Turker	EMO Kocaeli Branch
Emel Sakarya	RAYDER
Erhan Gocuklu	EMO Eskisehir Branch
Erhan Sezgin	ESTRAM
Feyzullah Gündoğdu	Kayseri Transportation
Hakan Güler	Sakarya University
Halil Ibrahim Bakar	EMO Bursa Branch
Halil Ibrahim Okumus	EMO Trabzon Branch
Huseyin Yesilseven	EMO Bursa Branch
Ilhan Metin	EMO Antalya Branch
Ilhan Yildirim	EMO Adana Branch
Mehmet Mak	EMO Adana Branch
Mehmet Ozdag	EMO Samsun Branch
Metin Uckun	MMO Eskisehir Branch
Mustafa Serdar Cinarli	EMO Izmir Branch
Nukhet Isikoglu	DTD
Okan Eryurt	THALES
Ozenc Akdag	EMO Ankara Branch
Riza Behcet Akcan	EMO Istanbul Branch
Saygin Onder Akal	EMO Samsun Branch
Sertan Dogan	MMO Eskisehir Branch
Tamer Karakurt	EMO Eskisehir Branch
Vahdettin Tekin	EMO Diyarbakir Branch

ORGANIZING COMMITTEE

Chairman

Osman Parlaktuna	Eskisehir Osmangazi University

Members

A. Levent Eguz	EMO Eskisehir Branc
Aykut Kozandagi	EMO Eskisehir Branch
Aylin Toren	EMO Eskisehir Branch
Cagdas Gorgulu	TCDD Transport
Cengiz Goltas	EMO
Cihan Uyanik	Eskisehir Osmangazi University
Deniz Kaplan	Eskisehir Municipality
Emrah Deniz	Karabuk University
Ender Kelleci	EMO Eskisehir Branch
Eyyup Sultan Baris	TUDEMSAS
Gulin Elibol	Eskisehir Osmangazi University
Gurcan Banger	Railway Systems Cluster
H. Suat Turker	EMO
Hakan Okten	TCDD
Hakan Tuna	EMO Eskisehir Branch
Hasan Huseyin Erkaya	Eskisehir Osmangazi University
Hatice Aydın	EMO Eskisehir Branch
Hayri Avci	TULOMSAS
Huseyin Onder	EMO
Ibrahim Aksoz	EMO
Ipek Ture Karan	EMO Eskisehir Branch
Irfan Senlik	EMO Bursa Branch
Kamil Arslan	Karabuk University
Kubulay Ozbek	EMO
Levent Celik	EMO Eskisehir Branch
M. Kenan Isik	Savronik
M. Savas Ozaydemir	Eskisehir Chamber of Industry
M. Turan Soylemez	Istanbul Technical University
Mahmut Demir	TUDEMSAS
Mehmet Bayraktutar	TCDD Transport
Mehmet Emin Akay	Karabuk University
Mehmet Peker	EMO
Melike Ozlem Bilgili	EMO
Metin özkan	Eskisehir Osmangazi University
Murat Esen	TULOMSAS
Mustafa Karasahin	Istanbul University
Mustafa Yasar	Karabuk University
Nadir Gürefe	Eskisehir Chamber of Industry
Nagehan Abacilar	EMO
Nedim Demirel	TCDD
Nuri Sezer	TUVASAS
Oguz Soylu	EMO Eskisehir Branch
Onur Ayan	Istanbul Technical University

Oya Kiraz	EMO
Omer Mete Kockar	Anadolu University
Omur Yildiz	EMO Eskisehir Branch
Remzi Cinar	EMO Bursa Branch
Rifat Edizkan	Eskisehir Osmangazi University
Serdar Ergen	EMO Eskisehir Branch
Suat Yalnızoglu	Tepebasi Municipality
Tunc Aladagli	EMO Bursa Branch

TECHNICAL COMMITTEE

A. Mete Dirik	Turkey
Abdurrahman Karamancıoglu	Turkey
Ahmet Yazici	Turkey
Alfredo Nunez	Nederland
Ali Osman Atahan	Turkey
Antonis Giannapoulos	Great Britain
Ata Mugan	Turkey
Bijan Moaveni	Iran
Bohumil Culek	Czech Republic
Burak Kaleci	Turkey
Bunyamin Tamyurek	Turkey
Cem Sevik	Turkey
Charles Watson	Great Britain
David Kirkwood	Great Britain
Emin Sunbuloglu	Turkey
Emrah Deniz	Turkey
Esin Karpat	Turkey
Eva Schmidova	Czech Republic
Fatih Karpat	Turkey
Frank Lademann	Germany
Fritz Busch	Germany
Gokhan Dindis	Turkey
Habibollah Molatefi	Iran
Hakan Guler	Turkey
Halil Karadeniz	Turkey
Harm Visser	Nederland
Jaroslav Mencik	Czech Republic
Kamil Aslan	Turkey
Kemal Keskin	Turkey
Mehmet Fidan	Turkey
Meserret Nalcakan	Turkey
Metin Akkok	Turkey
Metin Gokasan	Turkey
Metin Ozkan	Turkey
Mohamad Ali Sandidzadeh	Iran
Murat Karacasu	Turkey
Murat Uyar	Turkey
Mustafa Karasahin	Turkey

Mustafa Yasar	Turkey
Muzaffer Metin	Turkey
N. Ozlem Unverdi	Turkey
Necmettin Kaya	Turkey
Nil Mukherjee	Great Britain
Nizami Akturk	Turkey
Nurkan Yagiz	Turkey
Omur Akbayir	Turkey
Pasi Lautala	USA
Pavel Svanda	Czech Republic
Petr Voltr	Czech Republic
Rahmi Guclu	Turkey
Rob Goverde	Nederland
Semih Sezer	Turkey
Semiha Turkay	Turkey
Safak Bilgic	Turkey
Sener Agalar	Turkey
Stanislav Jovanovic	Serbia
Tuncay Ertas	Turkey
Tuncer Toprak	Turkey
Zahit Mecitoglu	Turkey
Zdenka Popovic	Serbia
Zeynep Gultekin Yildirim	Turkey
Zubeyde Ozturk	Turkey

CONTENTS

Dynamic Modelling and Numerical Simulation of a Tram Wheel Test Stand

Altan Onat[1],Abdulkadir Zirek[2], Petr Voltr[3]

[1]Electrical & Electronics Engineering Department, Faculty of Engineering,
Anadolu University, Eskişehir, Turkey
altanonat@anadolu.edu.tr
[2]Department of Transport Means and Diagnostics, Faculty of Transport Engineering,
University of Pardubice, Pardubice, Czech Republic
azirek@anadolu.edu.tr
[3]Educational and Research Centre in Transport, Faculty of Transport Engineering,
Pardubice, Czech Republic
Petr.Voltr@upce.cz

Abstract

Track experiments and tests for railway vehicles are challenging tasks. In order to realize methods and validate models which are developed for railway vehicle systems, roller–rig test equipments are widely used. In this study, a torsional dynamic model of a tram wheel test stand, which has a wheel on roller configuration and has been used for research purposes in faculty of transport engineering, university of Pardubice for many years, is proposed. Numerical simulations are validated by the measurements taken from this roller–rig. This model includes solution to geometrical, normal and tangential problems for wheel–rail interface and models of electric motors. Comparison with measurements shows that this modelling formalism is promising to test and verify proposed methods for the test stand and railway vehicle systems.

1. Introduction

Verification and validation for the performance and safety of railway vehicles are compulsory. These processes require the use of special vehicles, tracks, measurement devices and qualified staff as well. Therefore, verification and validation for the performance and safety of railway vehicles are costly.

Since the beginning of research for railway vehicles, researchers has sought different ways of verifying and validating their innovations, models and methods. Roller–rig test stands are proposed as a favorable solution to this problem. These test rigs includes rollers to simulate rails so that the motion of a wheelset, bogie or a vehicle can be inspected without field tests.

A wide variety of roller–rig configurations exist in the literature. As well as full scale roller–rigs, there are reduced scale ones to investigate special aspects of railway vehicles. Several roller–rig configurations are reported in [1]. Differences between wheel–rail and wheel–roller cases, various substitutions of rail with a roller are explained in [2, 3].

The roller–rig, which is considered in this study, has been used for research purposes in the faculty of transport engineering, university of Pardubice, Czech Republic. The researches carried out on this test stand focus on wheel–rail adhesion [4–6] and traction [7,8]. Additionally, there are future works about this test stand especially for testing new methodologies in model based condition monitoring. An example for such a methodology has already presented in [9].

In this study, a mathematical model of the test stand is composed. It includes the mathematical model of a permanent magnet synchronous motor, an asynchronous motor, contact between wheel and roller and the torsional dynamic model of the test stand. Comparison of simulation results for this model with respect to measurements shows that the model is suitable to reflect the physical structure of the test stand and use it for research purposes.

2. Tram Roller–Rig

Test stand includes a tram wheel and a roller manufactured from a railway wagon wheel. Wheel and roller are attached to an upright frame. The wheel is connected to a swinging arm with a pneumatic spring to provide normal force, the roller is connected to a base plate. In order to provide traction or braking on the tram wheel, the wheel is equipped with a torque–controlled permanent magnet synchronous motor (i.e. PMSM). An asynchronous motor is attached to the roller to keep constant speed, [6]. A diagram and the photos of the test stand can be seen in Fig. 1 and Fig. 2, respectively.

Air pressure in pneumatic spring is observed by a pressure transmitter. The incremental rotary encoders are mounted on both shafts to provide the angular velocities of the wheel (ω_w) and the rail roller (ω_r). The tangential force T and the coefficient of adhesion μ (ratio of the tangential force to the normal force) are determined from the output of a torque transducer on the roller shaft. Sensory information is collected by a data aquisition (i.e. DAQ) device and then they are processed. A similar roller–rig configuration is also reported in [10]. Characteristics of the PMSM are a nominal

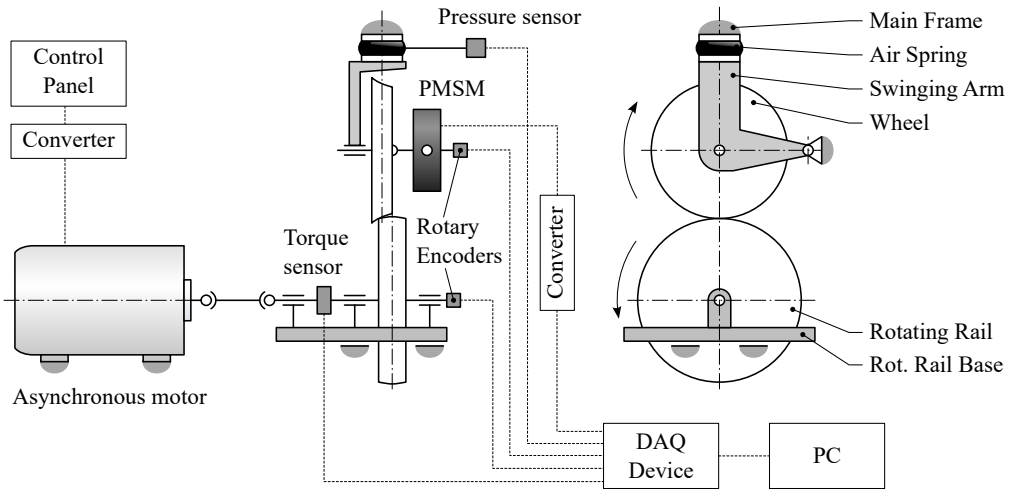

Fig. 1. Diagram of the test stand

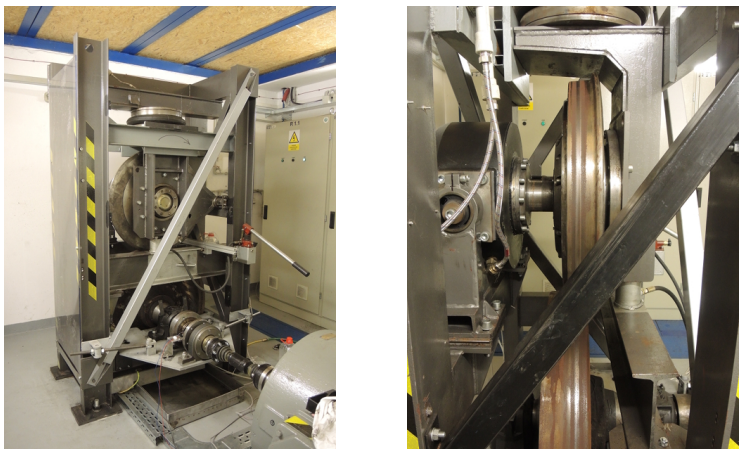

(a) **(b)**

Fig. 2. The tram wheel test rig in the laboratory of the University of Pardubice

power of 58 kW, a nominal torque of 852 Nm and maximum torque of 2000 Nm. Characteristics of the asynchronous motor connected to the roller are a nominal power of 55 kW and a nominal torque of 891 Nm. The nominal rolling diameter of the wheel is 700 mm and the nominal rolling diameter of the roller is 905 mm.

3. Models of the Electrical Motors

3.1. PMSM Model

Fig. 3 shows the dynamic equivalent circuit of the PMSM. Dynamic equations of the stator currents can be written as

$$\frac{d}{dt}i_{ds} = \frac{1}{L_{ds}}V_{ds} - \frac{R_s}{L_{ds}}i_{ds} + \frac{L_{qs}}{L_{ds}}p\omega i_{qs} \quad (1)$$

$$\frac{d}{dt}i_{qs} = \frac{1}{L_{qs}}V_{qs} - \frac{R_s}{L_{qs}}i_{qs} - \frac{L_{ds}}{L_{qs}}p\omega i_{ds} - \frac{\varphi}{L_{qs}}p\omega, \quad (2)$$

where V_{ds}, V_{qs} are $d-q$ axes voltages, i_{ds}, i_{qs} are $d-q$ axes cur-

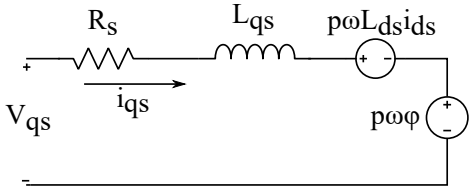

(a) q-axis circuit

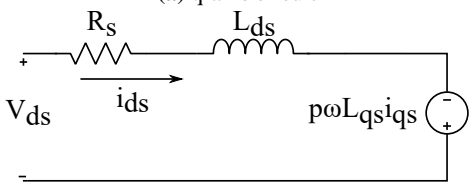

(b) d-axis circuit

Fig. 3. Equivalent circuit of PMSM

rents, p number of pole pairs, R_s is the resistance of stator windings, φ is the amplitude of the flux induced by permanent magnet of the rotor in the stator phases, L_{ds}, L_{qs} are $d-q$ axes inductances, ω is the angular velocity of the rotor. Electromagnetic torque of the motor can be calculated from

$$T_P = 1.5p\left[\varphi i_{qs} + \left(L_{ds} - L_{qs}\right) i_{qs} i_{ds}\right]. \tag{3}$$

Parameters of the PMSM, which are used in simulations, can be found in Table 1.

Table 1. Permanent magnet synchronous motor parameters [8]

Parameter (Nominal)	Value
Power	58 kW
I (Nominal Phase Current)	122 A
p	22
T_p	852 Nm
φ	0.2 Wb
ω	650 rpm
R_s	0.087 Ω
L_{ds}	0.8 mH
L_{qs}	0.8 mH

3.2. Asychronous Motor Model

Electrical motor, which is mounted on the roller, is used for breaking during operation. Several tests are conducted in order to determine an equivalent circuit model of the asynchronous motor, [11]. Thevenin equivalent circuit parameters for this motor obtained at 50 Hz can be found in Table 2. Volts per Hertz (i.e. V/f) open loop control methodology is used for motor control by using a rectifier and inverter couple. By considering the Thevenin equivalent circuit parameters which are provided in Table 2, mechanical torque of the asynchronous motor can be calculated as

$$T_A = \frac{3}{\omega_{syn}} \frac{V_{Th}^2}{\left(R_{Th} + \frac{R_2'}{s}\right)^2 + \left(X_{Th} + X_2'\right)^2} \frac{R_2'}{s}. \tag{4}$$

Table 2. Thevenin Equivalent Circuit Parameters of the Asynchronous Motor

V_{Th}	212.3438 V
R_{Th}	0.0226 Ω
X_{Th}	0.2007 Ω
$X_2^{'}$	0.3010 Ω
$R_2^{'}$	0.0181 Ω

4. Contact Model

Wheel and roller profiles are based on the theoretical profiles which are used in the tramway network of Prague, Czech Republic. Rolling radii for wheel–roller are measured by a diameter tape. These radii values can be used to calculate longitudinal curvatures and they are 0.9043 m for roller , 0.6964 m for wheel. Lateral curvatures and conicity angles are calculated by using analytical geometry and mathematical tools. Measured wheel–roller profiles are illustrated in Fig. 4.

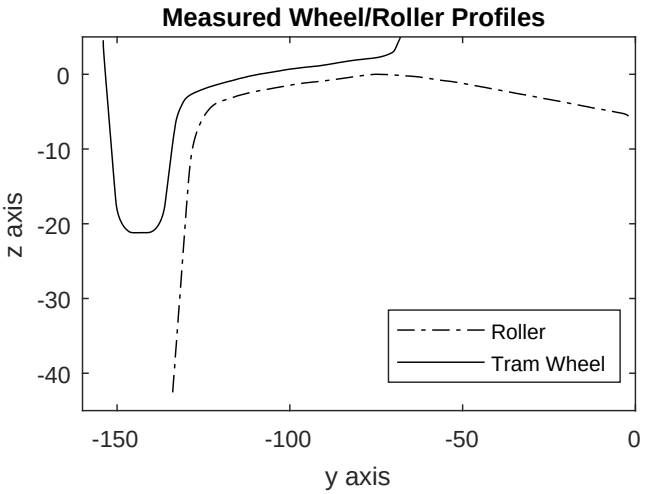

Fig. 4. Measured wheel–roller profiles

In order to find the contact point, quasi–elastic contact search formalism is considered. Quasi–elastic contact search uses elasticity of the wheel–roller (or rail). It is more realistic with respect to rigid contact search method. Furthermore, the computational complexity of this method is lower than the finite element method. Quasi–elastic contact search method is also used for a similar test stand in [12]. Results for the solution of geometrical problem are 0.0503 rad of contact angle, 3.4306 m^{-1} and 0.529 m^{-1} lateral curvatures for wheel–roller, respectively.

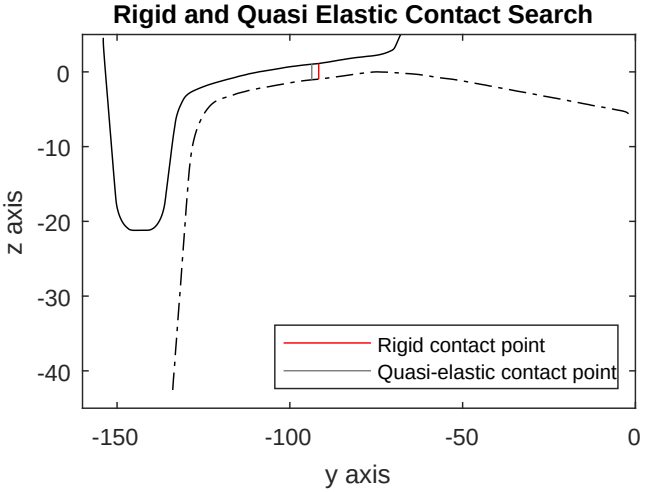

Fig. 5. Results for rigid and quasi–elastic contact search method

4.1. Normal Problem

Theory of Hertz is considered to find the contact area occurring between wheel–roller. Details of the considered solution methodology can be found in [13]. Elliptical contact patch dimensions are 2.605 mm and 2.622 mm semi–length and semi–width, respectively.

4.2. Adhesion Model

The dry surface is assumed between wheel–roller. Slip velocity dependent friction model, which is proposed in [14], is considered in simulations. Slip velocity is dependent on the dimensionless creep. Spin creep (1/m) and dimensionless translational creep can be expressed as

$$s_x = \frac{v_r - v_w}{v_r}, \tag{5a}$$

$$s_\phi = \frac{sin\delta_w}{r_{eq_x}}. \tag{5b}$$

In these equations v_w and v_r are wheel–roller translational velocities, respectively and δ_w is the contact angle. Wheel–roller case is different from the wheel–rail case. Therefore, spin creepage should be calculated by considering an equivalent radius and it is given as

$$\frac{1}{r_{eq_x}} = \frac{1}{r_{w_x}} + \frac{1}{r_{r_x}}, \tag{6}$$

where r_{w_x} and r_{r_x} are the rolling radii of the wheel–roller, respectively. Slip velocity is expressed as $w = s_x \times v_w$ and friction coefficient is given with respect to slip velocity as

$$\mu = \mu_0 \left[(1 - A)\, e^{-Bw} + A \right]. \tag{7}$$

Values for the parameters and their definitions are presented in Table 3 and they are based on the model parameters given for dry conditions in [14]. A comparison between adhesion model and the measurement is illustrated in Fig. 6. Adhesion measurements are taken by using the torque transducer mounted on the roller shaft.

Table 3. Parameters for friction coefficient model

μ_0	Maximum friciton coefficient	0.4
B (s/m)	Coefficient of exponential decrease	0.6
A	Ratio of limit friction coefficient μ_∞ to μ_0	0.4

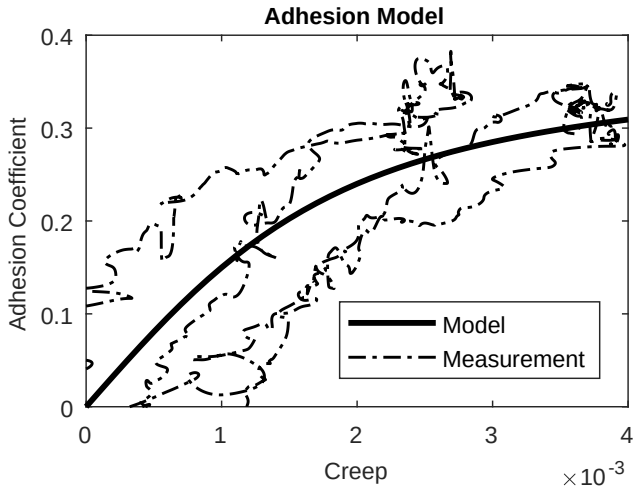

Fig. 6. Comparison of adhesion model with measurement

4.3. Tangential Problem

Creep force model, which is presented in [14], is used. Tangential creep force is described as

$$\mathbf{F} = -\frac{2F_n\mu}{\pi}\left(\frac{k_A\epsilon}{1+(k_A\epsilon)^2} + \arctan k_S\epsilon\right), \quad k_S \le k_A \le 1, \tag{8}$$

where F_n is the normal force, k_A and k_S are reduction factors for slip and adhesion areas on the contact patch, ϵ is the gradient of tangential stress in the adhesion area and it is expressed as

$$\epsilon = \frac{2}{3}\frac{C\pi a^2 b}{F_n\mu}s, \tag{9}$$

where s is the total slip, C is the contact shear stiffness, a, b are the semi–length and width of the contact patch. Details of this creep force model can be found in [9, 14]. Furthermore, the effect of spin on the lateral creep force is considered. Details of how spin causes an increase in lateral creep force can be found in [15].

5. Dynamical Model

Torques and creep force acting on the test stand is seen in Fig. 1. Dynamic model of the test stand is expressed as

$$\frac{d\dot{\omega}_r}{dt} = \frac{T_A + (F_x \times r_{r_x})}{J_{r_{total}}}, \tag{10a}$$

$$\frac{d\dot{\omega}_w}{dt} = \frac{-T_P - (F_x \times r_{w_x})}{J_{w_{total}}}, \tag{10b}$$

where moment of inertias (found by using a 3D modeling software) and their values are presented in Table 4 and T_A, T_P are the torques transmitted to the system by asynchronous motor and PMSM, respectively.

Table 4. Moment of inertias of the wheel–roller

$J_{w_{total}}$	Moment of inertia of the wheel (with connection components)	17.86 kgm^2
$J_{r_{total}}$	Moment of inertia of the roller (with connection components)	47.20 kgm^2

6. Results and Discussion

The torque request during the simulations is illustrated in Fig. 7. The asynchronous motor attached to the roller operates at 7.5 Hz synchronous frequency which corresponds to the 15 km/h translational velocity. Initial states (i.e. angular velocities) for wheel and roller are calculated as 12.16 rad/s and 9.36 rad/s for wheel–roller, respectively. Results are shown in Fig. 8 and 9. Simulation model results and measurements for angular velocities are in good agreement.

Actually, field oriented control method with front-end flux weakening controller, which is presented in [8], is used for the control of PMSM. However, the field oriented control method is only used for simulation purpose hereby. Even though two control methods have small differences, results and measurements are in very good agreement since two controller provides same results until

nominal speed is reached. Torque reference and the torque output taken from the controller are illustrated in Fig. 10. This simulation model reveals that it is promising and can be used for other research purposes such as testing different control, parameter estimation and condition monitoring algorithms on this test stand.

It is seen in Fig. 8 and Fig. 9 that there is noise in the measurements taken from the wheel–roller. Main reason of this noise is the mechanical imperfections in the system. Furthermore, angular velocities are obtained by using a numerical derivation procedure for rotary encoders attached to the wheel–roller. Measurements from rotary encoders provide angular positions of the wheel–roller and a simple numerical derivation procedure is applied in order to find angular velocities. It is a known fact that numerical derivation procedure amplifies the noise effect in such measurements and this is the second reason for such noise in the measurements.

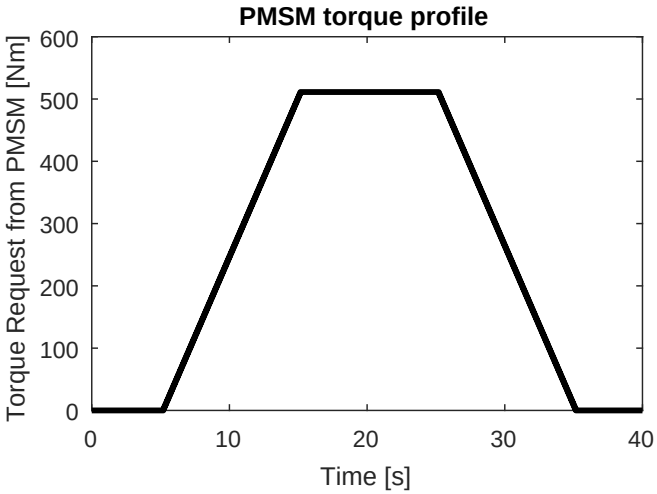

Fig. 7. Torque request from PMSM

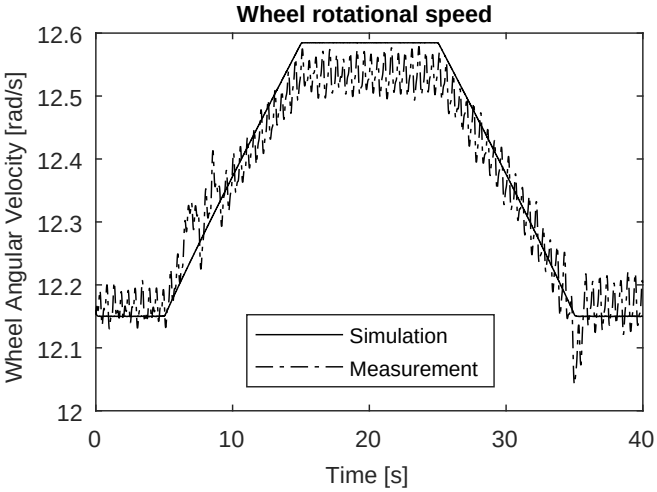

Fig. 8. Angular velocity of the wheel

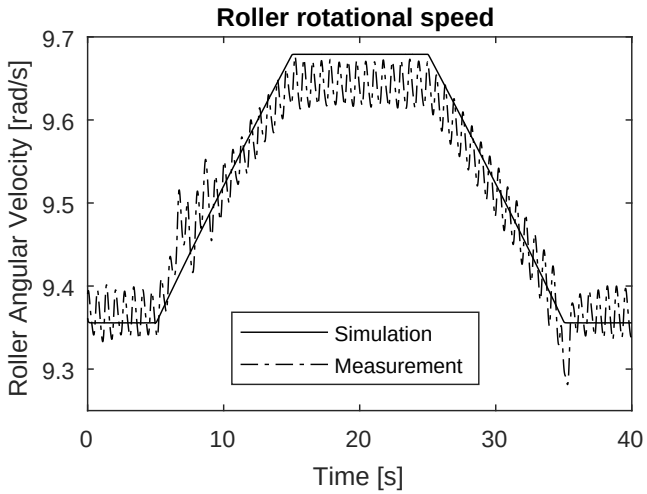

Fig. 9. Angular velocity of the roller

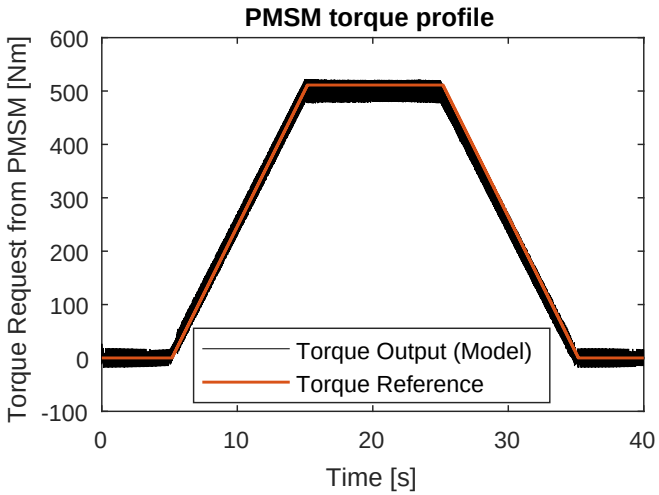

Fig. 10. Torque reference and torque output taken from PMSM model

7. Conclusion

In this study, a simulation model for a tram wheel test stand is presented. Firstly, mathematical models for electrical motors attached to the wheel–roller are expressed. Afterwards, a contact model is presented which provides solutions to geometrical, normal and tangential problem. Lastly, a torsional dynamic model of the test stand is given and results of the simulation model are compared with the measurements. This comparison shows that the proposed simulation model is promising to be used for different research purposes.

8. References

[1] Nicola Bosso, Maksym Spiryagin, Antonio Gugliotta, and Aurelio Somà. *Mechatronic modeling of real-time wheel-rail contact*. Springer, 2013.

[2] Petr Voltr. Simulation of wheel-rail contact conditions on

experimental equipment. *Railway Transport and Logistics*, XI:77–82, 2015.

[3] Binbin Liu and Stefano Bruni. Analysis of wheel-roller contact and comparison with the wheel-rail case. *Urban Rail Transit*, 1(4):215–226, 2015.

[4] Petr Voltr, Jaroslav Čáp, and Michael Lata. New practical results about adhesion limites obtained from experimental stand testing. *Scientific papers of the University of Pardubice. Series B, Jan Perner Transport Faculty. 15 (2009)*, 2009.

[5] P Voltr, M Lata, and O Černỳ. Measuring of wheel–rail adhesion characteristics at a test stand. *Engineering Mechanics*, page 181, 2012.

[6] Petr Voltr and Michael Lata. Transient wheel–rail adhesion characteristics under the cleaning effect of sliding. *Vehicle System Dynamics*, 53(5):605–618, 2015.

[7] O Cernỳ, J Šimánek, R Dolecek, and J Novák. Testing of robust control characteristics for traction pmsm. *PIERS2007*, pages 107–111, 2007.

[8] Radovan Doleček, Jaroslav Novák, and Ondřej Černỳ. Traction permanent magnet synchronous motor torque control with flux weakening. *Radioengineering*, 18(4):601–605, 2009.

[9] Altan Onat. *ESTIMATION OF STATES AND PARAMETERS FROM DYNAMIC RESPONSE OF WHEELSET*. PhD thesis, Faculty of Transport Engineering, University of Pardubice, 2017.

[10] SZ Meymand and M Ahmadian. Design, development, and calibration of a force-moment measurement system for wheel–rail contact mechanics in roller rigs. *Measurement*, 81:113–122, 2016.

[11] Paresh Chandra Sen. *Principles of electric machines and power electronics*. John Wiley & Sons, 2007.

[12] Andreas Heckmann, Alexander Keck, Ingo Kaiser, and Bernhard Kurzeck. The foundation of the dlr railwaydynamics library: the wheel-rail-contact. In *Proceedings of the 10 th International Modelica Conference; March 10-12; 2014; Lund; Sweden*, number 096, pages 465–475. Linköping University Electronic Press, 2014.

[13] Altan Onat, Petr Voltr, and Michael Lata. Nonlinear wheel/rail contact geometry characteristics & determination of hertzian contact. *Scientific papers of the University of Pardubice (Series B)*, 19:145–152, 2014.

[14] Oldrich Polach. Creep forces in simulations of traction vehicles running on adhesion limit. *Wear*, 258(7):992–1000, 2005.

[15] Oldrich Polach. A fast wheel-rail forces calculation computer code. *Vehicle System Dynamics*, 33:728–739, 2000.

New Pursuits on Public Transport Policies for Middle-sized Cities in Turkey: Erzincan as an Example Specific to Rail Systems

Hıdır Düzkaya, Hayri Ulvi, Abdullah Orman, Sema Sıvat

Gazi University
Urban Transportation Technology, Accessibility Implementation and Research Center (UTTAC),
06570 Ankara, Turkey
hduzkaya@gazi.edu.tr, hayriulvi@gazi.edu.tr, abdullah@gazi.edu.tr, svatsema@gmail.com

Abstract

Urbanization, which has been one of the most significant parameters of changing social structure since the beginning of 20th Century, has also brought urban transport problems. To cope with these transport problems, traditional vehicle priority policies must be abandoned; modern policies taking individual mobility into consideration must be considered. To increase that mobility, urban rail system projects, which have long been implemented in developed countries, have become widespread in Turkey. These projects that have become the main transport system in many Metropolitan Municipalities have recently begun to be implemented in middle-sized cities. This study reveals the developing role of rail systems in transport policies as a tool for social and economic development and explores traffic policy in Erzincan as an example for middle-sized cities in Turkey.

1. Introduction

Since the transition from conventional agricultural society to modern industrial society, technological improvements have developed transport systems, and these systems have increased social and economic mobility as one of the determinant factors in social development.

Social development theories reveal that social development depends on economic, social, and cultural revival, namely on mobility. These theories insist that development and improvement increase along with the increase in social mobility [1]. Transport technologies, as one of the most significant elements in development of economic, social, and cultural mobility, undertake critical functions such as productive use of natural resources, distribution of goods and services, and development of internal and external trade [2]. Urban transport systems are necessities to help the occurrence of social and cultural activities, along with interpersonal and social relations [1].

Transport needs, which in primitive societies were accomplished by walking and simple wheeled vehicles, since the beginning of 19th Century have gained another dimension with the development of faster and higher capacity transport vehicles using steam, electricity, and internal combustion. These technological pursuits, focusing on development of transport systems, caused rapid increase in individual automobile ownership and the number of motorized vehicles. To respond to the intensive infrastructure demand that followed this increase, some policies dependent on petrol and its derivatives followed between the 1950s and 1970s: removal of public transport vehicles from transport systems, annihilating urban rail systems —primarily trams—and extending road networks. In this period, traditional policies did not respond to the increase in the number of motorized vehicles; on the contrary, these policies contributed more and more to the complexity of existing problem.

Although traditional policies as responses to solve traffic congestion problems present short-term solutions, they increase the number of vehicles and trigger a new loop in which similar problems are continued to occur (Fig. 1) [3].

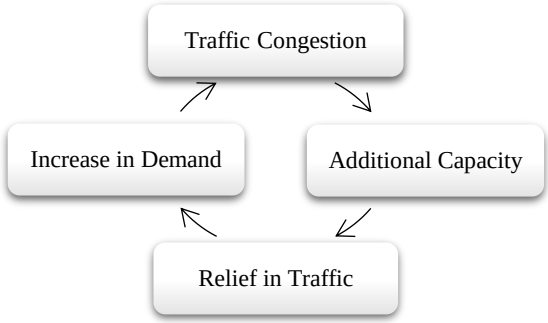

Figure 1. General Approach of Transport Systems

Increasing traffic congestion in urban transport since the 1970s and the economic effects of the global petrol crisis have made elimination of traditional vehicle priority approaches and implementation of contemporary human scale transport policies focusing on public transport inevitable [4]. Human-scale contemporary transport policies have been developed through strategies on establishment of safe public transport services, implementations that encourage private car owners to use public transport and discourage them from using their cars. Within the framework of these strategies, development of high capacity and integrated public transport systems, particularly rail systems, come into focus [3].

Urban public transport systems, set up for use of individuals, have an established tariff of fares, a route, timetable, stations, and on-line integrated rubber-wheeled or rail vehicle systems. Rubber-wheeled transport services are used on the routes that have lower passenger demand; rail systems are used on higher trip demand routes. Between these systems, light rail system (LRT), metro, suburban train, magnetic bearing, and monorail implementations have become prominent [5].

In the present research, the developing position of rail systems among public transport policies, development processes of rail systems in terms of legislation and implementation suited to Turkey, and implementation stages using Erzincan as an example as a middle-sized city will be explained.

2. Rail Systems in Public Transport Policies

Traditional transport policies that focus on increasing mobility of motorized vehicles that use fossil fuels have not been primarily preferable transport policies in the countries that are within the sphere of influence of European Union. Urban traffic intensity caused by low capacity and private vehicle transport, traffic congestion, air and noise pollution, as well as time and energy loss render this approach unsustainable. When modern approaches emphasizing human mobility rather than vehicles are investigated, public transport systems, particularly rail system implementations in coordination and integration with other systems, are the core of these policies. [1]. This section, which aims to give information about rail systems used in public transport policies, focuses on the topics such as first rail system implementation, historical development of these systems, and compares different rail system implementations.

The first rail systems were seen at the beginning of 19th Century: trams being moved on a line through horsepower. These implementations, seen in New York, New Orleans, Paris, London, Copenhagen and others, offered improvement of some parameters such as speed, size, and distance covered, together with the integration of electric motor technology into these systems since the beginning of the same century; these implementations constituted the backbone of public transport systems [6]. The first metro implementation in which electric systems were first being used was London metro (1863). Apart from London, short-distance implementations appeared around these dates in some cities like Budapest, Paris, and Istanbul [7]. After the first half of 20th Century, because these systems did solve the problems of traffic and infrastructure in relation to an increasing number of the number of vehicles, rail systems represented the main alternatives for transport policies that focused more on public transport systems. In this policy framework, underground metro system networks in city centers and suburban train lines at the outer parts of cities integrated with these metro lines were constructed. Through these public transport policies, in which an accessibility concept was taken into consideration, the target was to decrease the use of private car and to increase quality of life in cities [8]. When global scale examples of rail systems are investigated, the prominent examples are heavily populated greater cities like Shanghai, New York, Chicago, Paris, Moscow and London with their long and frequently used metro lines.

The first rail system implementation that integrated fossil fuel with motorized public transport services were tram and metro services in city centers and suburban train [9]. Recently, research into urban rail public transport systems and technological innovations have been changing the concepts behind rail systems and have generated new systems having more flexible activity areas; they defined by concepts as rapid-tram, light-metro or half-metro. These new systems will be defined light rail systems during the present research [10].

Suburban train systems, developed to transfer people to who are obliged to live at the outside of city centers city by the increasing population in modern cities and intensification of shopping and working activities in city centers, are one of the most significant alternatives with their high passenger capacity and transportation cost. This system, which can be used integrated with an inter-city railway system, is quite efficient in terms of energy consumption and operation costs; it is also safe and comfortable [9, 11]. Suburban train implementations are 1435-mm line-width systems fed by 15 to 25 kV line voltage via a catenary [12].

Urban rail public transport systems having the lowest passenger capacity system is the tram. This system, which moves on rails laid at the same level as the highway, is called a "street tram"; it can be operated in a mixed way with traffic and as a grade crossing, depending the topography [5]. These systems, which are usually driven by a driver, are dependent on road and traffic conditions: they are operated at 25–35 km/h, low operating speeds compared to other rail systems because they are intermixed with traffic, and because the distance between stops is short [6]. Tram systems are technically restricted to 1 to 3 carriages with 1435 mm track width; vehicle widths between 22002650 mm; catenary systems with a power supply density of 750/1500 VDC; maximum speeds of 60–70 km/h, average speeds of 2535 km/h; maximum passenger carrying capacity in one hour with 300–500 m distance between stations, 100–300 passengers; 4-6 axles with lengths 14–21 m; range from 7000 persons per hour up to 15,000 passengers by increasing speed, unit vehicle capacities ,and frequencies [9, 11]. Tram systems can be considered as the main transport system in the settlement units with lower population because of the maximum passenger carrying capacity, but they can also be used as an auxiliary transportation system integrated with LRT or metro systems in cities with high travel demand and high population [5]. In addition, if the tram system can be better organized and integrated with other urban transport systems, it can operate efficiently at lower capacities.

A transitional form between tram and metro systems, Light Rail Systems (LRT), has been used in many mainly European developed countries since the mid-1970s, can carry a maximum of 35,000 passengers in a single direction with less passenger capacity than subway. These systems, which are designated as fast trams, light metro, or pre-metro, are controlled by a driver on the main roads mostly supported by the open-closed tunnels, splitting, diving, viaducts, and special short tunnel techniques; they rarely by the signalization system [6, 11]. These systems, which are used intensively in railway public transportation, are often preferred because they are more flexible: they are adaptable to urban macro forms, can be operated in mixed traffic, have lower cost compared to metro systems, have the opportunity to make a flexible selection of the physical properties of the vehicles depending on the applications, have superior energy-saving and lower air pollution caused by petroleum-fueled vehicles, have a lower accident risk, and are more comfortable [6]. Light rail systems have a 1435-mm track width, 2200–2650-mm vehicle width, 750/1500 VDC supply voltage via catenary or third track systems, maximum 60–100 km speed, average 25–45 km operating speed, 2–7 bellows, capable of carrying an average of 250–300 passengers in single or multiple arrays with 4–10 axles, are 18- to 42-m in length, have a designed 600–1000m distance between stations, and a maximum passenger-carrying capacity of 35,000 passengers per direction in one hour [5, 12].

Metro systems, which constitute the main axis of public transport systems in greater cities with intense travel demands, can carry many more passengers with better comfort and safety compared to tram and light rail systems. Compared to other systems, initial investment and operation costs are higher; however, their ability to manage intensive travel demands easily using advanced signaling systems on private lines come into prominence. These systems are usually constructed underground to alleviate the surface traffic burden; but in the case of suitable

topography, options of either grade level or viaduct can be applied to reduce infrastructure costs [5]. Metro systems are heavy rail systems that have a 1435-mm rail width, 2650–3150 mm vehicle width, 750/1500 VDC supply voltage over catenary or third rail systems, maximum 80–100 km speed, an average operation speed of 45–60 km/h, carrying capacity average of 1200 to 2500 passengers, with 4-axes and up to 10 sets of multiple arrays, 180–200 m length, capable of traveling at an average of 20–40 hours per hour, and a maximum passenger-carrying capacity in one direction up to 100,000 passengers [6, 12]. Implementations commonly used in public transportation systems in urban areas can easily be compared using this information, see Table 1.

Table 1. Comparison of urban rail public transport implementations (İyinam and Öztürk, 2013: 3)

	Tram	LRT	Metro
Vehicle Capacity (passenger)	100–250	110–250	140–280
Vehicle Length (m)	14–35	14–54	15–23
Vehicle Width (m)	2.2–2.7	2.2–3.0	2.5–3.2
Number of Vehicle	1–3	1–4	1–10
Train Capacity (passenger / vehicle)	100–500	100–750	140–2400
Line Capacity (thousand passengers / h)	4–15	6–20	10–70
Maximum Speed (km / h)	60–70	60–100	80–100
Operating speed (km / h)	15–30	20–45	45–60
Emergency Brake Acceleration (m / sec^2)	2–3.7	2–3	1.1–2.1
Maximum Acceleration (m / sec^2)	1–1.9	1–1.7	1–1.4
Single Line Span (m)	3–3.35	3.4–3.6	3.7–4.3
Station Range (m)	300–500	500–1000	500–2000
Investment Cost (M $/km)	5–10	10–50	40–100
Percent of fully protected line	0–40	40–90	100

Urban rail systems as a significant component of modern public transport approach are preferred more as time passes, with their being comfortable and safer as well as their high passenger capacity and rapid transport time [5]. Together with the extended implementation of rail systems, technological improvements enable the development of many mixed rail and wheeled transport systems. In long-term public transport policies, which are formed by many factors such as existing population of cities, growth plans, and topography, it is required to find optimal solutions by integrating these new transport technologies.

Considering that rail system implementations in public transport policies have commonly been used in many developed and developing countries, it is significant to determine an eco-politic process that needs to be followed in development of rail system projects in Turkey. The upcoming section, in which this development process from legislation to implementation will be explained, investigates the development process of rail system implementations in Turkey in a general manner.

3. Rail Systems in Turkey from Legislation to Implementation

The first example of the use of rail systems in urban transport policies in Turkey is the Beyoğlu-Karaköy Tunnel: it began to operate in 1875 and is the world's third oldest metro. Subsequent urban rail systems were not included in transport policies until 1989, apart from several suburban railway examples from some Metropolitan Municipalities because of the Ottoman Empire decline, World Wars, and having taken rubber-wheeled transport policies preferred by political decision makers. Before the 21st Century, that rubber wheeled urban transport policies did not respond travel demand that had increased together with the increase in the population of larger cities made obvious the necessity to use rail systems in urban transport [13]. This section aims to answer some main issues as why to adopt rail system policies for urban transport in Turkey, which legislation to obey during implementation stage of these systems, the historical development of rail systems in Turkey and problems at the implementation stages.

Demographic change in Turkey, started in 1950s and experienced with significant part of rural population shift to cities, combined with irregular urbanization policies and generated important urban problems. One of the most important urban problem is the continuous increase in traffic intensification and transport problems. To cope with these problems, traditional motorized vehicle mobility-oriented transport policies have been abandoned, and rail systems have been moved to the core of urban transport policies, particularly in some heavily populated municipalities [14]. Rail systems in urban transport policies aim to resolve traffic congestion in city centers and on the main axes, to respond to travel demands of people at the outer parts of city centers, to eliminate existing deficiencies of public transport supply, to eliminate problems caused by intermediary public transport modes (like paratransit), to lower air pollution and noise levels, and to control urban settlement by supporting new development areas.

In Turkey, when the legislation on which rail system implementations depend is examined, the determinant role of development plans after 2000 can be observed. In the framework of related titles of 8th Five Year Development Plan prepared for the period 2000–2005, policies were proposed to increase traffic safety, increase the quality of public transport systems, develop pedestrian and bicycle transport, and for car parking management, taxi operation, and sea transport operation. In addition, the obligatory condition to implement a rail system is that the urban population under discussion needs to have at least one million people. The related titles of the 9th Five Year Development Plan, prepared for 2007 to 2013, put forth the policies of participatory, environmentally sensitive, and sustainable pedestrian and bicycle transport to overcome the problems caused by traffic. In the content of this plan, to have rail systems implemented, the travel demand of 15,000 persons per direction passenger/hour in peak hours is required rather than the population condition set in the previous plan. In the framework of the 10th Development Plan, covering the period 2014 to the present, pedestrian and bicycle lane implementation, integration of public transport systems, and smart transport systems have been given priority. It has been determined that minimum peak hour per direction travel demand in rail system investments is 7,000 for trams, 10,000 for light rail systems and 15,000 for metro systems [6]. However, it should not be ignored that lower capacity urban rail system preferences can also be created through an efficient feasibility, capacity, and volume calculation.

In cities that fulfill the conditions of development plans prior to investment, rather than considering rubber-wheeled and rail systems as alternative transport modes, these modes are as complementary modes. Following the year 2000, in some greater cities such as Istanbul, Ankara, Izmir, as well as Adana, Antalya, Bursa, Gaziantep, Kayseri, Konya, and Samsun that fulfilled necessary requirements in terms of population and travel demand, urban rail system projects were increasingly designed and implemented [5]. In the light of these developments, the total length of urban rail systems was 292 km in 2006, 477 in 2013, and it is expected to be 787 by 2018 [5]. Although the growth in rail system implementations demonstrates a significant transformation, considering the related statistics for Turkey and

global scale in comparison, it is obvious that only the very first steps of this transformation have been taken [5].

Traffic problems in Turkey, environmental problems caused by fossil fuels, and related economic problems make it inevitable that urban rail public transport systems will become widespread, as in many other cities. In addition, in cases where funds are insufficient to cover the investment costs of these systems, public administration—particularly local governments— might be harmed economically.

Together with larger cities, to have rail system projects, which have commonly implementation potential in also middle-sized cities, economically sustainable, implementation processes and criteria should be approached carefully. In the framework of realistic constraints, rail system projects, which contribute development of cities in the long run, need to be designed. At this stage, implementation procedures of rail systems as tools for public transport policies will be explained specific to city of Erzincan.

4. Implementation Processes of Rail Systems in Urban Transport Policies and Erzincan Example

Increasing urban population and mobility that have resulted from rapid urbanization dynamics in Turkey affects greater cities as well as developing middle-sized cities in many aspects—primarily transport problems. The classification based on the size of the city includes many criteria such as population size, function, and general settlement level. These criteria, which define medium-sized cities, vary from country to country [15]. In this framework, medium-sized cities in Turkey are those with a population of 50.000 to 500.000 when the population size and urban function are taken into consideration based on the study done by the State Planning Organization in 1987 [16]. This definition is widely used today, with the upper and lower limit under discussion [17-18].

In transportation policies of medium-sized cities, traditional transport systems are abandoned and modern transport technologies are adopted in response to increasing travel demand with increasing of urban population [19]. To create a long-term solution to the transportation problems in medium-sized cities, it has been necessary to prepare a Transport Master Plan (TMP) for the municipalities by specifying legal regulations [20].

According to Article 10 of the Regulation, *"Metropolitan municipalities and municipalities outside the borders of the metropolitan municipalities, having a population of over one hundred thousand, prepare a Transport Master Plan. These plans are made for a period of fifteen years and are renewed every five years. City plans and sustainable urban transport plans are handled together."*[20]. The responsibility of preparing the main transport plan is among the obligations of the greater cities in the framework of the Metropolitan Municipality Act of 2004. The related article also obliges cities with a population of over one hundred thousand, in the framework of the Metropolitan Municipality Act of 2004, to prepare the main transport plan as part of the obligations of the greater cities [21].

In the development phase of transport policies of cities in Turkey, the preparation of a Transport Master Plan has an important place, based on the legislation. The Transport Master Plan (TMP) studies contain the collection and evaluation of available information, the calibration and validation of the transportation demand forecasting model, the target year projections, the identification of the problems and bottlenecks in the current and target year structure, the identification of alternatives and testing with the transport model, and the strategic planning and programming of Transport Master Plan proposals and projects. Completed transport plans are first examined by the Ministry of Transport, Maritime Affairs and Communications and the General Directorate of Infrastructure Investments. After this review, the Transport Coordination Center and Municipal Council in the Metropolitan Municipalities, and local governments that are not Metropolitan Municipalities, are approved by the municipal council and are put into force [22].

In case the Transportation Master Plan recommends a railway system, metrobus, or cable system line within the scope of public transportation planning, to assess the applicability of these proposals and their financial and economic feasibility studies, preliminary / final projects and feasibility studies are prepared based on the design criteria published by the General Directorate of Infrastructure Investments of the Ministry of Transport, Maritime Affairs and Communications [22]. When the project as prepared and feasibility studies are approved by the ministry, the option of rail system is referred to Ministry of Development together with Council of Minister's Decision.

In cities with increasing population and growing transportation problems, the applicability of the proposed transportation projects is determined by the Transport Master Plan and additional studies on this plan. In this framework, Transport Master Plans are being produced in many cities, especially in greater cities, and applicable studies are becoming common [23]. In Turkey's medium-sized cities , the Transport Master Plan, which has become more and more widespread day by day, and the implementation processes of the projected rail system proposed by this plan will be explained using Erzincan as an example.

The Transport Master Plan study in Erzincan, which is in the foreground as one of the important cities of the region with its location, historical, and cultural richness and economic potential, started with the Mayor's authorization obtained from the Municipal Council in May 2016. After the protocol was signed between the municipality and Gazi University, the related work was carried out by the Urban Transportation Technology, Accessibility Implementation and Research Center (UTTAIC) within Gazi University; the completed plan was reviewed by the General Directorate of Infrastructure Investments of the Ministry of Transport, Maritime Affairs and Communications in April 2017 and rail system investment was found to be appropriate.

Within the scope of Transport Master Plan, 1260 household questionnaires for the 65 neighborhoods within the boundaries of Erzincan Municipality, there was traffic counting on 56 different sections considering the transport structure of the city; a get-on/get-off counting study on 11 bus lines of the municipality, pedestrian counting on 18 different roads and streets on which pedestrian flow and density is greatest; and pedestrian questionnaires on 21 different working areas [24].

Within the scope of the Transport Plan, moving in the direction of 2032 as target year to respond to the transportation demands of the developing city, scenarios have been developed in which the existing situation and probabilities are observed in short, medium, and long term. The initial scenario as the continuation of the present situation, rubber-wheeled public transport scenario, rail system development scenario, and rail system alternative scenarios are the different approaches that are put forth in the Transport Master Plan (TMP). The alternatives

generated by TMP have the power to influence the basic dynamics of existing situation. Scenarios developed for the Erzincan TMP such as travel cost, investment cost, air pollution, noise pollution energy consumption, and access time have been subjected to multi-criteria evaluation, and the least costly scenario—the rail system development scenario—was chosen [25].

The rail system project, which is among the scenarios of Erzincan TMP, is the Street Tram, which has the potential to respond to current travel demand and those in the future. According to this scenario, the planned system evolves in two stages. The first stage is projected to construct in the period between 2017 and 2018 and to be opened to service by the end of 2019. After the beginning of the operation of the first stage, 22.5 km in length, the goal is to complete the infrastructure works of the second stage in 2026 to 2027 and to integrate it into the system. At the first stage, it is assumed that the 22.5 km part of the project will be constructed between 2017 and 2018, and the system is projected to start operation during 2019. The infrastructure works of the second stage are planned to be completed and opened between 2026 and 2027 (Fig. 2) [25].

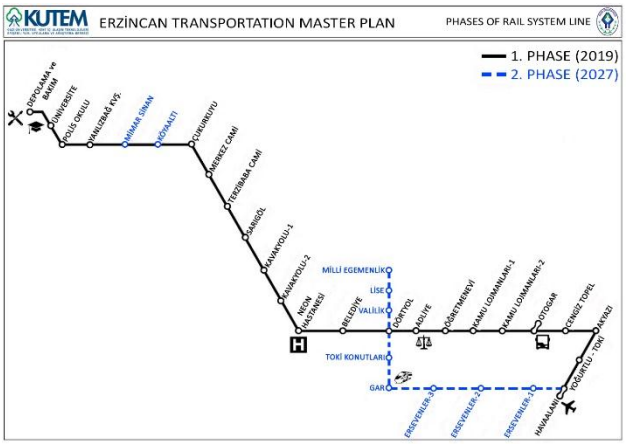

Figure 2. Erzincan Transportation Master Plan (TMP) Stages of Rail System Line

When the entire street tram line proposed for Erzincan city begins to operate in its circuit, 32 stops are planned to serve all the zones. These stops are positioned in a balanced manner in the regions where the commercial, educational, and residential areas of the city are concentrated, based on the city's Master Plan (Fig. 3). For the year 2019, the tram line is expected to carry 13,402 passengers in both directions and 7,860 passengers in a single direction during peak hours [26].

In the first stage, the length of the line is 22.5 km for 2019; it is planned that 109,170 passengers will travel at an average speed of 35 km / h per day. In 2027, the second stage of the project will be completed; and the total number of passengers after the construction of the 29.1 km line will reach 193.310 per day for 2027 [26]. Technical specifications such as speed, distance, travel time, rotation time, number of journeys, train capacity, peak one hour and maximum number of passengers, train number, train frequency, total capacity and number of required vehicles are presented in Table 2 by ten year intervals.

Within the scope of the project, a total of 14 vehicle purchases are foreseen in the first year, including 2 spare reserves in the first stage. To meet the increasing passenger capacity, the passenger projections are planned to supply 2 vehicles in 2022, 8 in 2027, 6 in 2032, 4 in 2037, and 26 in 2042 in [26]. The intervals at which the vehicles appear as recommended for the system are 5.5 minutes at peak hours and 10 minutes during the average daily general demand. Each set has a maximum capacity of 400 people. In bi-directional tram system proposed for the Erzincan tram line route, vehicle length is 40 m, vehicle width is 2.4 m, and vehicle height is projected to be 3.5 m [26].

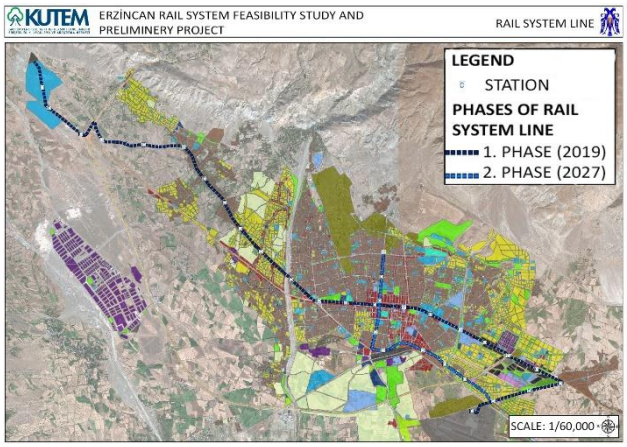

Figure 3. Erzincan Transportation Master Plan (TMP) Station Locations of Rail System

Table 2. General Characteristics of Rail System

	2019	2027	2037	2047
Speed (km / h)	35	35	35	35
Distance (km)	21	27.7	27.7	27.7
Duration (min)	36	47.5	47.5	47.5
Rotation Time (min)	79.7	105.6	105.6	105.6
Number of Trips	12	15	20	28
Array Capacity	400	400	400	400
Number of Passengers in Single Way at Peak Time (Passenger / Direction / Hour)	7.860	12.262	16.973	22.304
Peak Highest Cross-Section Value (Passenger / Direction / Time)	4.477	5.810	8.286	10.956
Number of Sequences	6	12	16	11 (22/2)
Expedition Frequency (min)	6	4	3	4,2
Total Capacity	4.4	6	8	11.2
Required Number of Vehicles	12 (+2)	22 (+2)	32 (+2)	42 (+2)

If the planned tram project is completed, the main revenue source will be the ticket sales to passengers. The expenditures of the tram during a given period consist of 3 items; investment costs of lines and fixed plants; investment expenditures for vehicles; and operating expenses. When similar projects are examined considering the slope, length and passenger density of the projects, the projected investment cost is 320,052,679 [26]. The project, which is planned to be financed by the state financing model, estimates that cash outflow can be recovered by 2022. The year in which the cumulative cash flow based on the repayment method are positive is the year 2024, which corresponds to the sixth year of the project [26].

The route planned in Erzincan TMP and the Erzincan Light Rail System Feasibility Study and Avant Projects approved by the General Directorate of Infrastructure Investments of the Ministry of Transport, Maritime Affairs and Communications combines all the terminal points (airport, high-speed railway, bus station) with the city center in the fastest and most convenient way. It facilitates the transition between different transportation types that operate intercity, and contributes a gain importance for the Erzincan

region. Other advantages of the project include; convenience of topography and road widths on the route; low expropriation costs; and the potential for generating benefits beyond the cost of the project. In addition, the proposed rail system route connects Erzincan University, which is the main arrival/departure point of daily trips for more than 25.000 people, with the city center by fully satisfying their transportation and accessibility needs and contributes to the relationship between city and university.

5. Conclusion

To solve the problems in urban transport resulting from urbanization and the increasing population in our country, it is necessary to make rail system projects more wide-reaching. In this process, rail systems in the public transport policies of Middle-sized cities in Turkey has been investigated using Erzincan, a medium-sized city, where construction of rail system projects is enhanced by the population size stated in the "Regulation on Procedures and Principles for Increasing Energy Efficiency in Transportation" is provided for, and settlement order and number of passenger are conveniently obtained. In the medium-sized cities that are like Erzincan in terms of population (a population of more than one hundred thousand), rail system proposals should be developed that are directly proportional to urban development in the framework of sustainable transportation policies, and proper interventions should be made in public transportation policies for proper use of resources.

Acknowledgment

In this study, the data of the Erzincan Urban Transportation Master Plan Project carried out in May / November 2016 period is utilized.

6. References

[1] M. Uzun, "Erzurum Hafif Raylı Sistem Projesi", Ener Strateji, Ankara, 2011.

[2] A.P. Akgüngör and A. Demirel, "Türkiye'deki Ulaştırma Sistemlerinin Analizi ve Ulaştırma Politikaları", *Pamukkale Üniversitesi Mühendislik Fakültesi Mühendislik Bilimleri Dergisi*, vol. 10, no. 3, pp. 423-430, 2004.

[3] M.K. Çubuk and M. Türkmen, "Ankara'da Raylı Ulaşım", *Gazi Üniversitesi Mühendislik Mimarlık Fakültesi Dergisi*, vol. 18, no. 1, pp. 125-144, 2003.

[4] İ. Ocak and E. Manisalı, "Kentsel Raylı Taşıma Üzerine Bir İnceleme (İstanbul Örneği)", *Sakarya Üniversitesi Fen Bilimleri Enstitüsü Dergisi*, vol. 10, no. 2, pp. 51-59, 2006.

[5] G. Baştürk, "Kent İçi Raylı Toplu Taşıma Sistemleri İncelemesi ve Dünya Örnekleri ile Karşılaştırılması", *Master Thesis, Ulaştırma, Denizcilik ve Haberleşme Bakanlığı*, Ankara, 2014.

[6] F. Cirit, "Sürdürülebilir Kentiçi Ulaşım Politikaları ve Toplu Taşıma Sistemlerinin Karşılaştırılması", *Master Thesis, Türkiye Cumhuriyeti Kalkınma Bakanlığı*, no. 2891, Ankara, 2014.

[7] A.F. İyinam and O. Öztürk, "İstanbul Metrosu'nun Bazı Avrupa Metrolarıyla Karşılaştırılması", in *2. Uluslararası Raylı Sistemler Mühendisliği Sempozyumu (ISERSE'13)*, Karabük, 2013, pp. 1-7.

[8] Z. Öztürk and M.T. Dündar, "Metro Sistemlerinde Yapım ve İşletme Maliyetlerinin Optimizasyonu İçin Bir Yaklaşım", in *2. Uluslararası Raylı Sistemler Mühendisliği Sempozyumu (ISERSE'13),* Karabük, 2013.

[9] C. Saatçioğlu and Y. Yaşarlar, "Kentiçi Ulaşımda Toplu Taşımacılık Sistemleri: İstanbul Örneği", *Kafkas Üniversitesi İktisadi ve İdari Bilimler Fakültesi Dergisi*, vol. 3, no. 3, pp. 117-144, 2012.

[10] G. Evren, "Türkiye'de Kentsel Ulaştırma Politikalarının Gereği", in *TMMOB MMO Kentiçi Ulaşımda Raylı Sistemler Sempozyumu Bildiriler Kitabı*, Eskişehir, 1999, pp. 85-92.

[11] M. Yüzügüllü, C. Özcan and İ. Baş, "Raylı Toplu taşım Sistemlerinin Türkiye'de Yapılması ve Yerli İmalat Olanakları", *Türkiye Mühendislik Haberleri*, vol. 384, pp. 48-52, 1996.

[12] S. Pampal, B. Kayranlı and D. Karakuş, "Raylı Ulaşım Sistemlerinden Kaynaklanan Çevresel Gürültünün İncelenmesi", in *Uluslararası 1. Trafik ve Yol Güvenliği Kongresi*, Ankara, 2002, pp. 180-189.

[13] E. Gedizlioğlu and K.S. Öğüt, "Türkiye'de Kentiçi Raylı Ulaşım Sistemleri", in *TMMOB MMO Kentiçi Ulaşımda Raylı Sistemler Sempozyumu Bildiriler Kitabı*, Eskişehir, 1999, pp. 73-84.

[14] R. Sevim, "İstanbul'da Kent İçi Raylı Sistemler ve Üstyapı Hesapları". M.S. Thesis, İstanbul Teknik Üniversitesi Fen Bilimleri Enstitüsü, İstanbul, 2007.

[15] A.N., Timor. "Orta Büyüklükteki Şehirler ve Taşıdıkları Önem", *Coğrafya Bölümü Dergisi*, pp.83-101, 1997.

[16] DPT, "Beşinci Beş Yıllık Kalkınma Planı", Ankara, 1985.

[17] U. Üzmez. "Türkiye'de Orta Ölçekli Kentsel Alanlar Sorununa Çözüm Arayışları: Zonguldak Örneği", *Gazi Üniversitesi İİBF Dergisi*, vol. 14, no. 2, pp. 127-158, 2012.

[18] P. Gökgür, İ.K. Altay and B.U. Alpay, "Çok Merkezlilik Orta Ölçekli Kent Kavramı; Söke Örneği". *Artium*, vol. 4, no. 2, pp. 1-12, 2016.

[19] M. Tanış and K. Öğüt, "Orta Ölçekli Kentler için Toplu Taşıma Seçeneklerinin Teknik ve Malî Karşılaştırması", in *5. Kentsel Altyapı Ulusal Sempozyumu*, Hatay, 2014, pp. 132-146.

[20] Ulaşımda Enerji Verimliliğinin Arttırılmasına İlişkin Usul ve Esaslar Hakkında Yönetmelik, T.C. Resmi Gazete, no. 26901, 9 Haziran 2008.

[21] Büyükşehir Belediyesi Kanunu, T.C. Resmi Gazete, no. 25531, 10 Temmuz 2004.

[22] Türkiye Belediyeler Birliği Ulaşım Çalışma Komisyonu, "Ulaşım Planlama Çalışmaları ve Ulaşım Ana Planı Hazırlama Kılavuzu", Ankara, 2014, pp. 6-16.

[23] M. Özalp and E. Öcalır, "Türkiye'de Kent İçi Ulaşım Planlaması Çalışmalarının Değerlendirilmesi", ODTÜ Mimarlık Fakültesi Dergisi, vol. 25, no. 2, pp. 71-97, 2008.

[24] Gazi Üniversitesi Kent İçi Ulaşım Teknolojileri Erişebilirlik, Uygulama ve Araştırma Merkezi (KUTEM), "Erzincan Belediyesi Ulaşım Ana Planı", C. 1, Ankara, 2017.

[25] Gazi Üniversitesi Kent İçi Ulaşım Teknolojileri Erişebilirlik, Uygulama ve Araştırma Merkezi (KUTEM), "Erzincan Belediyesi Ulaşım Ana Planı", C. 2, Ankara, 2017.

[26] Gazi Üniversitesi Kent İçi Ulaşım Teknolojileri Erişebilirlik, Uygulama ve Araştırma Merkezi (KUTEM), "Erzincan Belediyesi Raylı Sistem Fizibilite Etüdü ve Avan Projeleri", Ankara, 2017.

The Strategy of Battery Voltage Control using Hybrid PI+ANFIS Structure in Non-Inverting Buck-Boost Converter

Zafer ORTATEPE[1], Ahmet KARAARSLAN[1]

[1] The Faculty of Engineering and Natural Science, Ankara Yıldırım Beyazıt University, Ankara, Turkey
155106408@ybu.edu.tr, akaraarslan@ybu.edu.tr

Abstract

In this study, the battery voltage control strategy in railway vehicles with Non-Inverting Buck-Boost Converter (NIBBC) is investigated. For this purpose, a combination of Proportional-Integral (PI) and Adaptive Neuro Fuzzy Inference System (ANFIS) control methods which is known Hybrid PI+ANFIS is applied to the NIBBC and compared with the conventional PI control method. The NIBBC operated in constant output voltage mode however during extreme overload and different input voltage conditions to improve the power quality. In this study, ANFIS controller can adjust the appropriate PI parameters (K_p, K_i) for the purpose of solving the problems like rise time, settling time, and overshoot by online. Also PI controller gives the robustness and stability in steady-state. This method is simulated by Matlab/Simulink program. The simulation results show that battery management with NIBBC gives the better results with Hybrid PI+ANFIS compared to the conventional PI control method under various conditions.

1. Introduction

The railway industry has played an important role in modern transportation and social development due to its high capacity, high efficiency and low pollution. The power supply system in railway industry provides continuous and effective power for the trains in railway operation and great impact to its operations. Diesel and electrified railway vehicles which are frequently used today's technology contain a large number of DC/DC converters. But battery voltage control is always a problem for the railway industry. Voltage drops and losses take place in the battery that are not used for a long time. However, instantaneous voltage peak occurs when the vehicle is started for the first time. For this reason, the devices which are controlled by the battery, break down frequently. In this study, the Non-Inverting Buck-Boost Converter (NIBBC) control strategy has been proposed to keep the battery voltage keep constant.

DC/DC converters are widely used in industrial applications. A lot of control strategies are made on this area [1, 3]. In this study, it is analyzed to adjust the duty cycles of the converter switches for constant output voltage by using the combination of Proportional-Integral (PI) and Adaptive Neuro Fuzzy Inference System (ANFIS) control methods which is known Hybrid PI+ANFIS and performance evaluation is carried out. Conventional PI controller has a good static performance and robustness especially for linear and time-invariant systems, but a weak dynamic performance is unsatisfactory on nonlinear, time-varying and uncertain systems [4, 7]. Among the various techniques of artificial intelligence, the most popular and widely used techniques in control systems are the ANFIS controller [8, 9]. There are certain advantages in this control strategy; ANFIS does not need any mathematical model and it can give decisions by itself.

This study implements hybrid control into the NIBBC to improve disadvantages of conventional PI controller. ANFIS controller is applied for regulation of output voltage. Also PI controller gives the robustness and stability in steady-state. Simulation results show a better performance for hybrid PI+ANFIS controller compared to the conventional type. ANFIS controller can adjusts the PI parameters for achieve the optimal response of rise time, settling time, overshoot and steady-state error by tuning of PI parameters (K_p, K_i) online. While the system parameters of K_p and K_i values always constant with the conventional PI control method, the output of PI controller is trained with the artificial intelligence method which is known ANFIS and the output value is adjusted according to the error and the change rate of the error. Therefore, output which is less error rate and which is able to follow the reference better is obtained [10].

In this paper, NIBBC operating principle and circuit description detailed in section 2. Section 3 describes the control strategies of Hybrid PI+ANFIS controller. The performance analysis and test results are studied in section 4. The conclusion part is given in section 5, respectively.

2. Circuit Description and Operation

The control block diagram of NIBBC is shown in Fig. 1. The converter consists one inductor (L), one output capacitor (C), two switches (S_1, S_2) and two diodes (D_1, D_2). Also, NIBBC can work in three different modes and consists two cascade connected buck and boost converter in serial. When the output voltage is higher than the input; it can work in boost mode, as the input voltage decrease; it works in buck-boost mode when input voltage is within the range of output. Finally, if the output voltage is much lower than inputs it is in buck mode.

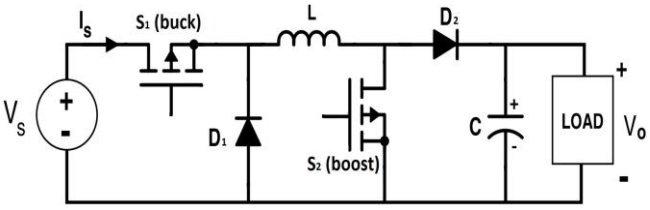

Fig. 1. The topology of two switched NIBBC converter.

If S_1 switch is always turn on, converter is controlled like a boost converter by the S_2 switch and If S_2 switch is always turn

off, converter is controlled like a buck converter by the S_1 switch. Also, it works in buck-boost mode when input voltage is within the range of output. In the steady state the relation between the input and output voltage is obtained by the following equations:

$$\frac{V_0}{V_{in}} = \frac{D_1}{1-D_2} \tag{1}$$

Which D_1 is the duty cycle of buck switch (S_1) and D_2 is the duty cycle of boost switch (S_2). Table 1 shows a summary of power converter operation in NIBBC.

Table 1. Operation principles of NIBBC.

Switch	Buck Mode	Buck-Boost Mode	Boost Mode
S1	On-off	On-off	on
S2	off	On-off	On-off
Average Load Voltage	$V_0 = D_1 V_{in}$	$V_0 = V_{in}\frac{D_1}{1-D_2}$	$V_0 = V_{in}\frac{1}{1-D_2}$

2.1. Analysis of Operation Modes

When the switch of S_1 is turn on in the buck mode operation, the current flows through L, charges its magnetic field and forces output capacitor to charge and supplying load. D_1 is off due to the positive on its cathode as in Fig. 2. When the switch S_1 is turn on, change of the current can be written in Eqs. (2).

$$\Delta i_{L(on)} = \frac{(V_{in} - V_o)}{L} D_1 T \tag{2}$$

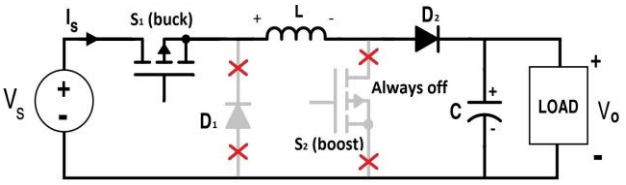

Fig. 2. Buck mode operation when the switch of S_1 is turn on.

It can be seen from the Fig. 3 that when the S_1 switch is turn off, Inductor (L) loses energy and reverses its polarity. Current flows through D_2 to the load.

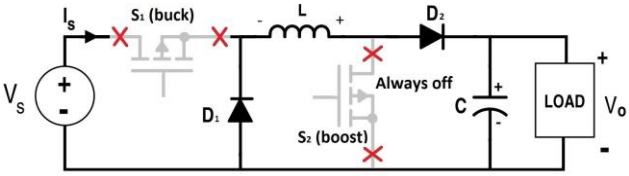

Fig. 3. Buck mode operation when the switch of S_1 is turn off.

The discharge voltage of L is collected in the capacitor to provide its voltage keep constant. If the value of capacitor (C) increases, the exponential curve reduces significantly and the inductor current decreases linearly. Therefore, the following equation is obtained;

$$\Delta i_{L(off)} = -\frac{V_o}{L}(1-D_1)T \tag{3}$$

Fig. 4 shows in boost converter mode. In this mode S_1 switch is always on. When the S_2 switch is turn on, inductor (L) charges its magnetic field. It holds anode of D_2 at ground potential and current passes through S_2 switch to supply negative terminal. During this time, the energy of capacitor flows to the load for the purpose of reduce the oscillation. The following equation can be written;

$$\Delta i_{L(on)} = \frac{V_{in}}{L} D_2 T \tag{4}$$

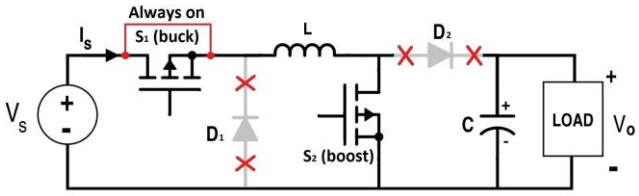

Fig. 4. Boost mode operation when the switch of S_2 is turn on.

When the S_2 switch is turn off as it can be seen from the Fig. 5 inductor (L) discharges and flows their stored energy to the capacitor. Magnetic field of the L begins to reduce with the reverse polarity. So that the output voltage becomes equal or greater than the input voltage.

$$\Delta i_{L(off)} = \frac{(V_{in} - V_o)}{L}(1-D_2)T \tag{5}$$

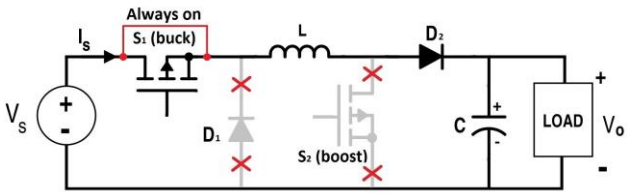

Fig. 5. Boost mode operation when the switch of S_2 is turn off.

3. Control Strategies and Algorithms of Converter

There are some control methods used in control systems. Each control methods have advantages and disadvantages. However, the main purpose of the system is to provide robustness, stability and fastness. In this study, Hybrid PI+ANFIS control method is implemented into voltage control loop and test results are compared with conventional PI control method.

3.1. Implementation of Conventional PI Controller

Conventional PI controller is most popular controller which is used in the converter applications. PI controller especially provides a good static performance for linear and time-invariant systems. As an example for the application of PI controller in industry, slow industrial process can be pointed; low percentage

overshoot and small settling time can be obtained by using this controller. Fig. 6 shows the topology of PI controlled NIBBC

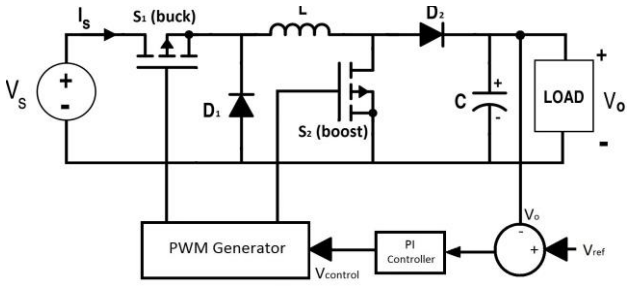

Fig. 6. The topology of PI controlled NIBBC.

The parameters contained are Proportional and Integral. The proportional part is responsible for following the desired set point, while the integral part account for the accumulation of past errors and the rate of change of error in the process respectively.

3.2. The Structure of ANFIS Controller

All AI techniques have its own abilities such as FL, ANN, genetic algorithms (GA) and expert systems. For example, while ANN is good at learning and describing examples, it is not good at how decisions are made. FL gives very good results in decision making, but it cannot generate the rule automatically in the decision-making process.

ANFIS approach is based on the idea of combining ANN's learning ability, finding the most appropriate rules and FL's decision-making like human. In this way, while ANN systems can be given the power to learn and calculate, FL can be given the ability to make decisions like human for the Anfis system. The architecture of the Anfis model proposed is shown in Fig. 7.

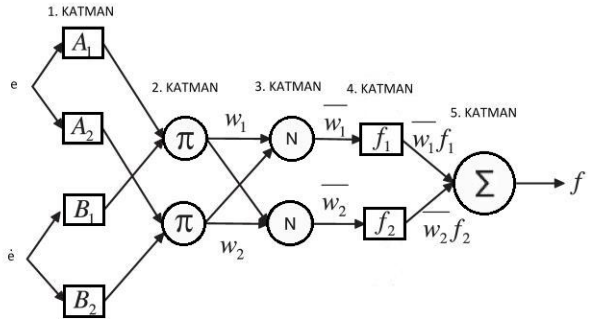

Fig. 7. The architecture model of ANFIS.

Layer 1: Each node corresponds to an input, with the "e" error and the "de" change of error. The data which is received from this layer transferred to the second layer without any processing or modification.

Layer 2: The layered representation of membership functions in the fuzzy control. Each node in this layer represents a fuzzy cluster and each is expressed by a Gaussian function.

$$t_{ij} = -\frac{(x_{ij} - m_{ij})^2}{(\delta_{ij})^2}, y_{ij} = f_{ij}(t_{ij}) = \exp(t_{ij}) \quad (6)$$

Layer 3: Each node in this layer represents a rule and the min operator is applied to the inputs of the nodes.

$$t_{ij} = \min(x_j, y_k), y_{jk} = f_{jk}(t_{jk}) = t_{jk} \quad (7)$$

Layer 4: The layer of defuzzification which the refinement and extraction is applied in fuzzy control. A rule given at each node in the defuzzification layer weighted result values are calculated.

$$a = \sum_{\substack{j=1 \\ k=1}}^{5} w_{jk} y_{jk}, b = \sum_{\substack{j=1 \\ k=1}}^{5} y_{jk}, t_0 = \frac{a}{b}, y_0 = f_0(t_0) = \frac{a}{b} \quad (8)$$

Layer 5: The output value of each node in the fourth layer is summed and resulting in the real value of the ANFIS system.

ANFIS controller adjusts the K_p and K_i parameters of PI controller using fuzzy adjuster. Coefficients of the conventional PI controller are not suitable for time-varying and nonlinear system because of adjustment trouble. Therefore, it is necessary to adjust the PI parameters automatically. Despite the conventional PI controller, Anfis controller is robust against dynamic changes in the system and does not need to know the whole system model. Therefore, Anfis controller shows the better performance than the conventional PI controller if the system is complex and undefined.

4. Training of the System

The proposed control method is trained by Matlab/Simulink program. The parameters used in converter topology are given in Table 2. Block diagram of the NIBBC that is controlled by Hybrid PI+ANFIS is shown in Fig. 8. The input and output data sets of proposed control technique is obtained from the conventional PI controller and compared to the constant frequency ramp signal for the purpose of adjust duty cycles of converter.

Table 2. Parameter used in NIBBC.

Output power	P_0	500 [W]
Output voltage	V_0	72 [V]
Input voltage	V_{in}	40-110 [V]
Switching frequency	f_s	20 [kHz]
Inductances value	L	10 [mH]
Output capacitor	C	100 [µF]

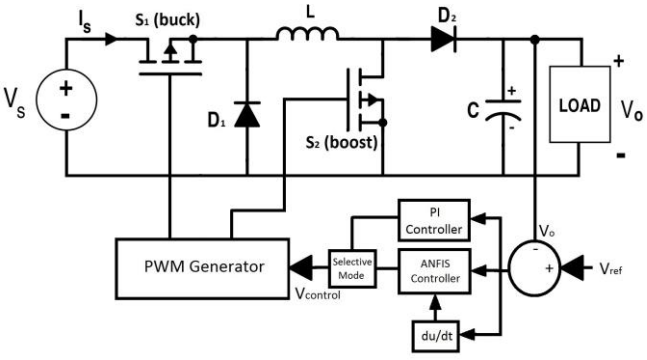

Fig. 8. The topology of proposed two switched NIBBC.

In this structure, controller output is selected by the expert for the purpose of PI or ANFIS output controller base on error and change of error. Three variables are needed to determine the selecting hybrid controller which are error, PI and ANFIS outputs. Flow chart of the selective mode is shown in Fig.9.

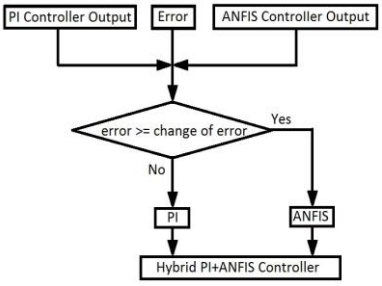

Fig. 9. Flowchart of the selective mode operation.

In the buck and boost modes of converter, there are four separate ANFIS structure. Each Proportional (K_p) and Integral (K_i) coefficients have been trained with input (error, derivative error) and output data of the conventional PI controller and carried out for a different operating conditions. The hybrid controller structure behaves like an online PI controller without the need to design and tune for different operating conditions. The loaded training data sets of the K_p and K_i coefficients of ANFIS are given in Fig. 10 (a), (b), (c) and (d), respectively.

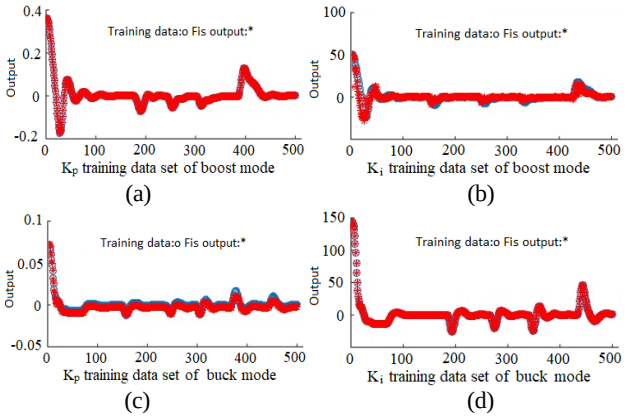

Fig. 10. (a) The plot of the K_p training data sets of boost mode, (b) the plot of the K_i training data sets of boost mode, (c) the plot of the K_p training data sets of buck mode, (d) the plot of the K_i training data sets of buck mode.

The plots of the rule surfaces are generated by ANFIS inference. The surfaces of ANFIS structure for NIBBC are shown in Fig. 11 (a), (b), (c) and (d), respectively. Fig. 11 shows that the output value for any combination of the two input values. Coefficients of the conventional PI controller are not often properly tuned for nonlinear and time-varying system. In this proposed controller, parameters are tuned by using ANFIS controller, which provide a nonlinear changing. In the next part, it will be discussed the impact of this parameter changes on the system.

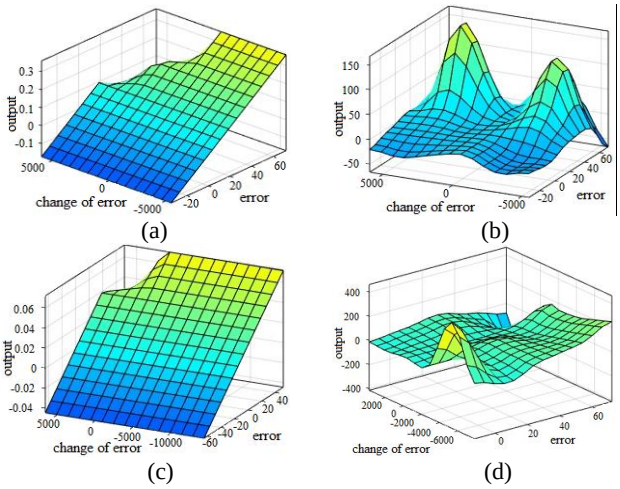

Fig. 11. (a) K_p surface of Boost mode, (b) K_i surface of Boost mode, (c) K_p surface of Buck mode, (d) K_i surface of Buck mode.

5. Performance Analysis and Test Results

Hybrid PI+ANFIS based control techniques have been proposed for NIBBC. In order to test the voltage stability and regulation performance of the proposed control method, different input voltage and load parameters were applied. The simulation studies are performed by MATLAB/Simulink program using ANFIS control method. Fig. 12 shows the topology of two switched NIBBC in Matlab/Simulink.

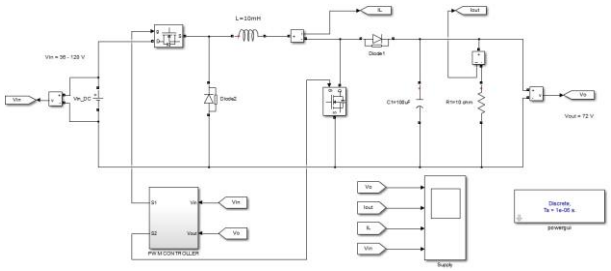

Fig. 12. NIBBC circuit diagram.

Fig. 13 shows the result of the converter for the case when the load of the converter is changed from 500 to 1000 W (change from full load to over load) and then again the power is changed from 1000 to 500 W (change from over load to full load) for conventional PI and Hybrid PI+ANFIS controllers, respectively.

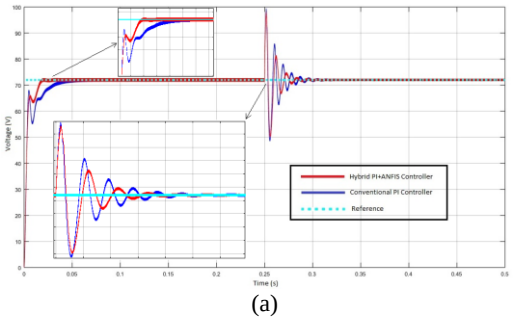

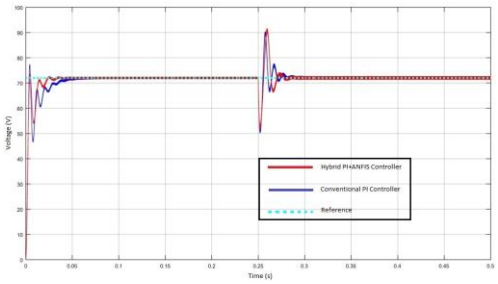

(b)

Fig. 13. Output voltage of conventional PI and Hybrid PI+ANFIS controller methods for different load changes: (a) from 500 to 1000 W (b) from 1000 to 500 W.

Fig. 14 shows the results of the converter for the case when the input voltage of NIBBC is changed from 40 to 110 V_{dc} and vice versa for conventional PI and Hybrid PI+ANFIS controller, respectively. The output power is kept constant (500W) during the input voltage changes.

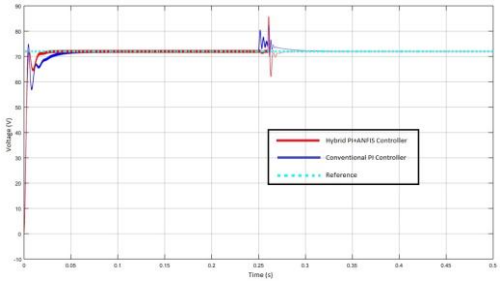

(a)

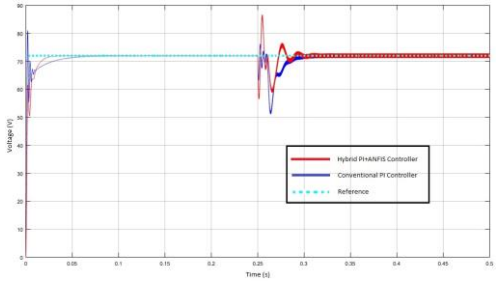

(b)

Fig. 14. Output voltage of conventional PI and Hybrid PI+ANFIS control methods for input voltage changes: (a) from 40 to 110 V_{dc} (b) from 110 to 40 V_{dc}.

Fig.13 and 14 show that the conventional controller responds slower than the other controller. Hybrid PI+ANFIS controller can be reached in a very short time despite the oscillation. Also settlement time for the hybrid controller was slower than conventional type. It reaches the reference voltage value in a very short time and then reduces the steady state error like an online tuned PI controller.

6. Conclusion

In this study, a nonlinear system controller Hybrid PI+ANFIS has been used to control the NIBBC. The conventional PI controllers of NIBBC have been replaced by Hybrid PI+ANFIS based controllers to make them more suitable for wide nonlinear and time-invariant operating conditions. Each of ANFIS structure have been trained with the two input (error, change of error) and one output data of the conventional PI controllers. The ANFIS training has been done by backpropagation learning algorithm and triangular membership functions with 5 input to learn the parameters related to membership functions and least mean squares estimation to determine the consequent parameters under 1000 epochs. The results show that the proposed Hybrid PI+ANFIS control strategy can achieve robustness in the steady state under wide input voltage and load variations.

References

[1] S.J. Jawhar, N.S. Marimuthu, N.A. Singh, “A Neuro-Fuzzy Controller for a Non Linear Power Electronic Boost Converter”, *IEEE International Conf. on Information and Automation*, pp. 394–397, 2006.

[2] B. Tarek, D. Said, M.H.E. Benbouzid, “Maximum Power Point Tracking Control for Photovoltaic Using Adaptive Neuro-Fuzzy "ANFIS"”, *IEEE International Conf. and Exhibition on Ecological Vehicles and Renewable Energies*, pp. 1–7, 2013.

[3] A. Karaarslan, "The Implementation of Bee Colony Optimization Algorithm to Sheppard-Taylor PFC Converter", *IEEE Transactions on Industrial Electronics*, vol. 60, no. 9, pp. 3711-3719, 2013.

[4] K. Boopathy, B.K. Boopathy, “Real-Time Buck Boost Converter with Improved Transient Response for battery Power Applications”, *Journal of Electrical Engineering*, pp. 1–6, 2011.

[5] A. Karaarslan, “The implementation of bee colony optimization control method for interleaved converter”, *Electrical Engineering*, vol. 97, pp. 1-11, 2015.

[6] A. Mittal, K. Arora, “Control of Wind Energy by Using Buck-Boost Converter”, *International Journal of Emerging Technology and Advanced Engineering*, pp. 293–300, 2015.

[7] A. Karaarslan, Z. Ortatepe, “The Application of ANFIS Control Method to AC-DC Single Phase PFC Converter”, *8th International Ege Energy Symposium and Exhibition (IEESE 2016)*, pp. 282-287, 2016.

[8] Z. Ortatepe, O. Parlaktuna, “Neuro Fuzzy Based Control of Two Degree of Freedom Robot Arm”, *Automatic Control Turkish National Committee National Meetings (TOK 2016)*, pp. 616-621, 2016.

[9] A. Hajizadeh, “Fuzzy/State-Feedback Control of a Non-Inverting Buck-Boost Converter for Fuel Cell Electric Vehicles”, *Iranica Journal of Energy & Environment*, vol. 5, pp. 34-41, 2014.

[10] R. Zaman, “Design of a Buck-Boost Converter and its Implementation in a Real System”, M.S. thesis, Department of Electrical and Electronics Engineering, Yaşar University, Turkey, 2016.

[11] J.K. Shiau, C.W. Ma, “Li-Ion Battery Charging with a Buck-Boost Power Converter for a Solar Powered Battery Management System”, *Energies*, vol. 6, pp. 1669-1699, 2013.

[12] D. Abd. Rahman, “Fpga-Based Digital Controller for DC-DC Converter”, M.S. thesis, Department of Electrical and Electronics Engineering, Tun Hussein Onn University, Malaysia, 2014.

Decreasing the Design and Testing Costs in the V-model

Mustafa Seçkin Durmuş[1], İlker Üstoğlu[2], and Lütfü Akçil[3]

[1]Pamukkale University, Denizli, Turkey
msdurmus@pau.edu.tr
[2]Yildiz Technical University, Istanbul, Turkey
ustoglu@yildiz.edu.tr
[3]Istanbul IT and Smart City Technologies Inc. (ISBAK), Istanbul, Turkey
lakcil@isbak.istanbul

Abstract

Software development for safety-critical systems are challenging, costly and time-consuming processes. If railway signaling system software (interlocking software) development is in question, this process is also mandated by railway-related functional safety standards. First recommendation of these standards is to use a software development process model, i.e. The V-model. However, this process may become inextricable even though the process is guided by safety-standards and outer notified bodies (NoBo). In particular, due to inadequate planning or recurrent testing the costs may increase dramatically. This paper explains a slight modification in the design phase of the V-model. The proposed modification ensures the requirement-software matchup and guarantees that all fault requirements are implemented in the software.

1. Introduction

Development of a software is a difficult process that needs to be handled very carefully. Sharing the tasks, calculation of manpower, determining work packages and many assignments shall be considered. Therefore, such processes are guided by software development process models, or in other word, software lifecycles. Among many software development models, V-model is a well-known software lifecycle which used for the development of safety-critical software.

Many studies can be found on different software lifecycles, decreasing the software costs, optimizing the man power, reasonable worst case analysis [1-5].

This paper explains the application of DES-based fault diagnosis in software component (module) design and the structure of the paper is as follows: V-model is explained in section 2, construction of the diagnoser and coding is explained in section 3 and a case is given in section 4. The paper ends with a conclusion in section 5.

2. V-model According to EN50128:2011

Safety-critical software development for railway control systems are mandated by the EN 50128 standard. This standard provides guidance for the preparation, development, implementation and maintenance of any railway-related software which includes safety functions. The steps of software development process, methods, techniques, role of people are explained in this EN standard. The EN 50128 is in conjunction with EN 50126 (where Reliability, Availability, Maintainability and Safety - RAMS is demonstrated) and EN 50129 (where requirements of safety related electronic systems for signaling is explained). The V-model, as defined in 50128:2011 [6], is shown in Fig. 1. As can be seen from Fig. 1, the lifecycle begins with a *Software Planning Phase* where Software Quality Assurance Plan (SQAP), Software Quality Assurance Verification Report, Software Verification Plan, Software Configuration Management Plan, Software Validation Plan and Software Maintenance Plan documents shall be prepared and shall be updated during the lifecycle.

Each phase has its own input documents and several output documents shall be prepared by responsible team members at the end of each phase. The list of 46 documents including their preparation phase and the responsible person are given in Table A.1 and Table C.1 of EN 50128:2011. The liability of each team member is also defined in Annex B from Table B.1 to Table B.10 in EN 50128:2011.

An important document is SQAP where the chosen lifecycle model, budgets, milestones of the project, roles of each team member, structure of the documentation, archiving, updating, writing and checking issues of the documents, the chosen methods, techniques and tools from related tables and etc. are defined.

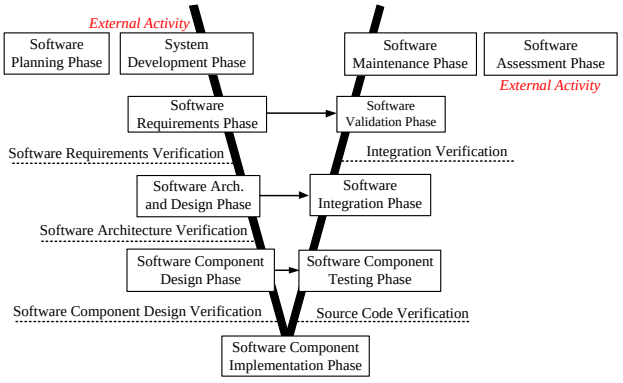

Fig. 1. V-model lifecycle [6]

The left side of the V-model can be considered as definition and design part whereas the right side of the V-model can be considered as testing part. Each phase shall be carried out by separate and distinct teams. The number of person may expand in the development process but this expansion shall be identified from the very beginning of the project. In [7], the change of the

total number of software development teams are illustrated as given in Fig. 2.

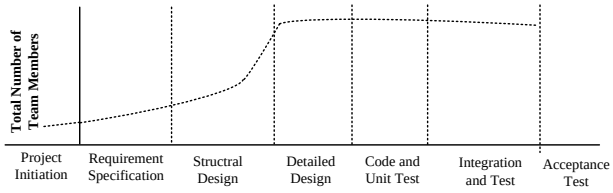

Fig. 2. Software development teams [7]

In addition to [7]; [8] illustrated the cost of detection of faults in the different phases of V-model (see Fig. 3).

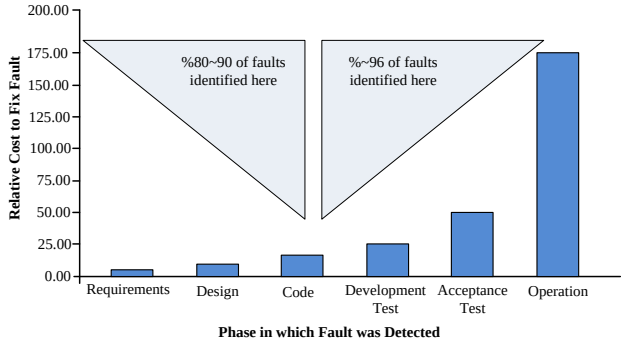

Fig. 3. Cost of detecting faults [8]

Additionally, the cost of fixing an error at the design phase is 3–8 units, whereas the cost of fixing an error at the testing phase is 21–78 units. Another study showed that, it is 5 times more expensive to fix a problem at the design stage than in the phase of initial requirements, 10 times more expensive to fix it through the coding phase, 20 to 50 times more expensive to fix it at acceptance testing and, 100 to 200 times more expensive to fix that error in the phase of operation [2], [5].

As it is obvious from Fig. 1, if a fault is detected in Software Component Testing Phase after Coding, the development process shall move back to the left side of the V-model. Depending on the type and number of faults, the requirements, the software architecture or software models shall be reviewed and fixed by responsible team members which will increase the costs dramatically.

In this study, it is shown that the software models (generic software blocks) can be checked by adding an intermediate step in the *Software Component Design Phase* of the V-model (see Fig. 4).

By adding this intermediate step, the designer checks if the developed software fulfills the software requirements related with faults or not, before passing to the Coding Phase.

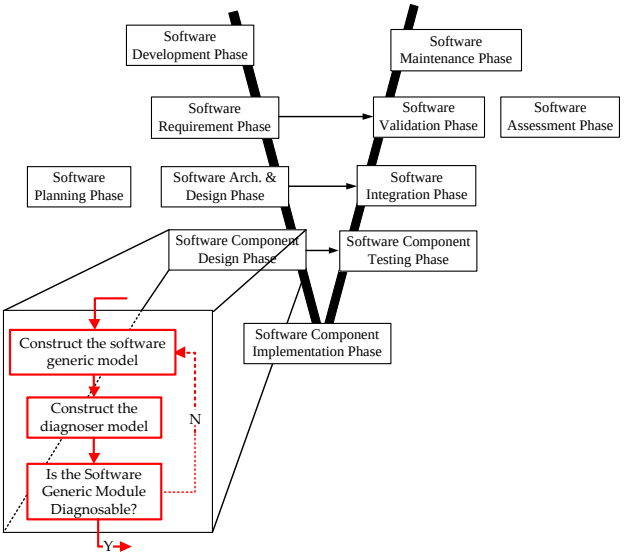

Fig. 4. V-model with diagnoser

3. Construction of the Diagnoser and Coding

Modeling (defined in Table A.17 of EN 50128:2011 [6]) is a must for the different phases of implementation of a software application. The use of *Modeling* is highly recommended for SIL3 by EN 50128:2011 in *Software Requirements Phase* (Table A.2 of EN 50128:2011), *Software Arch.&Design Phase* (Table A.3 of EN 50128:2011) and *Software Component Design Phase* (Table A.4 of EN 50128:2011). Recommended modeling methods are listed in Table A.17 of EN 50128 (see Table 1).

Table 1. A Part of recommendations of EN50128:2011 on *Modeling* [6]

Technique/Measure	Ref	SIL 3	SIL 4
.....	....	...	...
.....	....	...	...
4. Finite State Machines	D.27	HR	HR
5. Time Petri Nets	D.55	HR	HR
.....	....	...	...
.....	....	...	...
.....	....	...	...
11. Sequence Diagrams	D.67	HR	HR
Requirements: 1) A modeling guideline shall be defined and used. **2) At least one of the HR techniques shall be chosen.**			

Since 4 and 5 of Table 1 are also known as Discrete Event Systems (DES) based techniques, DES-based fault diagnosis methods are applicable. The diagnoser is built from the model itself and shall represent all fault types which are defined in *Software Requirements Phase*. As illustrated in Fig. 4, after construction of the model, designer shall construct diagnoser to check the diagnosability of the system.

DES-based fault diagnosis and the diagnosability is described by Sampath et al. [9] as the detection with a finite delay occurrence of failures of any type using the record of observable events. The diagnoser is obtained by using the system model itself and it observes online the behavior of the system [10]. For detailed explanation of DES-based fault

diagnosis and diagnoser construction for railways, the reader is referred to [9-12]. In order to apply DES-based fault diagnoses, the designer shall model the railway field components in the *Software Component Design Phase* of the V-model.

An example railway field is given in Fig. 5 (Eminonu tram station). The railway field given in Fig. 5 consists three different types of field components. To reduce the complexity, only the model of two-aspect signal and its diagnoser will be explained here.

The model of the component shall be constructed with respect to the software requirements. First of all, a two-aspect signal has two colors; green and red. Therefore, designer need two places to represent these states. As an operational requirement, the signal shall be red when the system started. Therefore, the designer shall put a token in the place which represents red color information. As a safety requirement, some signal combinations such as both signals (red and green) are lit at the same time or no signal indication shall be detected by the software. Hence, the designer shall add two more places to its model.

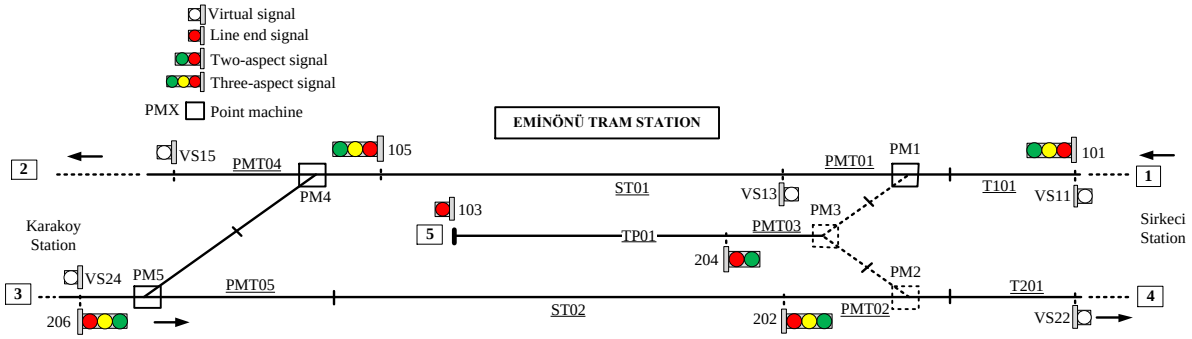

Fig. 5. Schematic representation of Eminonu tram stattion

The Petri net model of two-aspect signal is given in Fig. 6. Meanings of places and transitions are given in Table 2.

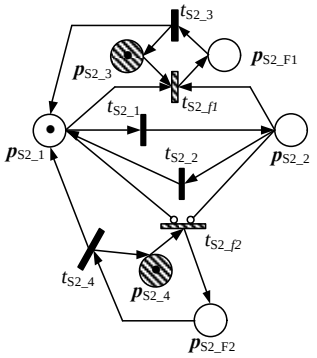

Fig. 6. Petri net model of two-aspect signal

Table 2. Meanings of places and transition of the model given in Fig. 6.

Place	Meaning	Transition	Meaning
p_{S2_1}	Signal is red	t_{S2_1}	Lit signal green
p_{S2_2}	Signal is green	t_{S2_2}	Lit signal red
p_{S2_3}	Color fault restriction	t_{S2_3}	Fault acknowledge
p_{S2_4}	Color fault restriction	t_{S2_4}	Fault acknowledge
p_{S2_F1}	Fault type F_1 has occurred (both signals are lit at the same time)	t_{S2_f1}	Occurrence of fault F_1
p_{S2_F2}	Fault type F_2 has occurred (no signal indication)	t_{S2_f2}	Occurrence of fault F_2

When the system has started, related signal will be red. After a route reservation, the signal can lit green. The striped places and transitions are named as unobservable places and unobservable transitions, respectively. In other words, it is not possible to trace the occurrence of event. For example, it is not possible to detect the occurrence moment of related fault but later, it is detected by the diagnoser. We cannot detect the time instance when both signals are lit but later, it is possible to detect it by feedback information on the signal card.

Later, the designer shall construct the diagnoser. The diagnoser consists of marking (1 or 0) which indicates the actual situation of the Petri net model given in Fig. 6. Additionally, the states of the diagnoser has fault label *N* or *F* which indicates that the related fault type has occurred or not. For the initial state the state of the diagnoser will be {(1,0,1,1,0,0,*N*)}, where observable place p_{S2_1} and unobservable places p_{S2_3} and p_{S2_4} contains one token and the rest have no tokens. Since there is no fault at the initial state, the initial state of the diagnoser is labeled with *N*. The diagnoser states are changed according to the event occurrences in the Petri net model. The diagnoser of the Petri net model given in Fig. 6 is given in Fig. 7.

The marking (state of the diagnoser) M_{S2_0} represents the initial marking. Due to the unobservable places and transitions, the states of the diagnoser changes by observing new markings or by observing new marking and observable transition occurrences. For instance, the state of the diagnoser changes from M_{S2_0} to M_{S2_1} by observing the new marking M_{S2_1} and occurrence of the transition t_{S2_1}. The new marking M_{S2_1} is also labeled by *N*, since there is no fault. Additionally, the state of the diagnoser changes from the initial marking M_{S2_0} to M_{S2_f1} by just observing the new marking M_{S2_f1}. The marking M_{S2_f1} is labeled by F_1, because the predetermined fault type F_1 (both signal colors are lit at the same time) has occurred.

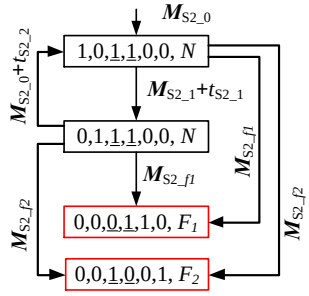

Fig. 7. Diagnoser of two-aspect signal

To achieve the diagnosis properly, the diagnoser given in Fig. 7 shall be diagnosable. In other words, *states of the diagnoser (the markings) does not include more than one fault label*. In addition to this, the diagnoser does not contain any Fi-indeterminate cycle [9]. In other words, *the diagnoser does not contain any cycle of faults*.

As can be seen from Fig. 4, if the constructed Petri net model is not diagnosable, then the designer shall revise the Petri net model and check the diagnosability once again. Diagnosability also ensures that all software requirements related to that component are fully implemented in the model. In particular, the software requirements related with the faulty conditions.

3.1. Coding the Diagnoser

Sequential Function Charts (SFC) and *Functional Block Diagrams* (FBD) are recommended in Table A1.6 of EN 50128:2011 standard. These two languages are used while coding the Petri net model and the diagnoser. The code for Petri net model of the two-aspect signal and its diagnoser is given in Fig. 8 and Fig. 9, respectively.

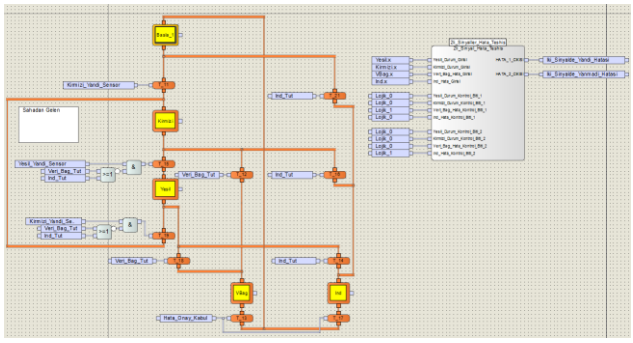

Fig. 8. The code for two-aspect signal with diagnoser

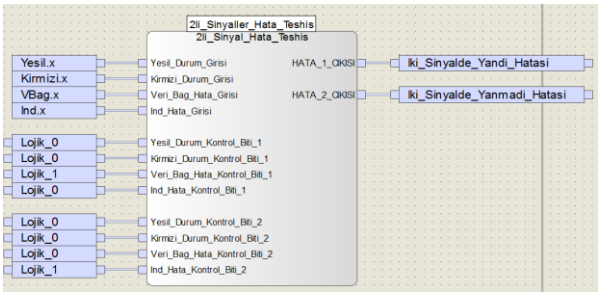

Fig. 9. Software block of diagnoser

As can be seen from the diagnoser block in Fig. 9, inputs of the diagnoser are the states of the Petri net model given in Fig. 6 and the diagnoser compares the actual states of the two-aspect signal with its faulty markings. When the actual states of the two-aspect signal is equal to ant faulty marking, then the diagnoser sets its related output (right side of the diagnoser).

4. Case Study: Eminonu Tram Station

Schematic representation of Eminonu tram station is given in Fig. 5. Eminonu tram station is located on T1 tram line of Metro Istanbul between Sirkeci and Karakoy stations.

According to the V-model given in Fig. 4, all components (signals, points, rail blocks and routes) are modeled by using Petri nets and their diagnosers are constructed in the *Software Component Design Phase*. Later, these software components are converted to PLC code to run on a fail-safe PLC in the *Software Component Implementation Phase*. The product of these previous phases are tested and verified in the *Software Component Testing Phase*.

Models and diagnosers are constructed according to the software component requirements document which include 93 requirements in total, are tested according to the software component testing document with 94 test cases. As a result of using diagnoser design and the use of diagnosable models, component tests are took only three days without any modeling errors. The setup of Eminonu tram station can be seen from Fig. 10.

A traffic control center is also designed to command the railway traffic in the station. The railway field is also simulated with another PLC. The hardware inside the panel on the right side can be considered as a Hardware-in-the-Loop (HIL) component.

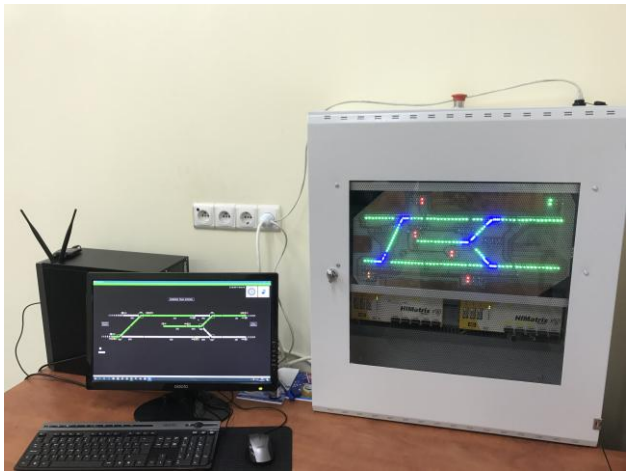

Fig. 10. The setup for Eminonu station

5. Conclusions

Software development processes are for safety-critical systems need to be managed very carefully and selflessly. Many software development processes has failed due to mismanagement or incomplete planning.

Design of a diagnoser allows designer to check software models are fully met or not with the *software component requirements*. Additionally, diagnoser design prevents designers

from software design errors (see [12]). Fixing these errors will be much more costly when they will later appear in the component tests.

Additionally, detection of an error in software component tests requires that the component model be revised, recoded and retested from the very beginning.

Acknowledgement

This work is supported by The Scientific and Technological Research Council of Turkey (TÜBİTAK) project number 115E394 – Fail-Safe PLC implementation of Interlocking System Design with Fault Diagnosis capability for Fixed-block Railway Signaling Systems.

6. References

[1] W. W. Royce, "Managing the Development of Large Software Systems: Concepts ad Techniques", *Proc. Wescon*, pp. *1-9*, 1970.

[2] B. W. Boehm, "Software Engineering Economics", *IEEE Transactions on Software Engineering*, vol. *SE-10*, no. *1*, pp. *4-21*, 1984.

[3] W. Boehm, "Verifying and Validating Software Requirements and Design Specifications", *IEEE Software*, vol. *1*, no. *1*, pp. *75-88*, 1984.

[4] B. Boehm, C. Abts, S. Chulani, "Software Development Cost Estimation Approaches – A Survey", *Annals of Software Engineering*, vol. *10*, pp. *177-205*, 2000.

[5] B. Haskins, J. Stecklein, B. Dick, G. Moroney, R. Lovell and J. Dabney, "Error Cost Escalation Through the Project Life Cycle", in *INCOSE International Symposium*, 2004, pp. 1723-1737.

[6] *EN 50128, Railway Applications, Communications, signalling and processing systems, Software for railway control and protection systems*, European Committee for Electrotechnical Standardization, Brussels, June 2011.

[7] P. Rook, "Controlling Software Projects", Software Engineering Journal, vol. *1*, no. *1*, pp. *7-16*, 1986.

[8] G. P. Brat, "Reducing V&V Cost of Flight Critical Systems: Myth or Reality?", in *AIAA Information Systems, AIAA SciTech Forum*, American Institute of Aeronautics and Astronautics, 2017, pp. 1-10.

[9] M. Sampath, R. Sengupta, S. Lafortune, K. Sinnamohideen and D. Teneketzis, "Diagnosability of discrete event systems", I*EEE Transactions on Automatic Control*, vol. *40*, no. *9*, pp. *1555-1575*, 1995.

[10] M. Sampath, R. Sengupta, S. Lafortune, K. Sinnamohideen, D. Teneketzis, "Failure diagnosis using discrete-event models", *IEEE Transactions on Control Systems Technology*, vol. *4*, no. *2*, pp. *105-124*, 1996.

[11] M.S. Durmuş, S. Takai, M.T. Söylemez, "Fault Diagnosis in Fixed-Block Railway Signaling Systems: A Discrete Event Systems Approach", *IEEJ Transactions on Electrical and Electronic Engineering*, vol. *9*, no. *5*, pp. *523- 531*, 2014.

[12] M. S. Durmuş, S. Takai, M. T. Söylemez, "Decision Making Strategies in Fixed-Block Railway Signaling Systems: A Discrete Event Systems Approach", *IEEJ Transactions on Electrical and Electronic Engineering*, ol. *10*, no. *2*, pp. *186-194*, 2015.

Wayside Diagnosis of Wheelset Faults of Metros using One-period Analysis

O. Kilinc[1], J. Vágner[2]

[1]Department of Transport Means and Diagnostics, Faculty of Transport Engineering,
Studentska 95; 530 09, Pardubice, Czech Republic
onur_kilinc@anadolu.edu.tr
[2]Department of Transport Means and Diagnostics, Faculty of Transport Engineering,
Studentska 95; 530 09, Pardubice, Czech Republic
jakub.vagner@upce.cz

Abstract

This research is focused on detection of wheelset faults of Prague metro train set of type 81-71M using vibration sensors on the wayside with the contribution of a novel one period analysis. Vibration sensor activities for each metro passing are recorded by two accelerometer sensors which are mounted on both right and left rail for all day while metros are in routine operation. Signal samples of two known faulty wheels of a wheelset on ID-108 metro are used as ground truth information in comparison to ID-119 healthy data. The database has 16 faulty signal samples against 16 healthy ones. Three different methodologies; Wavelet Packet Energy (WPE), Time-Domain Features (TDF) and Linear Configuration Pattern Kurtograms (LCP-K) are used with Fisher Linear Discriminant Analysis and Support Vector Machines classifiers. Outstanding results are observed among proposed techniques up to 100%. Proposed methods may be used for a cost-effective wayside diagnostic system for railway vehicles.

1. Introduction

Diagnosis of wheelsets of railway vehicles is crucial by means of safety of the run and preventing further damage on the components.

Condition monitoring of wheelsets of a railway vehicle is cumbersome with stationary techniques since multiple sensor allocation on each train is costly and maintaining sensor calibration over time is difficult unless a wayside diagnosis approach is employed. The main problem of a wayside diagnostic system is to achieve little number of false positives and false negatives in the detection. Once these conditions are satisfied, a cost-effective maintenance plan can be organized which is far more superior to scheduled or on-condition maintenance.

Recent studies shows that it is possible to detect wheelset bearing faults [1], wheel profile and wheel impact problems [2] and wheel defects [3] using wayside approaches. As reviewed in [2], there are various methods which are focused on wheelset related faults: Wheel profile condition monitoring by using a high speed camera is possible. However this method requires the railway vehicle operating at a very low speed and further image analysis. Utilizing ultrasonic signal processing statistical techniques is also promising for detecting cracked wheels [4]. Out-of-roundness, shelling and wheel flats can be detected using optical sensors, accelerometers and strain gages [5],[6].

All techniques pointed out in this study require an appropriate signal processing and identification (classification) phase since signals in wayside environment are highly affected by the environmental noise and interaction of different components between each other. Unless a dynamical modelling is to be used, signal based methods are generally based on band-pass filtering, wavelet and frequency spectrum analysis and Fast-Fourier Transform [7].

Another vital problematic is to determine how data acquisition and segmentation are to be done. Distinguishing between healthy and faulty cases requires a properly calibrated measurement instrumentation device and choosing a smart sampling window as it may overlap the information of nearby wheelsets and other structures.

This study is focused on the detection of wheel flats on metro train sets using vibration sensors on the wayside. Throughout the study, two vibration sensors are mounted on the rail with accompanying optical gates which provides speed calculation in a metro tunnel in Prague. After recording the signals that are related to healthy and faulty metro wheels, novel signal acquisition and feature extraction techniques are used to detect faulty conditions of the wheelsets with the help of the signal classifiers.

The paper is organized as follows: wayside measurement passage, signal acquisition and the preparation of the database are told in Section 2. Proposed feature extraction techniques are presented in Section 3. Analysis results are demonstrated in Section 4. Finally, conclusion part is given in Section 5.

2. Test Environment

In this study, measurements are carried out on a passage between Dejvická and Bořislavka metro stations which are located on Prague metro line-A. The operation speed of the metros in this passage are almost constant which provides stable and more standardized outputs preventing unexpected braking and structural noise. Two accelerometer sensors (Z_1 , Z_2) are mounted on the foot of both left and right rails which are supplemented by two optical gates (G_A , G_B) that detect wheelset positions with respect to time. Vibration sensors are handled by NI-cDAQ-9234 device and signals are recorded with sampling frequency of 51.2 kHz for vibration sensors to observe spiky behavior in the signal more precisely and 500 Hz for optical sensors. Signals are recorded for all day long when trains are in their routine operation. All measurements were carried out as the part of the project; Competence Centre of Railway Vehicles,

No. TAČR TE01020038. The wayside measurement set up is shown in Fig. 1.

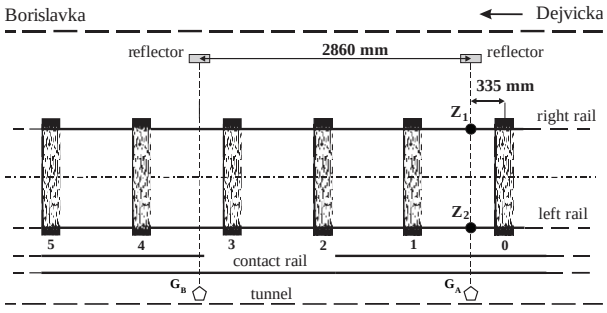

Fig. 1. Measurement system on the wayside passage

The metro train sets that are investigated in this research are identical (type 81-71M) by means of bogies and passenger cars (five passenger cars on each train set with 4-axle traction bogies).

Though there are a lot of passing available, the database is constructed by two trainsets; ID-108 with known wheel flats on both of the wheels on axle-7 and ID-119 which has healthy wheelsets on all of its bogies. In most cases faulty observations are far more than normal ones. Since eight passing of ID-108 train set is available for use with two sensors, the final database includes these 16 faulty signal segments against 16 healthy ones which are acquired from ID-119 metro train set to equalize the database.

Thanks to a novel technique which standardizes the signal segmentation for each wheelset passing; one-period analysis, a technique which calculates number of samples and positions respect to the sensor position so that each wheel is rotated only once, is used to finalize all signal samples on the database (Fig. 2, V: operational speed of the passing wheelset, r: wheel radius). Since wheel diameters vary significantly due to wear (0,730 – 0,785 m), the information of each wheel diameter is acquired from maintenance of train sets.

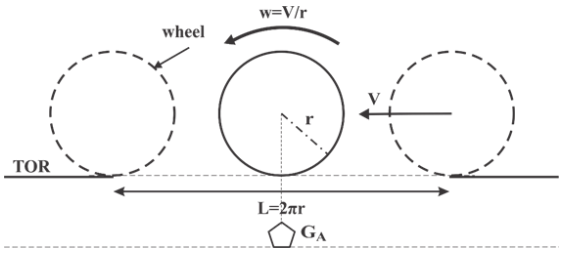

Fig. 2. Understanding one-period analysis

Constructed database is shown in Table 1 which leads to a two-class classification problem.

Table 1. Two-class database for wheel flat detection

TRAIN ID	Condition	Wheelsets	Sensors	Total Samples
119	Normal	2-17	Z1	16
108	Wheel flat	7	Z1-Z2	16

3. Proposed Techniques

In machine learning, it is vital to represent necessary information while discarding the irrelevant parts which provide computational efficiency and higher recognition rates regarding to the problem. Maintaining relevant information is generally performed by different feature extraction techniques which are specialized for the classification problem that is focused.

It is known that railway vehicle related signals have non-stationary characteristics in most cases [8]. In this study, three feature extraction techniques are proposed which are efficient in non-stationary signal processing. After feature extraction stage is completed, two state-of-art classifiers; Fisher Linear Discriminant Analysis [9] and Support Vector Machines with linear kernel [10] are employed in order to distinguish between healthy and faulty conditions of the metro wheelsets.

3.1. Wavelet Packet Energy

Wavelet techniques are based on discrete wavelet transform and have wide range of implementations in signal processing.

As an efficient feature extraction method for non-stationary signals, Wavelet Packet Transform (WPT) is introduced. In this method, Fourier spectrum of the signal is divided into desired number of frequency bands (L), which will change the frequency resolution according to the signal that is to be analyzed. The signals in the frequency bands are than filtered by low and high pass filters to achieve next level where the maximum number of components is $n = 2^L$. However, this signals are not time invariant and need further processing for a convenient feature extraction (Fig. 3).

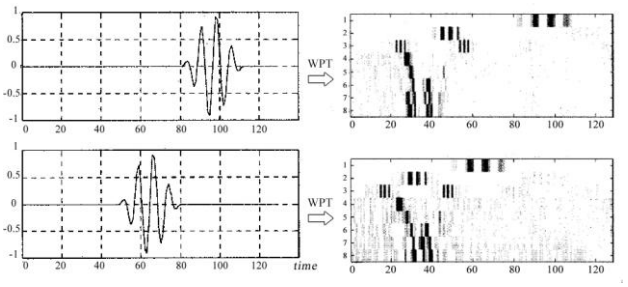

Fig. 3. Time shifted transients in time domain (left), resultant WPT of three-level (right)

Thanks to the Wavelet Packet Energy (WPE) that makes signal characteristics translation invariant [11]; energy calculation of each wavelet packet is carried out (Fig. 4). As seen in Fig. 4, the outputs of both transients are nearly the same.

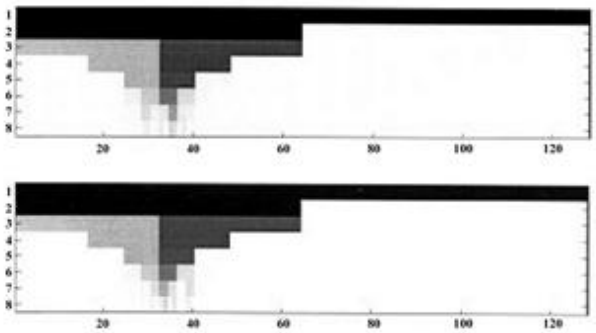

Fig. 4. The resultant WPE of three-level for the signals shown in Fig. 3

In this research, five-level wavelet packet energy (WPE_5) is used after Haar wavelets [12] (Fig. 5) are utilized in the WPT phase and the resultant feature vector size is 32 x 1.

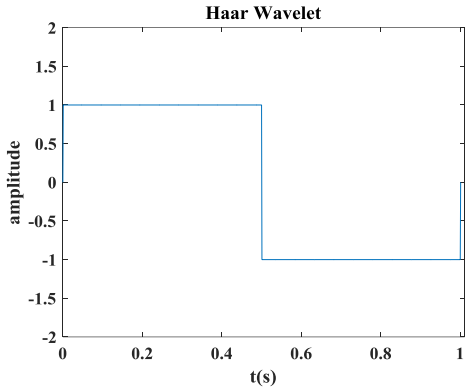

Fig. 5. Preferred wavelet function for WPT

3.2. Time Domain Features

Faulty components generally generate different signals than healthy ones, statistically. One very common technique is to calculate time-domain statistics from the segmented signals. In this research, besides regular time-domain statistics, kurtosis (1), skewness (2) and crest factor (3) are also calculated for the discrete signal $X[n]$ which is inspired by a recent research [13] about rotating machinery fault diagnosis.

$$X_{kurtosis} = \sum_{n=1}^{N} \frac{(X_n - \mu)^4}{N\sigma^4} - 3 \quad (1)$$

$$X_{skewness} \sum_{n=1}^{N} \frac{(X_n - \mu)^3}{(N-1)\sigma^3} \quad (2)$$

$$X_{crest\ factor} = 20 * \log_{10}\left(\frac{\max(x)}{\mathrm{rms}(x)}\right) \quad (3)$$

All time-domain features are calculated and concatenated in a 8 x 1 matrix for each signal sample (4).

$$TDF = \begin{bmatrix} energy, mean, std.dev, max, min, \\ kurtosis, skewness, crest\ factor \end{bmatrix}_{8x1} \quad (4)$$

3.3. Linear Configuration Pattern Kurtograms

In condition monitoring, Kurtograms are widely used especially in rotating machinery fault detection. Kurtogram approach is based on spectral kurtosis, which is a transformation of the signal into frequency-delta spectrum, that has previously introduced in the literature [14]. The main drawback of spectral kurtosis is its computational inefficiency. Thus, a few thousands of times faster algorithm is substituted so called Fast Kurtogram (FK) [15]. In FK, signal is divided into bands as it is in Short Time Fourier Transform (STFT) but in a different order so that maximum spectral kurtosis is shown in a grid view by means of intensity level which represents frequency-delta spectrum in a more appropriate way.

Local Configuration Pattern (LCP) is a descriptor based on Local Binary Patterns (LBP) [16] which is introduced in 2D pattern recognition. As an extension of LPB, LCP approach allows patterns to be detected on a 2D image rotationally invariant [17].

One crucial advantage of this technique is that it has a fixed output for the signal samples with different sizes. Thus, it always results 81 x 1 feature vectors independent from the input image. In the proposed LCP algorithm in this study, LCP window size is chosen as 16 x 16 which is proved to be successful for 128 x 128 image size.

Mechanical faults have shown different behavior than the normal signal in the Kurtograms. One example from the database of healthy and faulty wheelsets of metros is shown on Kurtograms, which are resized into 128 x 128 pixels, after dynamical one-period analysis takes place on signal samples.

Fig. 6. Sample faulty (a) and healthy (b) signals from vibration signals of metro wheelsets on Kurtogram

Combining these two techniques; Kurtogram and LCP, leads to the proposed Linear Configuration Pattern Kurtogram (LCP-K). The procedure of LCP-K implementation is shown in Fig. 7.

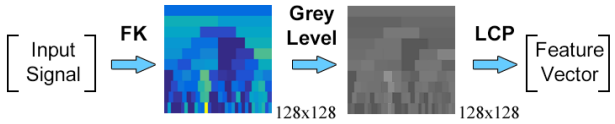

Fig. 7. Implementation of LCP-K on a one-dimensional signal

It is urgent to emphasize that signal samples ought to be segmented according to the rule of one-period analysis prior to FK approach to standardize the process.

Consequently, proposed LCP-K technique is considered to be a convenient way of describing signature of the failures.

The overall procedure of the proposed framework is shown in Fig 8.

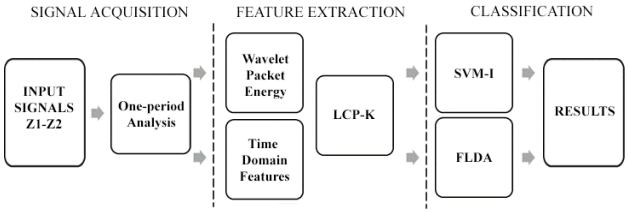

Fig. 8. Flowchart of the proposed wayside diagnosis system

4. Analysis Results

In the classification of healthy and faulty wheelset, two-state of art classifiers; Fisher Linear Discriminant Analysis (FLDA) and Support Vector Machines with linear kernel (SVM-I) are employed with 8-fold cross validation to achieve reliable results.

Table 2. Classification results after 8-fold cross validation

Classifier	Classification Accuracy (%)		
	WPE_5	**TDF**	**LCP-K**
SVM-I	90.6	**100**	90.6
FLDA	68.6	**100**	96.9

In the proposed framework best results are obtained only via 8-fold cross validation. Regarding to the results in Table 2, WPE_5 features have instable results indicating that this feature extraction method is less reliable in this duty. Proposed LCP-K feature extraction scheme have promising results in both of the classifiers but still not as efficient as TDF. It is also notable that, both SVM-I and FLDA classifiers can outperform each other in WPE_5 and LCP-K feature extraction techniques. Furthermore, in FLDA classification, both TDF and LCP-K has much better results up to 100%. It can be assumed that using either TDF or LCP-K feature extraction technique may be the most suitable way in detecting of wheel defects when vibration based diagnosis is performed.

5. Conclusion

This study investigates three feature extraction methodologies which are known to be efficient in mechanical fault diagnosis. Proposed techniques are utilized on the signals that are acquired by wayside passages of Prague metros with the novel one-period analysis technique which compensates the small changes in the vehicle operational speed.

Besides, all proposed feature extraction schemes allow a fixed sized output even if the duration of the signal varies due to speed or wheel diameters.

According to the results, both TDF and LCP-K are considered to be superior to conventional WPE features when FLDA classifier is used. The results show that it is possible to detect wheel flats with the TDF technique as 100%.

This framework may be used in achieving an efficient and cost-effective wayside diagnosis of wheelset related faults, which also ensures safety of the run, not only for metros but also any kind of railway vehicles.

6. Acknowledgement

This paper was supported by Technological Agency of Czech Republic within the Project No. TE 01020038.

7. References

[1] F. Liu, C. Shen, Q. He, A. Zhang, Y. Liu, and F. Kong, "Wayside bearing fault diagnosis based on a data-driven doppler effect eliminator and transient model analysis," *Sensors*, vol. 14, no. 5, pp. 8096–8125, May 2014.

[2] R. W. Ngigi, C. Pislaru, A. Ball, and F. Gu, "Modern techniques for condition monitoring of railway vehicle dynamics," *Journal of Physics: Conference Series*, vol. 364, p. 012016, May 2012.

[3] K. Jakimovska, V. Vasilev, N. Stoimenov, S. Gyoshev, and D. Karastoyanov, "Train control system for railway vehicles running at operational speed," *Manufacturing Engineering*, vol. 69, no. 2, pp. 86–92, 2015.

[4] B. Brickle, R. Morgan, E. Smith, J. Brosseau, and C. Pinney, "Identification of existing and new technologies for wheelset condition monitoring," TTCI Ltd, TTCI(UK), RSSB Report T607 UK P-07-005, 2008.

[5] V. Belotti, F. Crenna, R. C. Michelini, and G. B. Rossi, "Wheel-flat diagnostic tool via wavelet transform," *Mechanical Systems and Signal Processing*, vol. 20, no. 8, pp. 1953–1966, Nov. 2006.

[6] D. Barke and W. K. Chiu, "Structural health monitoring in the railway industry: a review," *Structural Health Monitoring*, vol. 4, no. 1, pp. 81–93, 2005.

[7] S. Bruni, R. Goodall, T. X. Mei, and H. Tsunashima, "Control and monitoring for railway vehicle dynamics," *Vehicle System Dynamics*, vol. 45, no. 7–8, pp. 743–779, Jul. 2007.

[8] C. Mao, Y. Jiang, D. Wang, X. Chen, and J. Tao, "Modeling and simulation of non-stationary vehicle vibration signals based on Hilbert spectrum," *Mechanical Systems and Signal Processing*, vol. 50–51, pp. 56–69, 2015.

[9] S. Ergin and O. Kilinc, "A new feature extraction framework based on wavelets for breast cancer diagnosis," *Computers in Biology and Medicine*, vol. 51, pp. 171–182, Aug. 2014.

[10] J. KIM, B.-S. Kim, and S. Savarese, "Comparing image classification methods: K-nearest-neighbor and support-vector-machines," presented at the 6th WSEAS international conference on Computer Engineering and Applications, Harvard, 2012, pp. 133–138.

[11] G. G. Yen and K.-C. Lin, "Wavelet packet feature extraction for vibration monitoring," *Industrial Electronics, IEEE Transactions on*, vol. 47, no. 3, pp. 650–667, 2000.

[12] L. Li, L. Qu, and X. Liao, "Haar wavelet for machine fault diagnosis," *Mechanical Systems and Signal Processing*, vol. 21, no. 4, pp. 1773–1786, May 2007.

[13] X. Yu, E. Ding, C. Chen, X. Liu, and L. Li, "A novel characteristic frequency bands extraction method for automatic bearing fault diagnosis based on Hilbert Huang transform," *Sensors*, vol. 15, no. 11, pp. 27869–27893, Nov. 2015.

[14] R. F. Dwyer, "Detection of non-Gaussian signals by frequency domain kurtosis estimation," in *Acoustics, Speech, and Signal Processing, IEEE International Conference*, 1983, vol. 8, pp. 607–610.

[15] J. Antoni, "Fast computation of the kurtogram for the detection of transient faults," *Mechanical Systems and Signal Processing*, vol. 21, no. 1, pp. 108–124, Jan. 2007.

[16] S.-R. Zhou, J.-P. Yin, and J.-M. Zhang, "Local binary pattern (LBP) and local phase quantization (LBQ) based on Gabor filter for face representation," *Neurocomputing*, vol. 116, pp. 260–264, Sep. 2013.

[17] Y. Guo, G. Zhao, and M. Pietikäinen, "Texture classification using a linear configuration model based descriptor," 2011, pp. 119.1–119.10.

Train Motion Dynamic Model Choices

Kemal Keskin[1] and Abdurrahman Karamancioglu[2]

Eskisehir Osmangazi University, Eskişehir, Turkey
kkeskin@ogu.edu.tr[1], akaraman@ogu.edu.tr[2]

Abstract

In this presentation it is intended to point out the necessity of realistic train dynamic models at different complexity levels for the research community studying energy optimal driving strategies, passenger comfort, cargo safety, and simulator development. It is stated that for the design of energy optimal driving strategies a point mass model of the train suffices. However, for passenger comfort, cargo safety, and driver training simulator development a dynamic model having lateral and vertical components in addition to the longitudinal components is needed.

1. Introduction

Train dynamics model is essential for building a train simulator. Having such simulator facilitates simulating scenarios which are impossible to exercise in reality. For instance, train behavior in steep gradients, frequent change of throttle positions, and using sudden brakes. Simulators are cost effective tools in driver training. They provide a mean for investigation of train accidents [1]. Train dynamics is is also useful in making driving strategy decisions. These decisions involve energy optimal train driving, reliable maneuvering and enhancing passenger comfort. Each of these objectives involves a certain complexity of the dynamics model. For instance, for the traction energy optimization a point mass model suffices [2], however, for the passenger comfort such a lumped model is not a solution; lateral and vertical components of the dynamic model must be considered.

In literature, there are two main train model approach that were taken into account by researchers for years. Single mass point approaches are generally based on open loop control. Various studies have been done considering single mass point approach. The common characteristic of these studies is ignoring train dynamics. Timetable scheduling and energy efficient travel between two subsequent stations are more concerned by these studies [3, 4, 5, 6, 7, 8].

The other train model approach is distributed mass model. For this approach in-train forces are important. Linear quadratic regulator (LQR) method was employed to optimize in-train forces and speed variation [9, 10]. Yang and Sun modeled the dynamics of a high speed train in cascade structure considering rolling resistance, aerodynamic drag and wind gust. They used H_2 / H_∞ controller to propose a robust cruise control system [11]. Most of studies which are employed distributed mass model are closed loop system.

2. Point Mass Model

Modeling a whole train set, that is, the locomotive and the rolling stock, as a point mass is widely used for analyzing and designing driving strategies for optimal energy purposes. This model is [2]:

$$\begin{aligned} \frac{dx}{dt} &= v \\ \frac{dv}{dt} &= \frac{F_t - F_b}{m} - R - R_g - R_c \end{aligned} \tag{1}$$

where x and v are position and speed of the train respectively. F_t is the tractive force, F_b is braking force, R is the rolling resistance of the train, R_g is the resistance caused by level change, and R_c is the railway curvature resistance, and m denotes mass of train. By this model, a train motion between successive stations which constitutes train's basic motion in a journey can be analyzed. Let us denote distance between stations be X, allowed maximum speed V and allowed travel time be T. Hence parameters are restricted with following limits:

$$0 \leq x \leq X, \quad 0 \leq v \leq V, \quad 0 \leq t \leq T \tag{2}$$

These constraints together with the dynamics (1) lead to an optimal control problem whose solution is a minimum drive strategy. It is well-known that driving strategies consist of ordering the four driving phases: (1) maximum traction, (2) cruising, (3) coasting, and (4) braking phases. For an optimal energy consumption it is possible that some of the phases may occur multiple times. This approach has been applied successfully to local railway lines [2].

3. Distributed Mass Model

In the most basic distributed model the locomotive and each wagon is considered as a point mass that interacts with preceding and succeeding wagons (or locomotive) through a coupling element. In a more developed model each vehicle's internal dynamics is taken into account. In such a case, the primary objective is to find linear and rotational motion variables as a function of time. These motion variables are described in Figure 1). In certain cases whole time graphics of these variables are not needed; their asymptotic behaviors, that is, whether they are stable or not, are sufficient.

Train's motion in the x,y, and z directions are called longitudinal, lateral, and vertical motions respectively. Rotations about these directions are called roll, pitch and yaw respectively. For reliable and comfortable travel, besides the linear motion variables, these

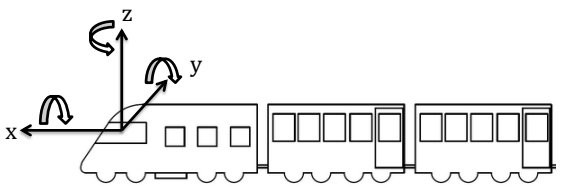

Fig. 1. Definition of train motion variables

rotational variables also interest the designer. Unfortunately, no single set of equations is good for such analysis. Regarding a specific vehicle configuration and a purpose of analysis,a suitable analysis method may be used. Below we review various motions which are encountered only in train motion analysis. The motion kinds to be discussed below are hunting motion, curving dynamics, creep dynamics, motion due to track cant angle, motion due to primary and secondary suspensions, and crosswind dynamics.

3.1. Hunting Motion

Due to conicity of the wheels, wheel cross section at contacting points are different for the left and right wheels. Therefore, at a given time interval each of the left and right wheels travel different distances. This causes vehicle to turn left or right depending on the initial state of the wheels. The turning directions alternate and display a sinusoidal motion in the y direction. This is a lateral motion and called hunting motion. Up to certain speed, called critical speed, hunting motions do not cause instability [16]. The critical speed can be increased by using linear dissipation devices [13].

The hunting motion's period depends on the distance between the wheel contacts, wheel radius, and wheel conicity. This period is calculated by Klingel's formula [16]:

$$f = \frac{v_0}{2\pi}\sqrt{\frac{\delta_0}{e_0 r_0}} \tag{3}$$

where r_0, e_0, δ_0, and v_0 are rolling radius, half the lateral distance of the wheel contact points, cone angle, and vehicle speed respectively. Because e_0 is fixed the frequency is increased by rising speed or cone angle or decreasing the wheel radius.

The frequency of the hunting motion above is obtained from a linear approximation of Klingel's equation. Since the original equation is nonlinear, the hunting motion dynamics is nonlinear.

Besides wheel-rail contact and conicity of the wheels there are other causes of the lateral dynamics. Lateral motion due to bogies and car bodies have frequencies 4-10 Hz and 1-2 Hz respectively [14, 15, 16]

3.2. Curving Dynamics

Curve track may be represented by two arcs having the same center but different radius. One of the wheels in a wheelset goes along the outer rail and the other goes along the inner rail. In the curves wheel along the outer track must travel more distance compared to the one along the inner rail. For this to happen without derailing the wheel-rail contact positions must adopt itself suitable. Of course, this can happen if the speed is below certain critical speed.

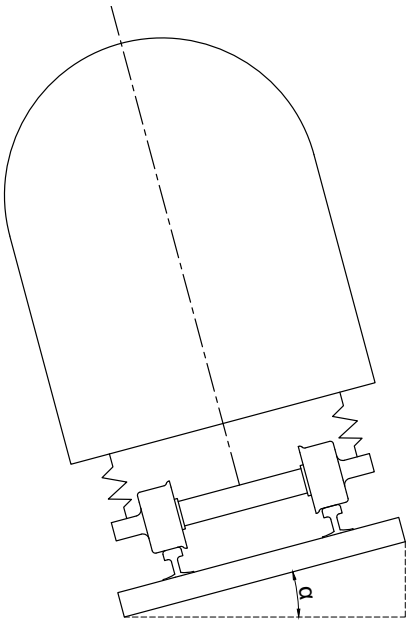

Fig. 2. An illustration of track cant angle

3.3. Creep Dynamics

Creep in rail is defined as the longitudinal and lateral movements of the rails in the track [**?**]. It results from pressing of two rigid bodies against each other and allowed to roll over each other. Creep in the rails occurs generally in the phases of start or break of the rail vehicle. A secondary reason for the creep is due to the environmental temperature changes. Following a creep, rails do not preserve their straightness anymore, they buckle in the lateral directions. Depending on the size of the buckling, rail vehicles face derailment upon exceeding certain speed limits.

Considering a rail vehicle and a track together as the system, it is hard to predict track positions where creep has occurred. However, to find out the maximum allowed buckling, simulations for certain degrees of creep may be performed.

3.4. Track Cant Angle

If one of the rail has higher altitude compared to the other then track plane makes an angle with the horizontal plane. This angle is called the cant angle. If correctly designed, cant angle support the stability at curving motions. However on a tangent track it may be viewed as a track irregularity and harm the stability.

3.5. Motions Due to Primary and Secondary Suspensions

Primary and secondary suspensions are the suspensions between wheelsets and bogies, and bogies and car bodies respectively. These suspensions cause both lateral and vertical motions. For small amplitude motions they are modeled by linear spring and damper components. Higher amplitudes may cause instability. To avoid instability bumpstops and air springs can be used [].

3.6. Crosswind Motion

As the speed of the trains increase they face larger aerodynamic forces during their travel modes. The lateral components of such forces may cause motion instability and overturn the vehicles. Constructing heavier train sets is a solution but it is not desired in terms of fuel efficiency, and in terms of track maintenance costs[17]. For an analysis of crosswind dynamics an aerodynamics model of a rail vehicle must be built. Such modelling involves computational fluid dynamics model and wind tunnel tests.

4. Conclusion

Point mass train model ignores some detail dynamics of train. Hence optimization method gets rid of complex processes relevant to dynamics, however, some constraints are ignored. This model may be appropriate for short trains and it must be considered for problems which does not need detailed dynamics of train such as energy efficient train operation, timetable and speed profile optimization problems. Distributed mass train model is closed loop control system which may control the interaction between train parts separately. This model has the advantage of more realistic results, however, it makes the optimization problem more complex. Hence this model may be suitable for long heavy haul trains or high speed trains which need to know detailed interactions between train's separate systems such as braking and traction.

5. References

[1] M.J. Arsahd, Attiq-ur-Rehman, A. I. Durrani, and H. Ahmad, "Mathematical modelling of train dynamics: A step towards pc train simulator.", *Journal of Faculty of Engineering & Technology*, vol. 20, no. 1, pp: 38-53, 2013

[2] K. Keskin and A. Karamancioglu, "Energy-Efficient Train Operation Using Nature-Inspired Algorithms," *Journal of Advanced Transportation*, vol. 2017, Article ID 6173795, 12 pages, 2017. doi:10.1155/2017/6173795

[3] P. Howlett, "An Optimal Strategy for the Control of a Train," *J. Austral. Math. Soc. Ser. B*, vol. 31, pp. 454-471, 1990.

[4] C. Jiaxin, P. Howlett, "Application of Critical Velocities to the Minimisation of Fuel Consumption in the Control of Trains," *Automatica*, vol. 28, no. 1, pp. 165-169, Jan. 1992.

[5] P. Howlett, "Optimal Strategies for the Control of a Train", *Automatica*, vol. 32, no. 4, pp. 519-532, 1996

[6] P. Howlett, "The optimal Control of a Train," *Annals of Operations Research*, vol. 98, pp. 65-87, 2000.

[7] E. Khmelnitsky, "On an Optimal Control Problem of Train Operation," *IEEE Transaction on Automatic Control*, vol. 45, no. 7, Jul. 2000.

[8] X. Yang, B. Ning, X. Li, T. Tang, "A Two-Objective Timetable Optimization Model in Subway Systems", *IEEE Transactions on Intelligent Transportation Systems*, Vol. 15, No. 5, 2014.

[9] P. Gruber, M. Bayoumi, "Suboptimal control strategies for multilocomotive powered trains", *IEEE Transactions on Automatic Control*, 27, 536-546, 1982.

[10] M. Chou, X. Xia, "Optimal cruise control of heavy-haul trains equipped with electronically controlled pneumatic brake systems", *Control Engineering Practice*, 15(5), 511-519, 2007

[11] C. Yang, Y. Sun, "Mixed H_2/H_∞ cruise controller design for high speed train", *International Journal of Control*, 74, 905-920, 2001.

[12] V. K. Garg and R. V. Dukkipati, "Dynamics of railway vehicle systems", *Academic Press*, 1984

[13] D. Baldovin, S. Baldovin, "The Influence of the Wheel Conicity and the Creep Force Coefficients to the Hunting Motion Stability of a Bogie with Independently Rotating Wheelsets", *Analele Universitatii Eftimie Murgu Resita: Fascicola I, Inginerie*, pp 11-18, XIX, 2012.

[14] E. Andersson, M. Berg and S. Stichel, "Rail Vehicle Dynamics", *Dep. of Aeronautical and Vehicle Engineering, Royal Institute of Technology (KTH)*, Stockholm, Sweden, 2007.

[15] S. Iwnicki (editor), "Handbook of Railway Vehicle Dynamics",Textbook,ISBN 978-0-8493-3321-7, *CRC Press, Taylor & Francis*, Boca Raton, USA, 2006.

[16] K. Knothe and S. Stichel, "Schienenfahrzeugdynamik", Textbook, ISBN 3-540- 43429-1,*Springer*, Berlin, Germany, 2003.

[17] D. Thomas, "On Rail Vehicle Dynamics in Unsteady Crosswind Conditions", *Studies Related to Modelling, Model Validation and Active Suspension*, Doctoral thesis, Royal Institute of Technology, 2013

Hough Cross-Section through Sinusoid of Vanishing Point for Image based Obstacle Detection on Railways using Drones

Seçkin Uluskan[1]

[1]Anadolu University, Vocational School of Transportation,
Rail Systems Electrical and Electronics Technologies, Turkey
seckinuluskan@anadolu.edu.tr

Abstract

This study proposes an image based obstacle detection system by means of drones. Drones have a great potential to be used in railway obstacle detection by periodically and locally inspecting the railways. In this study, a Hough transform based obstacle detection system for railways is introduced. This study suggests to monitor the cross-section of the Hough transform along the sinusoid of the vanishing point of the rails to detect any obstacle. By this way, two dimensional information of the Hough transform is reduced to a one-dimensional information where all Hough peaks can be simultaneously observed. This will yield a less complex algorithm for mini drones. To test the performance of the proposed solution, railway animation videos are created to perfectly simulate real scenarios in which drones are recording videos over the railway. It is shown that the proposed solution is quite successful in detecting obstacles along the railways.

1. Introduction

The railways provide people with a safe and convenient way of transportation, therefore the popularity and the importance of rail transportation increase all around the world. This situation accelerates the railway researches which aim to develop advanced railway technologies. Railway safety is one of the major issue of the railway research. The level crossing accidents (an important subject in railway safety) are defined as the accidents in which the train crashes to other vehicles, pedestrians or other objects which are temporarily present at or near the railway [1]. The level crossing accidents constitutes a great portion (26 percent) of all the railway accidents [1].

In order to avoid level crossing accidents or to prevent trains to crash any object on the rail during their travels, some automated obstacle detection systems were previously proposed. Two different strategies can be applied to detect obstacles on the railway. First strategy is to install stable sensors such as inductive loops, magnetometers, pneumatic tubes, piezoelectric cables etc. along the railways. This solution engages inexpensive materials yet their installation and maintenance result in significant costs [2]. Second strategy is to install sensors directly on the train to detect obstacle in front of it. These equipments can be thermal cameras, lasers, radars, ultrasonic sensors and finally video cameras [2]. These sensors are typically more expensive to acquire, however this strategy requires only very a few number of these sensors because they are only installed on the train. At this point, drones can provide a combined solution where these expensive sensors are carried along the railway. Drones which carry these sensors can periodically and locally inspect the railways. This study proposes an image based obstacle detection system by means of drones as shown in Fig.1.

Previously, some image based obstacle detection systems are proposed specifically for railways. In one of the earlier study on this subject, several image processing methods are introduced to detect obstacle on the railway for automated trains [3]. These methods are track gaps, edge elements, gray value variance and correlation along the track etc. In another study [4], image sensors are installed in front of a train to obtain a real-time obstacle detection system. Again, several methods are introduced such rail continuity and rail surface brightness etc. Stereo camera systems are also used to obtain a 3D-vision based obstacle detection for automated trains [5]. Finally, Hough transform is used as the major tool in obstacle detection in railways [6].

Drones recently became so popular that they are used in a wide range of applications. Consequently, railway technologies are also engaging drones to meet a lot of different needs. Drones are mostly being adopted to monitor railway infrastructure and detect or early alert any possible defect along the railway [7].

This study introduces a Hough transform based obstacle detection systems for railways. This study suggests to monitor the cross-section of the Hough transform along the sinusoid of the vanishing point of the rails to detect any obstacle on the railway. By this way, two dimensional information of the Hough transform will be reduced to a one-dimensional information where all Hough peaks can be simultaneously observed. This will yield a less complex algorithm for mini drones. To test the performance of the proposed solution, railway animation videos are created to perfectly simulate the real scenarios in which drones are recording videos over the railway. It is shown that the proposed solution is quite successful in detecting obstacles along the railways.

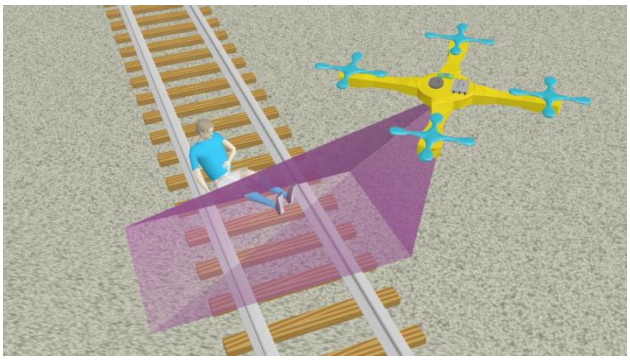

Fig. 1. Obstacle Detection system for railroads using Drones and image processing

2. Method

2.1. Hough Transform of The Railway

To detect obstacles on railways using images recorded by drones, this study proposes a Hough transform based solution. Before applying Hough transform, the images are subjected to edge detection as shown in Fig.1.a and 1.b. In Fig.1.a, an aerial image of the railway is shown, and Fig.1.b shows its new version after edge detection. Any line on the edge detected image can be represented by its polar coordinates [8],

$$\cos(\theta)\,.\,x + \sin(\theta)\,.\,y = \rho \qquad (1)$$

where ρ is the distance of the line to the origin and θ is the angular coordinate as shown in Fig.1.a. The main idea of the Hough transform is that any point in the edge detected image can be represented by all the lines which pass through this point:

$$\rho(\theta) = \cos(\theta)\,.\,x_a + \sin(\theta)\,.\,y_a \qquad (2)$$

where $(x_a\,, y_a)$ is the location of the point within the edge detected image. The function $\rho(\theta)$ which relates ρ to θ, in fact, is a sinusoidal curve [9], therefore, equation (2) can be rewritten as the following:

$$\rho(\theta) = d.\cos(\theta - \alpha) \qquad (3)$$

where d and α are the parameters which are defined as:

$$\alpha = \cos^{-1}\left(\frac{x_a}{\sqrt{{x_a}^2 + {y_a}^2}}\right) \text{ and } d = \sqrt{{x_a}^2 + {y_a}^2} \qquad (4)$$

Finally, Hough transform is the collection of all the sinusoids of the points within an edge detected image. The Hough transform of Fig.1.b can be seen in Fig.1.c. The sinusoids of the points which belong to a specific line in the edge detected image will overlap each other around the polar parameters of this specific line. Therefore, a line in the edge detected image will create a peak (called Hough peak) within the Hough transform of the image.

The Hough peaks which are associated with the railway are pointed by a rectangle in Fig.1.c. In order to better observe these Hough peaks, we can zoom into this rectangle. Therefore, Fig.1.d shows this region more closely where Hough peaks are more visible. As seen, several Hough peaks exists in Fig.1.d. The Hough peaks of the railway are scattered such that they constitute two distinct groups. The Hough peaks which occur around $25 < \theta < 35$ are associated to the left part and the Hough peaks which occur around $42 < \theta < 47$ are associated to the right part of the railway.

The idea of this paper is that any obstacle on the railway will reduce the strengths of these Hough peaks. An obstacle on the railway will create a disturbance on the aerial image, so they can mask either the left or right part of the railway. Consequently, the Hough peaks can lose their strengths or even disappear. Therefore, we need to monitor these Hough peaks to detect the obstacles on the railway. This paper finds a smart way to monitor all these Hough peaks simultaneously by means of the vanishing point. Two dimensional information of the Hough transform will be reduced to a one-dimensional information where all Hough peaks can be observed.

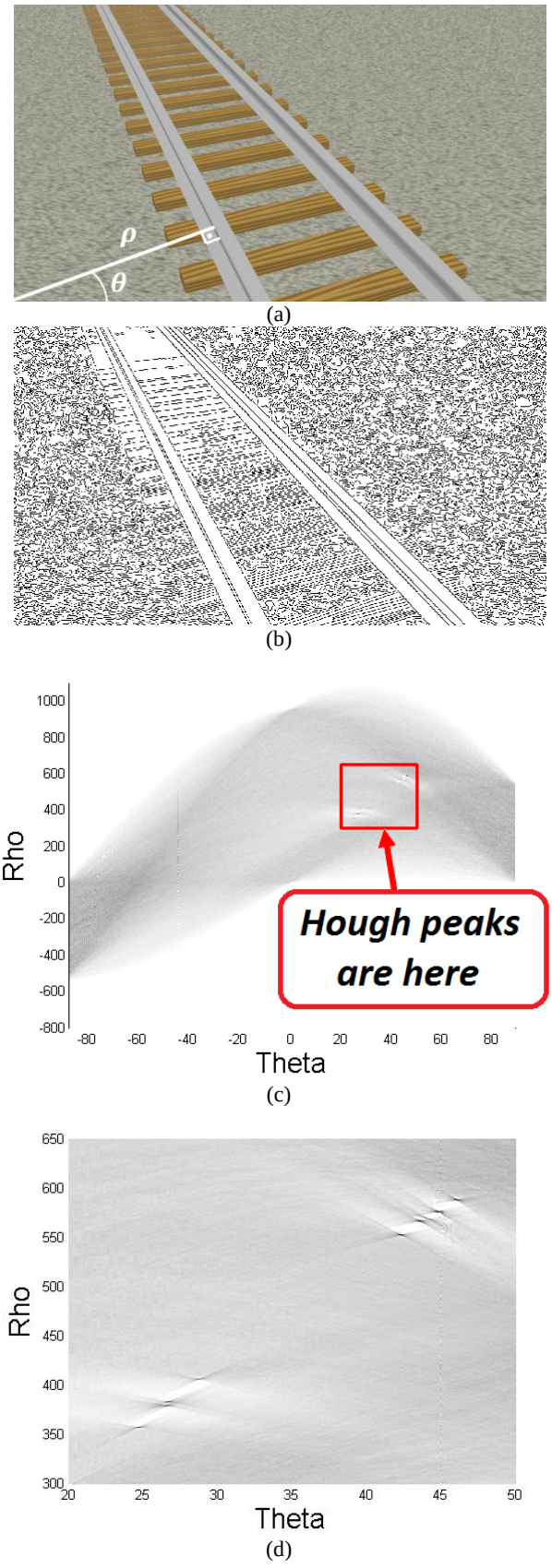

Fig. 1. (a) Original railway image, (b) edge detection, (c) Hough transform of the railway image, (d) Hough peaks

2.1. Hough Cross-Section through the Sinusoid of the Vanishing Point of the Rails

In a two dimensional image of a three dimensional space, parallel structures or lines in this three dimensional space appear to intersect at a specific point. This specific point is called as the vanishing point of these lines [10]. Therefore, all the lines associated with the left and right parts of the railway must pass through a single vanishing point because they are all parallel to each other. Fig.2.a shows the vanishing point of the rails for the railway image shown in Fig.1.a. The vanishing point can stay within or out of the borders of the image as shown in Fig.2.a. This study will utilize the sinusoid of the vanishing point of the rails to simultaneously monitor all the Hough peaks associated with the railway.

The vanishing points can be calculated by means of Hough transform. First, the best fitting sinusoid (Fig.2.b) which passes through the Hough peaks must be estimated [11]. This study utilizes nonlinear least squares estimation to accurately find the parameters of the sinusoid of the vanishing point,

$$(\hat{d}, \hat{\alpha}) = \underset{(d,\alpha)}{\operatorname{argmin}} \sum_{i=1}^{N} (\rho_i - d.\cos(\theta_i - \alpha))^2 \qquad (5)$$

where (ρ_i, θ_i) is the location of the ith Hough peak and N is the total number of all the Hough peaks. When this best fitting sinusoid is converted back to its corresponding point in the original image, then the vanishing point is obtained,

$$x_{vanish} = \hat{d}\,.\cos(\hat{\alpha}) \text{ and } y_{vanish} = \hat{d}\,.\sin(\hat{\alpha}) \qquad (6)$$

In this study, the drone which flies over the railway will be inspecting if there is any change in the levels of the Hough peaks associated with the railway. Therefore, if the drone investigates the complete 2D Hough transform for each image, it will be an inefficient algorithm, because most parts of Hough transform is irrelevant to the task. This paper finds a smart way to reduce the two dimensional information of the Hough transform to a one-dimensional information. It is known that all Hough peaks are located along the sinusoid of the vanishing point. If the Hough transform is considered as a 3D surface, then a cross section of this 3D surface can be obtained along the sinusoid of the vanishing point as shown in Fig.2.c. As seen in Fig.2.c, this cross section includes all the information regarding to the Hough peaks. Finally, monitoring this cross section will be an convenient way to detect obstacles on the railways.

3. Obstacle Detection System for Railways

In this section, the obstacle detection system that is created will be presented by means of railway animation videos to perfectly simulate the real scenarios in which drones are recording videos over the railway.

3.1. Railway Videos for Simulation

Before testing the obstacle detection system which is based on Hough transform, a couple of animation videos are created to simulate the real videos which are recorded by drones moving over the railway. It is assumed that the drone is flying along the railway and recording videos as depicted in Fig.1.

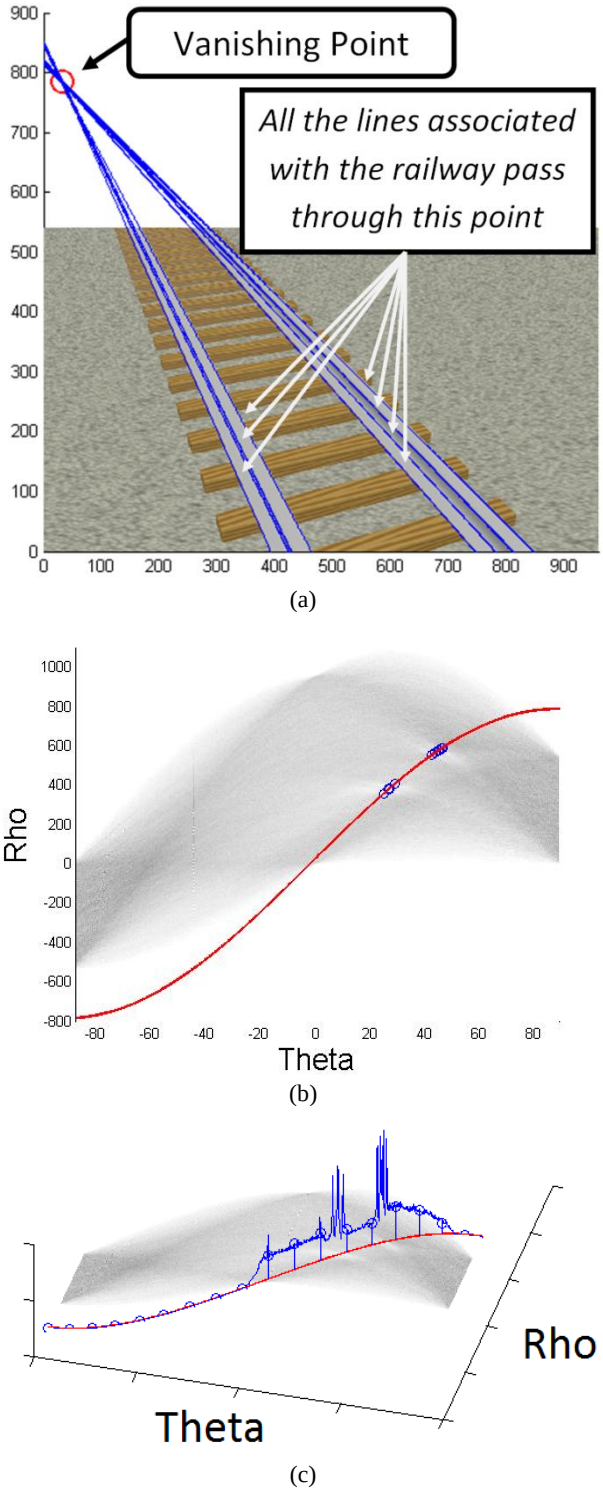

(a)

(b)

(c)

Fig. 2. (a) Illustration of the vanishing point on the railway image, (b) The sinusoid of the vanishing point which is estimated by nonlinear least squares, (c) 3D view of the cross-section of the Hough transform through the sinusoid of vanishing point

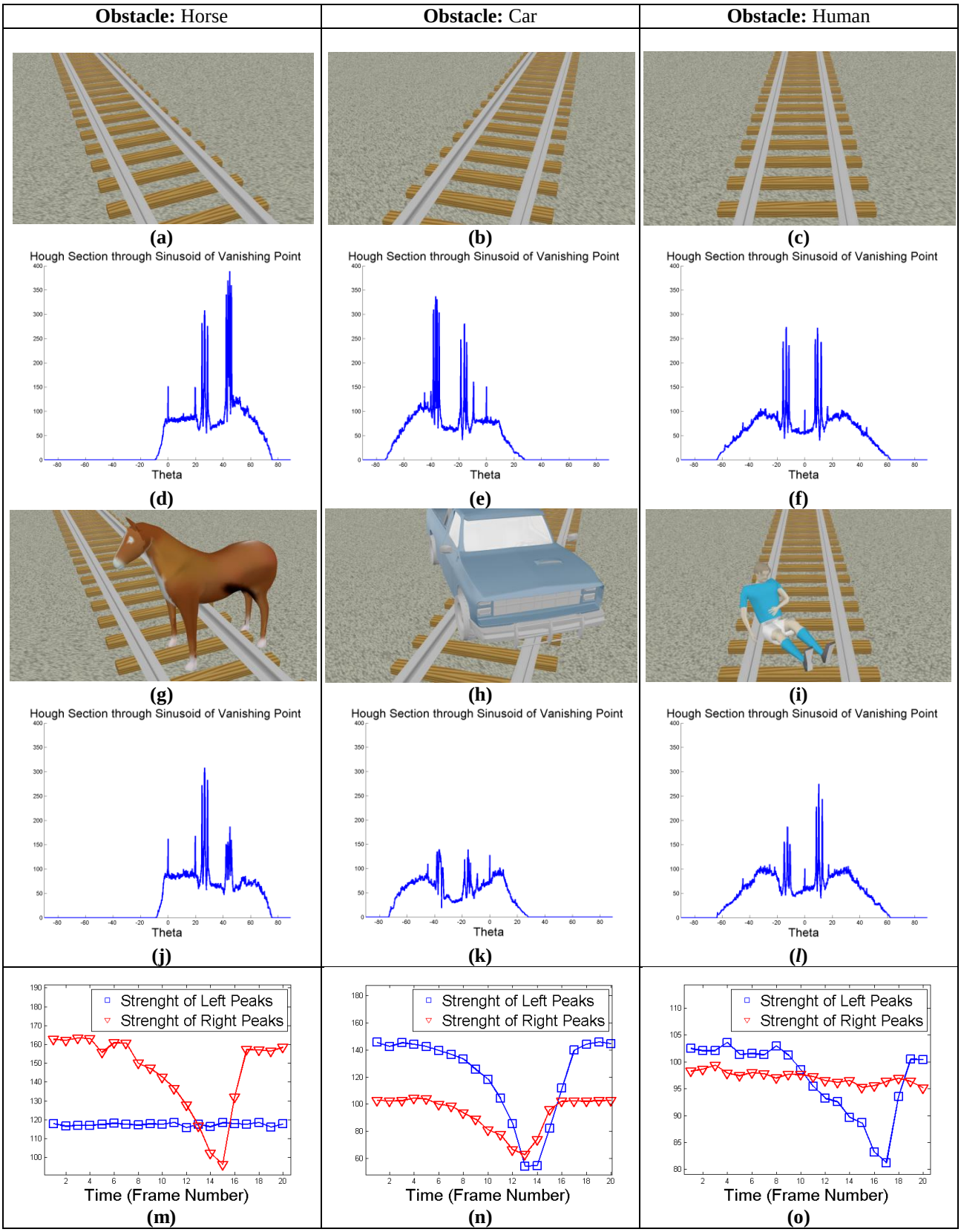

Fig. 3. Three different simulation results for three different types of obstacles i.e. Horse, Car and Human. The obstacles on the railway can be detected by means of Hough Peaks Tracking Timelines.

In each video, the drone starts to fly 3 meters over the empty railway. After a while it encounters an obstacle which stays on the railway. The frame rate of the videos are set to be high enough, so the obstacles enter gradually into the scene. Finally, the drone leaves the obstacle behind and continues to record the video of the empty railway. Fig.3 shows three different videos with three different obstacles namely a horse, a car and a human. These videos involve not only different types of obstacles, but also different points of view with respect to railway.

4.2. Obstacle Detection for Railway Videos

In order to detect if there is any obstacle on the railway, the drone takes the Hough transform of the first frame that it records. For this first frame, it determines the location of the Hough peaks, and it estimates the parameters of the sinusoid of the vanishing point as shown in Eq. 5. Then, it obtains the Hough cross-section along the sinusoid of the vanishing point as depicted in Fig.2.c. The drone preserves its perspective along its flight over the railway, so it has a stationary point of view with respect to the railway during its flight. This stationary point of view allows the drone to skip the step where the parameters of the sinusoid of the vanishing point is calculated. Consequently, after taking the Hough transform of the image, it can directly extract the Hough cross section along the sinusoid of the vanishing point for the succeeding frames. Whenever drone changes its point of view, it must recalculate the parameters of the sinusoid of the vanishing point.

The Hough cross section of a frame includes a couple of local maxima which can be divided into two groups corresponding to the right and the left part of the railway. In Fig.3.a, the right part of railway appears to be longer than left part within the image, so this results in higher Hough peaks in the right group as seen in Fig.3.d. As the obstacle enters into the scene as seen in Fig.3.g, the right sided Hough peaks decrease while left sided peaks stay unchanged as shown in Fig.3.j. This is because the obstacle only masks the right side of the railway.

In Fig.3.b, because of a different point of view, the left part of railway appears to be longer than right part within the image, so this results in higher Hough peaks in left group as seen in Fig.3.e. As the obstacle enters into the scene as seen in Fig.3.h, both the right and left sided Hough peaks decrease as shown in Fig.3.k. Because the obstacle is a large one (i.e. a car), it masks both side of the railway. In Fig.3.c, because the drone views the rail at the middle, both sides of the railway appear to be equal each other within the image, so this results equal levels of Hough peaks in left and right groups as seen in Fig.3.f. As the obstacle enters into the scene as seen in Fig.3.i, the left sided Hough peaks decrease while right sided peaks stay unchanged as shown in Fig.3.*l*. This is because the obstacle only masks the left side of the railway.

If the averages of Hough cross sections around the right and left sided peaks are taken separately for each frame, then two different plots can be obtained for a single video. As seen in Fig.3.m, the plot of right part experiences a decrease which is successively followed by an increase to the previous level, whereas the plot of left part remains unchanged during the video. This alerts that there exists an obstacle on the right part of railway. Similarly, as seen in Fig.3.n, both the right and left parts' plots experience a decrease followed by an increase simultaneously. This alerts that there exists an obstacle on both the side of railway. Finally, in Fig.3.o, the left part's plot experiences a decrease because there is a human on the left part of the railway.

As mentioned above, because of the high level frame rate, the obstacle enters into scene gradually. In other words, initially the legs of the horse enters into scene, then its body and its head appear successively at the top of image. This results in a gentle slope while the plots decrease. However, they experience a sharp increase after reaching minimum. This situation occurs because while the obstacle gradually appears at the top image, it quickly vanishes at the bottom image when the drone leaves the obstacle behind. Any fluctuation on these tracks can be conveniently tracked to detect any possible obstacle. Of course, only a decrease followed by an increase means there exists an obstacle on the railway. A permanent decrease in both of the plots most probably means that the drone has lost its point of view, so it must recalculate the vanishing point.

4. Conclusions

Drones have a great potential to be used in railway obstacle detection by periodically and locally inspecting the railways. This study proposes an image based obstacle detection system by means of drones. A convenient Hough transform based solution is proposed for real-time applications to be handled by mini drones. Experiments with animation videos simulating real scenarios illustrated that the proposed solution is quite successful in detecting obstacles on the railways.

7. References

[1] European Union Agency for Railways, *Railway Safety Performance in the European Union*, (2016), Available: https://erail.era.europa.eu/documents/SPR.pdf

[2] Punekar, N. S., & Raut, A. A., "Improving Railway Safety with Obstacle Detection and Tracking System using GPS-GSM Model", *International Journal of Science & Engineering Research*, vol. 4, no.8, pp. 288-292, 2013.

[3] Ruder, M., Mohler, N., & Ahmed, F. (2003). "An obstacle detection system for automated trains", In IEEE Intelligent Vehicles Symposium, pp. 180-185, 2003

[4] Ukai, M., Nassu, B., T., Nagamine, N., Watanabe, M., Inaba, T., "Obstacle Detection on Railway Track by Fusing Radar and Image Sensor", in *World congress on railway research*. 2008.

[5] Weichselbaum, J., Zinner, C., Gebauer, O., & Pree, W., "Accurate 3D-vision-based obstacle detection for an autonomous train", *Computers in Industry*, vol. 64, no. 9, pp. 1209-1220, 2013.

[6] Rodriguez, L. F., Uribe, J. A., Bonilla, J. V., "Obstacle detection over rails using hough transform". Image, Signal Processing, Artificial Vision Sympos., pp. 317-322, 2012.

[7] Flammini, F., Pragliola, C., & Smarra, G. "Railway infrastructure monitoring by drones". in International Conference on ESARS-ITEC , November, 2016.

[8] Illingworth, J., & Kittler, J., "A survey of the Hough transform", *Computer vision, graphics, and image processing*, vol. 44, no.1, pp. 87-116, 1988

[9] Saleh, B. "Introduction to subsurface imaging". Cambridge University Press. New York, 2011.

[10] Chen, X., Jia, R., Ren, H., & Zhang, Y., "A new vanishing point detection algorithm based on Hough transform", *Third International Joint Conference on Computational Science and Optimization (CSO)*, 2010, pp. 440-443.

[11] Papusha, I., & Ho, M. (2010), *Hough Transform for Directional Orientation*, Online resource, Available: http://www.ivanpapusha.com/pdf/hough_directional.pdf

The Availability Evaluation of Fallback Signaling for CBTC System

Vedat SÖYLEMEZ[1], Mehmet Turan SÖYLEMEZ[2]

[1]Istanbul Metropolitan Municipality, Istanbul, Turkey
vedat.soylemez@ibb.gov.tr
[2]Control Engineering Department, Istanbul Technical University, Istanbul, Turkey
soylemezm@itu.edu.tr

Abstract

Communication based train control (CBTC) systems are the state-of-the-art train control systems that have been applied throughout metro lines. When a failure occurs in a CBTC system, other operational scenarios are used to continue the railway service, e.g. degraded mode, reduced speed. Signaling system failures have great effect on availability and safety of such systems. To reduce human interventions and minimize operational disruptions, fallback signaling can be designed with a CBTC system. In this paper, one of the RAMS parameters, availability is examined to evaluate the necessity of fallback system in the event of a subsystem failure.

1. Introduction

Over the last decade, there has been a huge focus on rail transport due to reasons including environmental awareness, increased urbanization, population growth, and it being a more energy efficient, safer, higher capacity and higher speed transport alternative [1]. The railway system consists of many internal disciplines and the signaling system is an essential part of the railway. Its principal task to ensure that trains run safely.

From the point of signaling type, there are two main approaches: fixed block and moving block. In the fixed block signaling the track is divided into small sections (blocks) and block lengths are determined by track layout, train performance and operational requirements. Only one train can occupy a block at any time. In the moving block, on the other hand, there are no physical blocks and each train is considered as a block. Distance between two consecutive trains based on the speed can be reduced to a safety margin. CBTC systems employ the moving block concept. Compared with traditional fixed block systems, moving block systems are able to offer high availability, reliability and safety in operations due to distinctly different system configuration and components used in the approach [2]. With moving block signaling, minimum headways as low as 60 seconds are achievable. [3]

Signaling system is one of the most costly parts of the railway system. Also due to employment in traffic intensive environments, CBTC systems demand high availability. RAMS (Reliability, Availability, Maintenance and Safety) of the railway system describes the confidence with which the system can guarantee the achievement of this goal. RAMS requirements related with railway network are described in EN 50126 standard. System availability is the result of reliability and maintainability being implemented as basic requirements in the design of the signaling system.

CBTC systems employ redundant computer-based equipment to provide very high levels of reliability and availability [4]. When a failure occurs in the railway signaling system, other operational scenarios are used to continue railway service, e.g. degraded mode, reduced speed. For some reasons such as failure of equipment, mixed operation, upgrade of signaling system, control of maintenance vehicles, a secondary train detection system or secondary train protection system can be designed with CBTC system as fallback.

In this paper, the need for a fallback signaling system with CBTC systems is examined in terms of availability.

2. Communication Based Train Control System

CBTC systems are the state-of-the-art train control systems that has been applied widely to metro projects. CBTC is a continuous automatic train control system utilizing high-resolution train location determination, independent of track circuits; continuous, high capacity, bidirectional train-to-wayside data communications; and train borne and wayside processors capable of implementing vital functions [5].

CBTC does not only provide for the highest levels of train protection but also it enables the maximum return on the investment into rail transit infrastructure through optimized line capacity and passenger throughput and reduced operating/maintenance costs [6]. CBTC system allows trains to operate at short headways and use the maximum speed allowed on the line.

In signaling systems, the train position is used for many important decisions, such as: train separation, end of track, train routing, train protection, level crossing, coupling, rollback, over speed, door control and station stopping. In today's CBTC systems, train detection is determined by the train itself. Each train calculates its own speed, direction, location and integrity by using devices such as tachometers, accelerometers, global positioning system (GPS), loop transpositions, Doppler radar, balises and digital track maps. To increase location accuracy, balises are mounted between rails. Balises give the fixed reference location information. As the train passes over the balises, it takes the reference location information via balises antenna and compares it to the measured value. Between stations, positioning can be calculated with the resolution of 0.25 meter to 10 meter range [5].

In traditional signaling system track is divided into blocks and safe train separation changes based on the block length. In CBTC systems, the distance between two trains is instantaneously calculated the according to the position of the front train and continuously updated. Each train's position is continuously reported to the wayside controller (ZC) over the

data communication system. CBTC employ two techniques for safe train separation: virtual block and moving block. Virtual blocks are a software equivalents of physical track circuits separating trains in a fixed block train control system [7]. In moving block signaling each train is considered as a block and system continuously calculate the protected section around each moving train. Additionally, the interlocking conditions that are pre-requisite for safe train movement are continuously monitored by a wayside controller.

CBTC system can be considered as a closed loop control system because each train communicates continuously and bi-directionally with the wayside controllers. Since the position of each train is known, the distance between the two trains may be reduced to the safety margin. Based on the information received from all trains currently on the track, as well as a train's braking capability, the zone controller calculates the maximum speed and distance the train is permitted to travel, collectively known as "limit of movement authority" (LMA), and sends it to the train [1]. A movement authority includes a physical track point or limit, which the train's front end cannot proceed beyond [8]. A "brick wall" assumption is used to calculate the most restrictive braking distance considering that the preceding train is stopped at the LMA point, despite the actual speed of the train [9]. The zone controller knows all the physical and geographical features of the zone in order to control the trains in its area.

CBTC systems can implement the interlocking functions in two ways: the first is by having separate devices, i.e., one device for the interlocking function (interlocking controller) and another for CBTC safe train separation (zone controller) [7]. Interlocking is responsible for route setting for trains. Interlocking also controls the trackside equipment such as point machines, platform screen doors. CBTC shall determine the limit of safe route ahead of the train from the most restrictive inputs from occupation track ahead, end of track, opposing traffic direction ahead and interlocking status [10].

Onboard control unit creates the speed-distance profile based on the topological data, gradient, static line speed, location of the balises, switches, stopping points, overlap area etc. Onboard control system can be considered as a closed loop speed control system. According to information received from subsystems (balises antenna, traction/brake, odometer etc.), onboard subsystem supervises the movement authority and initiates an emergency brake in case of violation of limits.

3. Fallback Signaling for CBTC System

The fallback train control operation is based on the fixed block train separation principle. In fig. 1, a sample fallback signaling layout is given. The safe train separation and train protection in fallback level relies on the fixed blocks that are interlocking routes and on the signal aspect controlled by the interlocking. The routes are generally given by the path between two signals. The train separation is ensured by the interlocking which is based on a conventional route process. Fallback system can be built using signals and track circuits or axle counters. Track circuits are used to determine the location of trains and signals give the information about clear ahead of signal to the driver. A train operates only in one control level at the same time. Fallback system can be used for degraded operation (e.g. if the ZC or DCS (Data Communication System) failure), mixed operation, upgrade of signaling level and safety considerations. Onboard control unit is able to detect the CBTC or fallback mode. In case of failure of communication system (either onboard or wayside) or the train borne positioning system, or zone controller, onboard subsystem provides a transition from CBTC to degraded mode operation. The headway supported by a fallback signaling system depends on the length of secondary train detection sections.

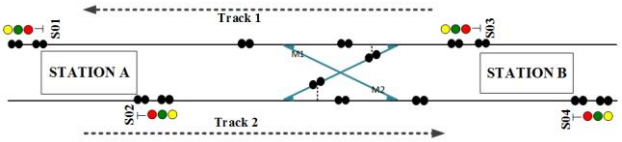

Fig. 1. Track layout for fallback signaling.

4. Availability Analysis

Safety-critical system is a system whose a failure has the direct potential to cause harm, injury, loss of life or damage to the environment. Many signaling systems nowadays are designed on the basis of electrical, electronic, or programmable electronic (E/E/PE) technology. Signaling systems have a complex structure in which a large number of electronic equipment interact. Defects that may occur in these systems may cause loss of life and property. Reliability, Availability, Maintainability and Safety (RAMS) techniques have been applied in order to reduce such risks. RAMS process begins with determining the parameters that the system must provide. The EN 50126 standard describes the requirements for the RAMS of the railway signaling system and how this process will be carried out. According to EN 50126, availability ability of a system is defined as being in a state to perform a required function: under given conditions, at a given instant of time the ability of a system to perform a required function: under given conditions, over a given time interval [11].

Since a system is considered reliable as long as it does not fail, there is a very close relationship between reliability and failure. Failure can occur randomly at any time. The frequency at which these failures occur is the rate of failure. The failure rate is denoted by λ in the reliability and unit is generally given as failure per hour or FIT. λ is determined on the base of statistical data with the formula given in equation 1. Here, N_f is the number of failed units during the time period t, and Ns is the quantity of failure free systems in a given time interval (0, t).

$$\lambda = \frac{N_f}{N_s \times t} \tag{1}$$

Systems can fail at any time interval, so a continuous time modeling will be appropriate. After the failure data are collected, a histogram corresponding to the failure data is generated and then probability density function is obtained. Probability density function and reliability are denoted respectively by f(t) and R(t). The relationship between them is given in equation 2 [12].

$$f(t) = -\frac{dR(t)}{dt} \tag{2}$$

Availability will vary depending on both the reliability and system maintenance strategy. There are two main ways of measuring availability. The first method of measuring

availability is through equation 3 [12]. Here, MTBF is the average time period of a failure/repair cycle. It includes time to failure, any time required to detect the failure, and actual repair time. MTTR is the average time required to move from unsuccessful operation to successful operation. The parameter related to MTTR is the repair rate, μ.

$$A = \frac{MTBF}{MTBF + MTTR} \tag{3}$$

The second method would be from an operational perspective and is measured using equation 4 [13]. Here, MTBM is the mean time between maintenance and MDT is mean down time. MTBM depends upon both MTBF and preventative maintenance. MDT depends on a number of factors: failure detection time, mobilization and repair time, time for test and accept repair, time to put back into service etc.

$$A = \frac{MTBM}{MTBM + MDT} \tag{4}$$

4.1. Markov Theory

Markov modelling is a very flexible technique for reliability and availability analysis of complex systems. It is widely used to quantify system dependability in areas such as performance, availability, reliability and safety [14]. In a Markov model, the system is modeled as a state machine with each state representing some characteristic of interest for the system [12]. The system begins with an initial state and transitions from one state to another after a time that is exponentially distributed. Since the exponential distribution is memoryless, the next state of the system depends only on the present state and does not depend on when the last transition occurred. If a state in the Markov Chain has no transitions leaving it, then that state is called an absorbing state.

Markov models are also classified into discrete time Markov chains (DTMC) or continuous time Markov chains (CTMC), depending on when the state changes. A Continuous-Time Markov Chain (CTMC) is one in which changes to the system can happen at any time along a continuous interval. i and j are elements of the sample space, the transition probabilities are calculated according to (5) [12]. p_{ij} is the probability of transition to j when the system is in state i.

$$p_{ij}(t) = P[X(t) = j \,|\, X(0) = i] \tag{5}$$

Markov chain has a transition matrix that provides the probabilities of changing from one state to another state. In equation (6), the general form of transition matrix is given [12].

$$TM = \begin{pmatrix} p_{11} & p_{12} & \cdots & p_{1n} \\ p_{21} & p_{22} & \cdots & p_{2n} \\ \vdots & \vdots & \ddots & \vdots \\ p_{n1} & p_{n2} & \cdots & p_{nn} \end{pmatrix} \tag{6}$$

State probabilities are obtained based on the state-space equations. The complete solution (probabilities dynamically change over time) or steady-state solution (asymptotic state probabilities) can be solved by (7) [12].

$$\begin{pmatrix} \frac{dP_1(t)}{dt} \\ \frac{dP_2(t)}{dt} \\ \vdots \\ \frac{dP_n(t)}{dt} \end{pmatrix} = \begin{pmatrix} p_{11} & p_{12} & \cdots & p_{1n} \\ p_{21} & p_{22} & \cdots & p_{2n} \\ \vdots & \vdots & \ddots & \vdots \\ p_{n1} & p_{n2} & \cdots & p_{nn} \end{pmatrix} \begin{pmatrix} P_1(t) \\ P_2(t) \\ \vdots \\ P_n(t) \end{pmatrix} \tag{7}$$

4.2. CBTC Markov Model

CBTC system consists of many subsystem and components. From a system point of view, we can divide the CBTC system into 6 subsystems: ATS (Automatic Train Supervision), DCS, ZC, IXL (Interlocking), Switch, and OBCU (Onboard Control Unit). If all subsystems correctly are working then the system is available and any failure in these subsystems directly lead to a failure. In Fig. 2 CBTC system is depicted as a block diagram. The onboard control system is considered as a whole: odometer, balises transmission module, controller, onboard communication system, traction/brake subsystem and HMI. The switch block includes all the switches on the line and the same applies to other equipment. The failure probability distribution of each subsystem will be assumed exponential. Hence, the failure rates and restore rates are fixed.

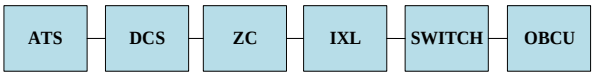

Fig. 2 Block diagram of CBTC system.

System's reliability in serial structures are calculated by multiplying the reliability values of each subsystem. Random failure rates about the subsystems are given in table 3. In the following analysis, systematic faults will not be considered.

Table 1. Failure and repair rates of subsystems.

Subsystem	λ(1/h)	μ(1/h)
DCS	10^{-6}	4/3
ZC	3×10^{-6}	4/3
Switch	10^{-6}	2/3
IXL	3.3×10^{-6}	4/3
ATS	10^{-6}	4/3
OBCU	8×10^{-6}	3/2

The state-space diagram for the Markov process visualized in Fig. 3 shows the different states of the system and the possible transitions between them. Initial state is S0 state. S1, S2, S3, S4, S5 and S6 show the failure states. From equation (8) and (9) state probabilities are obtained.

$$\frac{dP_0(t)}{dt} = -\sum_{i=1}^{6} \lambda_i \times P_0(t) + \sum_{i=1}^{6} \mu_i \times P_i(t) \tag{8}$$

$$\frac{dP_i(t)}{dt} = \lambda_i \times P_0(t) - \mu_i \times P_i(t) \tag{9}$$

Using Laplace transform, state probabilities are calculated from (10).

$$P_i(s) = \frac{\lambda_i}{s + \mu_i} \times P_0(s) \qquad i \neq 0 \tag{10}$$

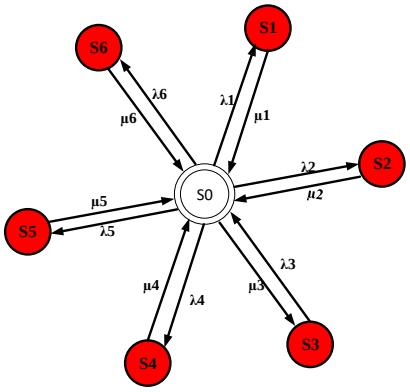

Fig. 3. CBTC Markov model.

If the system is in state S0, then the system is available to operation. As a result, the steady state availability is calculated from P0 or multiplication of availability of all subsystems. The availability and reliability of a 1oo1 system are calculated by following formulas.

$$R_{CBTC}(t) = e^{-\lambda_{CBTC} \times t} \tag{11}$$

$$A_k(t) = \frac{\mu_k}{\lambda_k + \mu_k} + \frac{\lambda_k}{\lambda_k + \mu_k} e^{-(\lambda_k + \mu_k)t} \tag{12}$$

$$A_{CBTC}(t) = \prod_{k=1}^{6} A_k(t) \tag{13}$$

The steady state availability of the CBTC system of Istanbul M2 Metro line is calculated as 0.9998356 by the help of MATLAB and using the data in table 1.

4.3. Markov Model of Fallback Signaling for CBTC

To build the Markov model of CBTC system with Fallback, we consider the system as a primary and backup system. The voter selects the operation mode (CBTC or degraded) between the primary and backup based on the status of subsystems. They are interconnected. IXL, Switch, ATS and OBCU are common elements used by both CBTC and the backup system. This is shown in Fig. 4. Markov model becomes large and unwieldy as the system size increases and thus it is difficult to construct and solve Markov models for large systems [14]. To overcome state explosion, common elements are considered as a subsystem in the Markov model. Fig. 5 shows the Markov model of fallback signaling for CBTC system. This model assumes that the voter is perfect (%100 reliable and available).

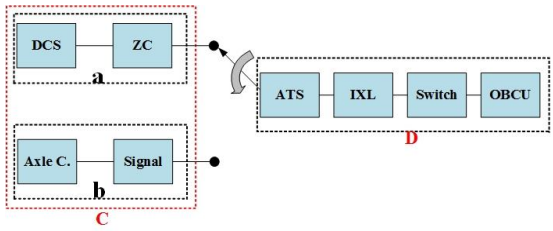

Fig. 4. Block diagram of CBTC with fallback system

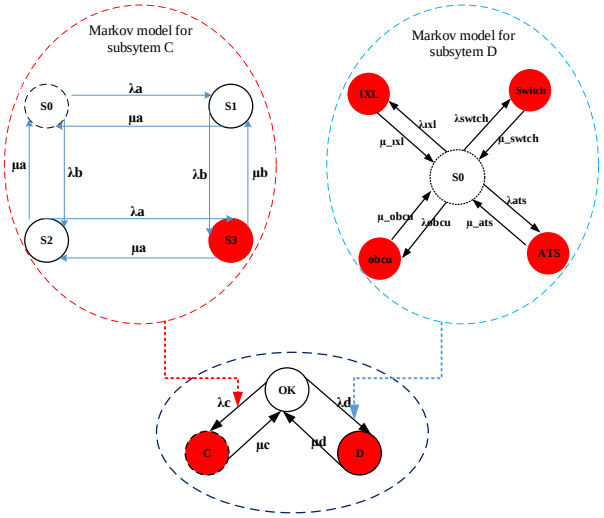

Fig. 5. Markov models of C and D subsystems.

The subsystem C consists of elements a and b. Using (14) and (15), failure rates and repair rates of elements a and b can be calculated.

$$\frac{1}{\lambda_a} = \frac{1}{\lambda_{DCS} + \lambda_{ZC}}$$
$$\frac{1}{\mu_a} = \frac{\lambda_{DCS} \times \mu_{DCS} + \lambda_{ZC} \times \mu_{ZC}}{\lambda_{DCS} + \lambda_{ZC}} \tag{14}$$

$$\frac{1}{\lambda_b} = \frac{1}{\lambda_{axle} + \lambda_{signal}}$$
$$\frac{1}{\mu_b} = \frac{\lambda_{axle} \times \mu_{axle} + \lambda_{signal} \times \mu_{signal}}{\lambda_{axle} + \lambda_{signal}} \tag{15}$$

To solve the state probabilities of subsystem C, Laplace transform can be used as follows:

$$\begin{aligned} sP_0(s) + 1 &= -(\lambda_a + \lambda_b)P_0(s) + P_1(s)\mu_a + P_2(s)\mu_b \\ sP_1(s) &= \lambda_a P_0(s) - (\lambda_b - \mu_a)P_1(s) + \mu_b P_3(s) \\ sP_2(s) &= \lambda_b P_0(s) - (\lambda_a - \mu_b)P_2(s) + \mu_a P_3(s) \\ sP_3(s) &= \lambda_b P_0(s) + \lambda_a P_2(s) - (\mu_b + \mu_a)P_3(s) \end{aligned} \tag{16}$$

According to the Markov model, S0, S1 and S2 are available states. Availability of subsystem C can be obtained by summing the probabilities of these states. Using Matlab, the steady-state availability is obtained as.

$$A_C(t) = \lim_{t \to \infty} A_C(t) = \frac{\lambda_a \lambda_b}{(\lambda_a + \mu_a)(\lambda_b + \mu_b)} \tag{17}$$

Subsystem D consists of serial components. Using (12) and (13), availability of subsystem D can be easily calculated. Finally, there are two series subsystems. System availability can be solved as.

$$A(t) = A_C(t) A_D(t) \tag{18}$$

For Istanbul M2 metro line, given that 100 axle counters and 40 signals are used for fallback signaling, we can compare the pure CBTC and CBTC with fallback. Failure and repair rates of axle counters and signals are given in table 2. From table 2 and

(18), the availability of CBTC system with fallback is calculated as 0.99985368.

Table 2. Failure and repair rates of fallback elements

Subsystem	λ(1/h)	μ(1/h)	Quantity
Axle Counter	2.5×10^{-6}	4/3	100
Signal	3×10^{-6}	4/3	40

CBTC systems are generally designed for 30 years. In terms of comparison of operational disruption, expected down times are given in table 3. As can be seen from this table, there is only a difference of 4 hours expected down time between the two systems.

Table 3. Down time comparison

System	Availability	Down Time
CBTC	0.9998356	34.2
CBTC&Fallback	0.9998536	30.44

5. Conclusions

Experience shows that the secondary detection constitutes 20 to 50% of the investment cost of a CBTC system for a green field project [4]. This cost depends on the number of axle counters and signal equipment, software complexity and the type of fallback system to be used (detection or protection). Also logistics costs increase as more equipment is being employed. Failures that occur in the secondary train control system while the CBTC is the primary system will not affect the operation of the system but there will be an extra cost in terms of maintenance. In terms of failure, CBTC systems have highly reliable equipment. In addition to this, adequate redundancy is built in these systems to avoid any repercussions due to a single point failure [15]. The calculations in this paper show that using a backup system in addition to a CBTC system does not increase the reliability of the system notably. Therefore using such fallback systems need to be reconsidered, and should be avoided unless they are necessary due to other reasons such as mixed mode operation, starting with a brownfield or safety considerations.

6. References

[1] J. Farooq and S. Jose, "Radio Communication for Communications-Based Train Control (CBTC): A tutorial and survey", *IEEE Communications Surveys & Tutorials*, vol. *99*, pp. *1-1*, 2017.

[2] W. Haifeng, T. Tao, R. Clive and G. Chunhai, "A novel framework for supporting the design of moving block train control system schemes", IMechE Part F: Journal of Rail and Rapid Transit, vol. *228*, no. *7*, pp. *784-793*, 2013.

[3] R. John Hill and L. J. Bond, "Modelling moving-block railway signaling systems using discrete-event simulation", Proceedings of the IEEE/ASME Joint Railroad Conference, pp. *105-111*, 1995.

[4] S. Lacroix, "Balancing the need for secondary train detection in UTO projects, in order to optimize CBTC capital investment and operating cost", SYSTRA, 2015.

[5] IEEE Standard for Communications-Based Train Control (CBTC) Performance and Functional Requirements," in *IEEE Std 1474.1-1999*, 1999.

[6] A. Rumsey, "Communications Based Train Control A Product or a Strategy?", in *IRSE Seminar*, London, UK., 2011, pp. *5-23*.

[7] R. D. Pascoe and T. N. Eichorn, "What is communication-based train control?", in *IEEE Vehicular Technology Magazine*, vol. 4, no. 4, pp. 16-21, December 2009.

[8] S. Maharaja, and M. Varghese, " Train Control System for Efficient Track Usage and Reduce Road Traffic ", IOSR Journal of Computer Engineering, vol. *9*, no. *6*, pp. *13-18*, *2013*.

[9] W. C. Carreño, "Efficient driving of CBTC ATO operated trains ", PhD. thesis, Sustainable Energy Technologies and Strategies**,** Pontificia Comillas, Madrid, Spain, 2017.

[10] IEEE Draft Recommended Practice for Communications-Based Train Control (CBTC) System Design and Functional Allocations," in IEEE Unapproved Draft Std P1474.3_D11.0, Jan 2008.

[11] EN 50126: The specification and demonstration of Reliability, Availability, Maintainability and Safety (RAMS)," in *European Committee for Electrotechnical Standardization*, 1999.

[12] Z. Taylor and S. Ranganathan, "Designing High Availability Systems: Design for Six Sigma and Classical Reliability Techniques with Practical Real-Life Examples ", John Wiley & Sons, Inc., 2014.

[13] H. P. Barringer and P. E. Barringer, "Availability, Reliability, Maintainability, and Capability", Triplex Chapter of the Vibrations Institute, Texas, Feb 1997.

[14] K. S. Son, D. H. Kim, C. H. Kim and H. G. Kang, "Study on the systematic approach of Markov modelling for dependability analysis of complex fault-tolerant features with voting logics", ELSEVIER Reliability Engineering and System Safety, vol. *150*, pp. *44-57*, 2016.

[15] Y. R. Bhardwaj, "Fall Back Signaling for communication Based Train Control- Luxury or Necessity", in *IRSE NEWS*, vol. *208*, pp. *13-17*, Feb 2015.

Linear Prediction of Traction Motor's Efficiency by the Information of Speed, Current and Moment

Mehmet Fidan[1], Mine Sertsöz[1], and Mehmet Kurban[2]

[1]Anadolu University, Vocational School of Transportation, Eskisehir, Turkey
mfidan@anadolu.edu.tr, msertsoz@anadolu.edu.tr
[2]Bilecik Şeyh Edebali University, Department of Electrical&Electronics Engineering, Bilecik, Turkey
mkurban@bilecik.edu.tr

Abstract

Asynchronous induction motors are the most preferable motors for the locomotives because of their simple but robust structure. The efficiency of the preferred motor is crucial for the limitation of the load pulled by the locomotive and suitability for the geographic conditions. In this study, a linear prediction based method is proposed for the forecasting the efficiency of the motor by using its speed, current and moment information. Before the predictor is applied, the statistical relations between efficiency and moment, efficiency and speed, efficiency and current of the motor are also analyzed and presented.

1. Introduction

Induction motors can be designed for various torque, various rotation speed and various drawn current parameters according to its usage. Therefore this different designs cause different efficiency percentages on the output of the motors. When the power of the motor is increased, the efficiency of the motor should also be increased, because of avoiding undesired amount of loss power. On the other hand how can we sure that we reach the desired efficiency percentage without complex and time-consuming power measurements and calculations? The observations show that there are strong correlations between efficiency and three critical parameters of the motor: drawn current, moment and rotation speed, which are presented in details in Section-2.

These correlations give the opportunity to construct a predictor function for the efficiency depending to current, moment and speed. In the literature, interpolation [1], extrapolation [2], Kalman filtering [3], Moving Average [4], Autoregressive Moving Average [5], Neural Networks [6], exponential smoothing [7], linear prediction [8], Markov chains [9] and HMM[10] are the most used methods for the prediction. In addition various parameters of the induction motors are predicted by the soft computing approach [11]. In-line testing of permanent excited rotors is also one of the recent methods which is used for prediction of the electric motor performance [12]. A predictive method is applied in another work for determining the remaining range of the motor vehicle by the data of energy consumption [13]. In this study linear prediction is preferred, which uses correlation coefficients between current sample, and past samples of a signal. In the proposed method, current sample is taken as efficiency percentage and current, moment and speed values are used instead of past samples. The strong correlations which are presented in Section-2, plays the main role for choosing this linear prediction method. In Section-3 the details of the linear prediction method and the obtained equations for the prediction are explained.

In Section-4, the performances of the proposed predictors which use different combinations of the current, speed and moment values as input vectors, are presented comparatively and in Section-5 the obtained performances are analyzed and some possible ideas are listed for the future work.

2. Correlations of Efficiency of Motor with Drawn Current, Output Moment and Rotation Speed

The main parameter which gives a numerical magnitude for the correlation of two phenomena is covariance[14], if these phenomena thought as random variables as shown in (1).

$$Cov(X,Y) = E[XY] - E[X]E[Y] \quad (1)$$

In (1), $E[\cdot]$ denotes the expected or mean value of the phenomenon. In discrete variables, covariance can be calculated by (2) from the samples measured for these two variables.

$$Cov(X,Y) = \frac{1}{n^2}\sum_{i=1}^{n}\sum_{j=1}^{n}(x_i - E[X])\left(y_j - E[Y]\right) \quad (2)$$

According to Eq-2, some idea can be obtained about the relation of events *X* and *Y*. However this covariance value is dependent to the magnitude of standard deviations of *X* and *Y*. This dependency is avoiding objectivity of the value. To discard the effects of standard deviations of *X* and *Y* and to normalize the value between 1 and -1, covariance value should be divided by standard deviations of *X* and *Y*. According to this division, Pearson Correlation Coefficient[15] is obtained as (3).

$$\rho(X,Y) = \frac{Cov(X,Y)}{\sigma_X \sigma_Y} \quad (3)$$

For obtaining Pearson Correlation Coefficient between efficiency and moment, efficiency and drawn current and efficiency and rotation speed, various data for the various size of induction motors are needed. For this purpose, the catalogue parameters of GAMAK which is the company producing various size of induction motors are used[16].

These parameters are listed in Table 1.

Table 1. Induction Motor Parameters for Different Sizes

Motor kW	Speed (RPM)	Current (Ampere)	Moment (Nm)	Efficiency (%)
5,50	1465	11,2	35,9	87.9
7,5	1465	15,4	48,9	89
11	1465	21,3	71,7	90
15	1465	29,4	97,8	90.6
18,5	1470	34,5	120	91.3
22	1470	42,5	143	91.7
30	1470	55	195	92.5
37	1470	67	240	92.7
45	1470	80	292	93.3
55	1475	96	356	93.7
75	1480	133	484	94
90	1480	158	581	94.3
110	1485	195	707	94.5
132	1485	230	849	94.7
160	1485	280	1029	94.9
185	1485	323	1190	94.9
200	1485	350	1286	95

If (3) is applied on Eq-1, the Pearson Correlation Coefficients are found as shown in Table-2.

Table 2. Pearson Correlation Coefficients

$\boldsymbol{\rho(E,S)}$	$\boldsymbol{\rho(E,C)}$	$\boldsymbol{\rho(E,M)}$
0.8993	0.8234	0.8241

Note: E,S,C,M denotes Efficiency, Speed, Current and Moment respectively.

According to Table 2, it can be said that most correlated parameter with efficiency is rotation speed and least correlated parameter with efficiency is drawn current. However, both parameters have strong correlations with efficiency, which gives the opportunity to construct a linear predictor for efficiency.

3. Linear Prediction Model

Assume that $\widehat{E_{\mathrm{i}}}$ is the prediction value of efficiency. Then there are four linear predictors are proposed as (4), (5), (6) and (7) respectively.

$$\widehat{E_{\mathrm{i},all}} = a_M M_{i,Norm} + a_C C_{i,Norm} + a_S S_{i,Norm} + \min(E) \tag{4}$$

$$\widehat{E_{\mathrm{i},MC}} = b_M M_{i,Norm} + b_C C_{i,Norm} + \min(E) \tag{5}$$

$$\widehat{E_{\mathrm{i},CS}} = c_C C_{i,Norm} + c_S S_{i,Norm} + \min(E) \tag{6}$$

$$\widehat{E_{\mathrm{i},MS}} = d_M M_{i,Norm} + d_S C_{i,Norm} + \min(E) \tag{7}$$

For a successive prediction, input parameters of the predictors are normalized as in (8)

$$X_{i,Norm} = \frac{X_i - \min(X)}{max(X_i - min(X))} \tag{8}$$

The coefficients of the predictor $\widehat{E_{\mathrm{i},all}}$ is calculated by the correlation matrix as in (9).

$$\begin{bmatrix} a_M \\ a_C \\ a_S \end{bmatrix} = K \cdot \begin{bmatrix} \rho(E,E) & \rho(E,M) & \rho(E,C) \\ \rho(E,M) & \rho(E,E) & \rho(E,S) \\ \rho(E,C) & \rho(E,S) & \rho(E,E) \end{bmatrix}^{-1} \cdot \begin{bmatrix} \rho(E,M) \\ \rho(E,C) \\ \rho(E,S) \end{bmatrix} \qquad K = max\big(E_i - min(E)\big) \tag{9}$$

The coefficients of the predictor $\widehat{E_{\mathrm{i},MC}}$ is calculated by the correlation matrix as in (10).

$$\begin{bmatrix} b_M \\ b_C \end{bmatrix} = K \cdot \begin{bmatrix} \rho(E,E) & \rho(E,M) \\ \rho(E,C) & \rho(E,E) \end{bmatrix}^{-1} \cdot \begin{bmatrix} \rho(E,M) \\ \rho(E,C) \end{bmatrix} \qquad K = max\big(E_i - min(E)\big) \tag{10}$$

The coefficients of the predictor $\widehat{E_{\mathrm{i},CS}}$ is calculated by the correlation matrix as in (11).

$$\begin{bmatrix} c_C \\ c_S \end{bmatrix} = K \cdot \begin{bmatrix} \rho(E,E) & \rho(E,C) \\ \rho(E,S) & \rho(E,E) \end{bmatrix}^{-1} \cdot \begin{bmatrix} \rho(E,C) \\ \rho(E,S) \end{bmatrix} \qquad K = max\big(E_i - min(E)\big) \tag{11}$$

The coefficients of the predictor $\widehat{E_{\mathrm{i},MS}}$ is calculated by the correlation matrix as in (12).

$$\begin{bmatrix} d_M \\ d_S \end{bmatrix} = K \cdot \begin{bmatrix} \rho(E,E) & \rho(E,M) \\ \rho(E,S) & \rho(E,E) \end{bmatrix}^{-1} \cdot \begin{bmatrix} \rho(E,M) \\ \rho(E,S) \end{bmatrix} \qquad K = max\big(E_i - min(E)\big) \tag{12}$$

For the Table 1, the predictor equations are found as in (13), (14), (15) and (16) respectively.

$$\widehat{E_{\mathrm{i},all}} = 1.92 M_{i,Norm} - 0.30 C_{i,Norm} + 5.07 S_{i,Norm} + 87.9 \tag{13}$$

$$\widehat{E_{\mathrm{i},MC}} = 3.21 M_{i,Norm} + 3.20 C_{i,Norm} + 87.9 \tag{14}$$

$$\widehat{E_{\mathrm{i},CS}} = 2.27 C_{i,Norm} + 4.35 S_{i,Norm} + 87.9 \tag{15}$$

$$\widehat{E_{\mathrm{i},MS}} = 2.28 M_{i,Norm} + 4.34 C_{i,Norm} + 87.9 \tag{16}$$

$\widehat{E_{\mathrm{i},CS}}$ and $\widehat{E_{\mathrm{i},MS}}$ have close coefficients because normalized current data and normalized moment data are so close to each other because of linear dependency.

4. Comparative Results

According to the predictor equations, the predicted current values are found as in Table 3.

Table 3. Prediction Values of Proposed Predictors

Exact Efficiency	$\widehat{E_{i,all}}$	$\widehat{E_{i,MC}}$	$\widehat{E_{i,CS}}$	$\widehat{E_{i,MS}}$
87.9	87.9	87.9	87.9	87.9
89	87.916	87.973	87.928	87.924
90	87.946	88.087	87.968	87.865
90.6	87.979	88.231	88.022	88.013
91.3	89.277	88.336	89.142	89.138
91.7	89.305	88.471	89.196	89.180
92.5	89.374	88.723	89.280	89.274
92.7	89.432	88.952	89.360	89.356
93.3	89.5	89.208	89.447	89.451
93.7	90.853	89.524	90.640	90.652
94	92.285	90.202	91.974	91.970
94.3	93.412	90.688	92.142	92.146
94.5	93.841	91.361	93.476	93.461
94.7	94.028	92.057	93.710	93.719
94.9	94.261	92.992	94.045	94.047
94.9	94.471	93.812	94.333	94.340
95	94.595	94.314	94.514	94.514

The best way to measure the performance of a predictor is calculating mean error (ME) and root mean square error (RMSE) of the predictor. These are shown in Table 4.

Table 4. ME and RMSE of the Proposed Predictors

	$\widehat{E_{i,all}}$	$\widehat{E_{i,MC}}$	$\widehat{E_{i,CS}}$	$\widehat{E_{i,MS}}$
ME	1.7427	2.5981	1.8779	1.8796
RMSE	2.0756	2.8864	2.1783	2.1800

5. Conclusions

According to the Table-4, it can be deduced that using moment and drawn current data in a single prediction model is not an efficient idea, because they have the same information according to linear dependency. However if the speed data is used in any predictor, the predictor gives better results because of strong correlation with efficiency. Naturally, if both speed, current and moment data is used in the predictor, predictor gives the best result. Furthermore, the results shows that the weakest correlation of the motor efficiency is with the parameter of moment and the strongest correlation is with the parameter of speed.

Some environmental effects can change the accuracy of the predictions. The quality of the A.C. power used for driving the motor is one of these effects. Low quality A.C. power can cause unexpected synchronization problems, which causes necessity of more complex models for efficiency prediction. In additional high ambient temperature can cause irrational behaviors on electrical motor, which obstructs accurate efficiency predictions.

There can be used another parameter as temperature of the motor or noise of the motor instead of current data for obtaining better predictions in the future works. In addition, PCA can be applied to input vectors for filtering unnecessarily repeated knowledge in the input parameters. Moreover, the variety of the motors can be enhanced for obtaining more comprehensive prediction model. Finally the prediction model can be improved by choosing a suitable ARMA model, or NN model.

6. References

[1] R.E. Crochiere and L.R. Rabiner, "Multirate Digital Signal Processing." Englewood Cliffs, NJ: Prentice–Hall, 1983.

[2] J. Scott Armstrong; Fred Collopy, *"Causal Forces: Structuring Knowledge for Time-series Extrapolation"*, Journal of Forecasting. **12**: 103–115, 1993.

[3] Paul Zarchan; Howard Musoff, . "*Fundamentals of Kalman Filtering: A Practical Approach*." American Institute of Aeronautics and Astronautics, Incorporated, 2000.

[4] *Statistical Analysis*, Ya-lun Chou, Holt International, ISBN:0-03-089422-0, section 17.9. 1975.

[5] Hannan, Edward James, "*Multiple time series*. Wiley series in probability and mathematical statistics." New York: John Wiley and Sons, 1970.

[6] Mandic, Danilo P., and Jonathon A. Chambers. *Recurrent neural networks for prediction: learning algorithms, architectures and stability*. New York: John Wiley, 2001.

[7] "NIST/SEMATECH e-Handbook of Statistical Methods, 6.4.3.1. Single Exponential Smoothing". *NIST*. Retrieved 2017-07-05.

[8] Hayes, M. H., "Statistical Digital Signal Processing and Modeling". New York: J. Wiley & Sons. ISBN 978-0471594314, 1996.

[9] Richard Serfozo, "*Basics of Applied Stochastic Processes"*, Springer Science & Business Media. p. 2. ISBN 978-3-540-89332-5, 2009.

[10] Lawrence R. Rabiner, *"A tutorial on Hidden Markov Models and selected applications in speech recognition"* (PDF). Proceedings of the *IEEE*. **77** (2): 257–286. doi:10.1109/5.18626, 1989.

[11] A. Soni and L. Daniel, "*A Soft Computing Approach For Prediction of Reactive Power Drawn By Induction Motor"*, International Journal of Innovative Research in Engineering Applications. 1(2):89-96, 2016.

[12] Abersfelder, Sandra, et al. *"Prediction of electric motor performance by in-line testing of permanent excited rotors."* Electric Drives Production Conference (EDPC), 2016 6th International. IEEE, 2016.

[13] Klimesch, Michael, Andreas Lamprecht, and Sascha Kulnick. "Method for determining the remaining range of a motor vehicle, and motor vehicle." U.S. Patent No. 9,662,996. 30 May 2017.

[14] Hazewinkel, Michiel, ed. , *"Covariance"*, *Encyclopedia of Mathematics*, Springer, ISBN: 978-1-55608-010-4, 2001.

[15] "SPSS Tutorials: Pearson Correlation", Retrieved 2017-05-14.

[16] http://www.gamak.com/Uploads/Files/2016-04-27-032451.pdf

Vibration Mitigation of Railway Bridge Using Magnetorheological Damper

Arif Ulu[1], Mahmut Paksoy[1], Muzaffer Metin[1] and Murat Emre Yücel[1]

[1]Department of Mechanical Engineering, Yildiz Technical University, Turkey
uluarif1@gmail.com, mpaksoy@yildiz.edu.tr, mmetin@yildiz.edu.tr, emreyucel1987@gmail.com

Abstract

The purpose of this study is to analyze the railway bridge vibrations and control their negative effects through semi active Magnetorheological (MR) damper. Dynamic analysis of a railway bridge subjected to the moving load is performed. The real structural parameters are used and the six axle train is simulated as moving loads. The railway bridge is modeled as Euler-Bernoulli beam theory and it is discretized through Galerkin method. To mitigate the bridge vibrations, MR damper with a Fuzzy Logic based controller is positioned at the ends of the bridge. The simulations of the system are performed by Matlab software. Finally, the results are examined both in the time and frequency domains.

1. Introduction

Because of the increasing air pollution and traffic problems, the importance of rail vehicles gained importance as a mass transportation system. In addition, the railway bridges have become a part of the transportation, as well. With the development of materials and construction technology, the bridges are enabled to be built light and slender which made the bridges prone to the vibrations triggered by high-speed rail vehicles while passing. As a consequence, the vibrations of railway bridges are considered as a significant factor in bridge design [1].

The dynamic behavior of railway bridges under moving load is a complicated and challenging phenomenon and is drawn the attention of scientists and engineers due to the complex structure of Railway Bridges. The interaction between rail vehicle and bridge creates a dynamic effect. The most crucial parameters determining the dynamic response of bridges are rail vehicle speed, characteristics of bridge and rail irregularity. The safety is expected to be maximum while the comfort of the rail vehicles is minimum. In order to do so, the controlling of rail superstructures and rail bridges, as well as the vehicle suspension are significant. In addition, the vibration control of a rail bridge is better both for its life and the rail vehicles on the bridge if any.

The structural damping while exposed to the vibrations is the typical characteristics of bridges as well as the civil structures are. Yet, that damping is regarded as insufficient. So, when the disturbance force is applied, it may cause strong and long-lasting vibrations. Hence, the semi-active suspension to mitigate vibrations is investigated.

When we review literature, it shows that the structural control of the railway bridges subjected to the moving load is studied by many researchers. The bridge can be modeled as a simply supported Euler-Bernoulli beam [2] and the train mass at a constant speed is modeled as a time and spatially changing load. Doing that, the vehicle dynamics can be neglected [3]. These models were adopted subsequently in the related study [4-5]. On the other hand, several researches on bridges' dynamic response under the moving load, demonstrate the effects of moving the train.

The suspension types are separated into three groups which are active, semi-active and passive suspensions. However, only the semi-active one and the active one can be controlled. The idea in implementing a semi-active suspension is to change active force generator with adaptive elements that can shift the rate of energy dissipation in response to a momentary condition of motion. The force of suspension can be controlled through active causes in response to sensory feedback, whereas the actuators are used in active controllers to implement an independent force on suspension [6]. We could say that semi-active systems are more practical than passive systems and less expensive and complicated than active systems [7]. It is widely known that the MR damper is quite feasible and reliable to implement in reducing vibrations [8] since its performance is better than passive suspension as its power requirements are low and its hardware is inexpensive than active suspension [9]. Usually, the MR damper-based semi-active controller works through a two-step progress. Firstly, a system controller designates the desired control force in respect of the responses; then damper controller sets the command applied to the MR damper so that it can track the desired control force. Hence, the successful application of the MR damper-based semi-active controller is depended on two aspects: One of them is to select a proper control strategy and the other is to establish the accurate damper controller [10].

In this paper, the vibration of railway bridges subjected to the moving load is investigated. The bridge model is taken into consideration as a simple support beam. As the model is a continuous one, it is changed to discrete model through the Galerkin method and its vibration is investigated when subjected to the force which is due to the train passing on the bridge. To mitigate vibrations, two symmetric MR dampers are applied to the bridge from the bottom. Fuzzy logic control method is used on MR dampers to determine the voltage input. Controlled and uncontrolled results are analyzed.

2. Mathematical Modeling

Fig. 1 shows that a model of railway bridge. Bridge modeled as Euler-Bernoulli beam which is constant cross-section, homogeneous and simply-supported. At that time MR dampers that modelled as Modified Boucwen Model, located on two sides of bridge. In addition, forces thought as axial forces of railway train axles.

$$m\frac{\partial^2 w(x,t)}{\partial t^2}+c\frac{\partial w(x,t)}{\partial t}+EI\frac{\partial^4 w(x,t)}{\partial x^4}= \sum_{j=1}^{6}\delta(x-vt)P_j+\sum_{j=1}^{2}\delta(x=x_{dj})F_{MRj} \tag{1}$$

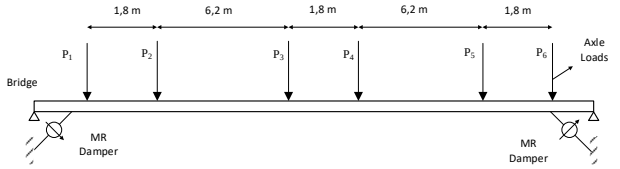

Fig. 1. Railway bridge with MR dampers acted on moving axle loads

where *EI*, *m*, *c* and *w(x,t)* were flexural rigidity mass per length, the damping coefficient and transverse displacement of bridge at point *x* and time *t*, respectively. Parameters of bridge were given in Table 1. Right hand of equation is axial forces (*P*) represented by Dirac-delta function and MR damper forces. Dirac-delta function $\delta(x)$ was thought as a unit concentered force acting at point $x = 0$. Dirac-delta function was defined in Eq. 2.

$$\int_a^b \delta(x - vt) f(x) dx = f(\xi) \text{ for } a < \xi < b \tag{2}$$

By using Galerkin method transverse function *w (x, t)* was transformed into two separate functions Eq. 3. It was selected a sinus function $\left(\sin\frac{i\pi x}{L}\right)$ depending on *x*, in order to satisfy boundary conditions.

$$w(x,t) = \sum_{i=1}^{N} T(t) \sin\frac{i\pi x}{L} \qquad i = 1,2,...,N \tag{3}$$

Trial function (3) is implemented in Eq. (1), multiplied full equation with trial function and integrated from *0* to *L*. Finally, a partial differential equation (Eq. 1) is turned into ordinary differential equation (Eq. 4).

$$m\ddot{T}_i(t) + c\dot{T}_i(t) + EI\left(\frac{i\pi}{L}\right)^4 T_i(t) = \sum_{j=1}^{6} \frac{2P_j}{L} sin\left(\frac{i\pi(vt - L_j)}{L}\right) + \sum_{j=1}^{2} \frac{2F_{MRj}}{L} sin\left(\frac{i\pi x_{dj}}{L}\right) i = 1,2,3,\ldots,N \tag{4}$$

At the right-hand side of equation, there are eight forces. First six forces are moving forces that represented train axle loads. L_1, L_2… are distance from first wheel (Fig. 1). The last ones are the MR damper forces that were located two sides (x_{d1}, x_{d2}) of bridge.

Damping of bridge is modeled as Rayleigh structural damping [2], depended on mass, rigidity and natural frequencies of the bridge (Eq. 5-6). ω_i, ω_j is represented natural frequencies of the simply supported bridge.

$$c = a_0 m + a_1 k \tag{5}$$

$$a_0 = \xi\frac{2\omega_i\omega_j}{\omega_i + \omega_j}\,;\; a_1 = \xi\frac{2}{\omega_i + \omega_j} \tag{6}$$

As mentioned above, MR Dampers modeled modified Boucwen Model that related equations are given Eq. 7-12 [12].

$$\dot{z} = -\gamma|\dot{x} - \dot{y}||z|^{n-1} z - \beta(\dot{x} - \dot{y})|z|^n + A(\dot{x} - \dot{y}) \tag{7}$$

$$\dot{y} = \frac{1}{c_0 + c_1}\left[az + c_0\dot{x} + k_0(x - y)\right] \tag{8}$$

in which k_1 is the accumulator stiffness; c_0 is the viscous damping at larger velocities; c_1 is viscous damping for force roll-off at low velocities; x_0, is the initial displacement of spring k_1; and *A, β, γ* and *n* are the constants about MR Damper that force was calculated as Eq. 9 [12].

$$\begin{aligned} F_{MR} &= az + c_0(\dot{x} - \dot{y}) + k_0(x - y) + k_1(x - x_0) \\ &= c_1\dot{y} + k_1(x - x_0) \end{aligned} \tag{9}$$

c_0, c_1 and *a* have form of third-order polynomial with respect to electrical current *i*, expressed as Eq.10-12.

$$a(i) = 16566i^3 - 87071i^2 + 168326i + 15114 \tag{10}$$

$$c_0(i) = 437097i^3 - 1545407i^2 + 1641376i + 457741 \tag{11}$$

$$c_1(i) = -9363108i^3 + 5334183i^2 + 48788640i - 2791630 \tag{12}$$

Table 1. Properties of Railway Bridge [11]

Young's modulus (N/m^2)	210x10^9
Area moment of inertia (m^4)	0.61
Mass per length (kg/m)	18400
Length of the beam (m)	42
Moving load (N)	80000
Damping Ratio	0.1
MR Damper Locations (m)	5, 37

Table 2. Model Parameters of MR Damper [12]

A (m^{-1})	2769
β, γ (m^{-1})	647.46
k_0 (N/m)	137810
n	10
x_0 (m)	0.18
k_1 (N/m)	617.31

Table 3. ABB railway vehicle parameters [13]

Length (m)	23.2
Width (m)	2.65
Passengers capacity	257
Max. design axle load (kN)	80
Wheel diameter (m)	0.68-0.6
Wheel width (m)	0.125
Max. Speed (km/h)	80

Fig. 2. ABB railway vehicle

3. Fuzzy Control Design

FLC (Fuzzy logic based controllers) are frequently used in vibration reduction problems. Classical Fuzzy Logic Controller is used in this paper which based on two input one output FLC structure. The overall structure of used controller is shown in Figure 3.

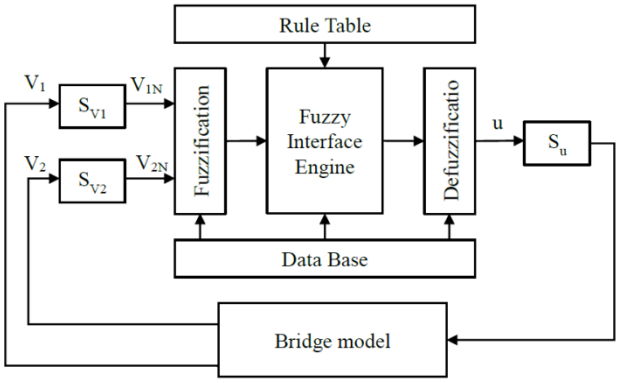

Fig. 3. Block diagram of the two input one output Fuzzy Logic Controller

The structure of fuzzy logic controller has two inputs, and one output. The inputs are respectively "V_1" which is defined as the velocity of middle point of bridge model; and "V_2" which is defined as the velocity of the upper end point of MR damper. Linguistic variables which imply inputs and output are classified as: NB NM NS ZO PS PM PB. Inputs and output are all normalized in the interval of [-1, 1] as well as outputs are normalized at range of [0, 1] as shown in Figure 4. Linguistic values which are used as output values are in the following; ZO, VS, S, SM, M, B, VB.

The variables are scaled with coefficient of S_{V1}, S_{V2} and S_u. The fuzzy control rule is in the form of:

IF $e=E_i$ **and** $de=dE_j$ **than** $V=V_{(i,j)}$

These rules are written in a rule base look-up table which is shown in Table 4. The rule base structure is Mamdani type.

The linguistic labels used to describe the Fuzzy sets are 'Negative Big' (NB), 'Negative Medium' (NM) 'Negative Small' (NS), 'Zero' (ZO), 'Positive Small' (PS), 'Positive Medium' (PM), 'Positive Big' (PB) Very small (VS), Small (S), Small Medium (SM), Medium (M), Big (B), Very Big (VB). It is possible to assign the set of decision rules as shown in Table 1. These rules contain the input/the output relationships that define the control strategy. Each control input has seven fuzzy sets so that there are 49 fuzzy rules.

Table 4. Rules of Fuzzy Logic Controller

V1/V2	NB	NM	NS	ZO	PS	PM	PB
NB	SM	S	VS	ZO	VS	S	SM
NM	M	SM	VS	ZO	VS	SM	M
NS	B	M	S	ZO	S	M	B
ZO	VB	B	SM	ZO	SM	B	VB
PS	B	M	S	ZO	S	M	B
PM	M	SM	VS	ZO	VS	SM	M
PB	SM	S	VS	ZO	VS	S	SM

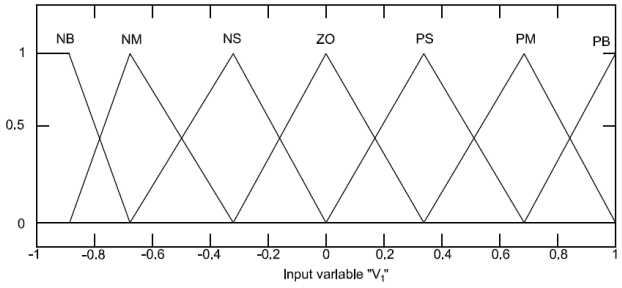

(a)

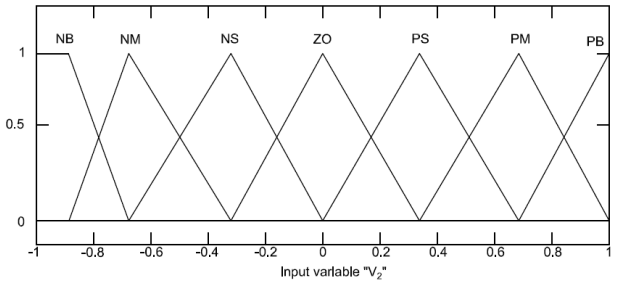

(b)

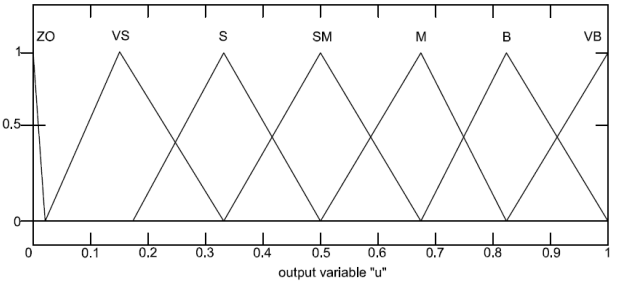

(c)

Fig. 4. Membership functions of inputs V_1 (a), V_2 (b) and output u (c).

4. Simulations

According to Eq. 4, for 5 modes of bridge is considered. It was enough for the responses of the bridge. MR Damper models and bridge equations with fuzzy control tools are simulated in MATLAB-Simulink and performed in ode45 solver.

In all analysis train's speed was fixed to maximum speed of 80 km/h for urban transportation. Moving loads are acting on bridge during 2.853 seconds. In uncontrolled system, supplied electrical current is fixed 0.05 A.

Fig. 3-5 shows the dynamic responses of midpoint of the railway bridge. Blue straight and red dashed lines show the uncontrolled and fuzzy controlled system, respectively. Maximum values of bridge responses are suppressed successfully, especially in velocity and acceleration. Also, settlement time of controlled bridge vibrations turns out to be better than uncontrolled system.

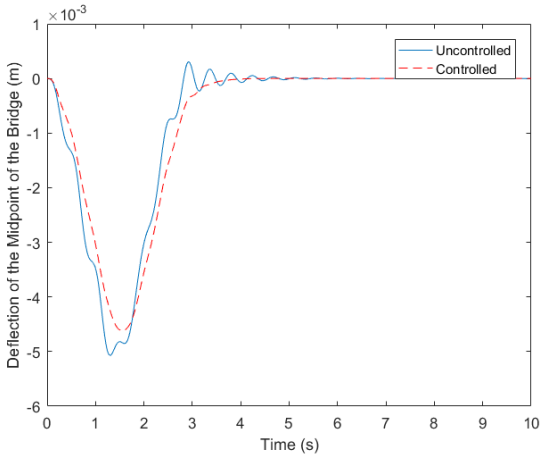

Fig. 3. Displacement of the midpoint of the railway bridge

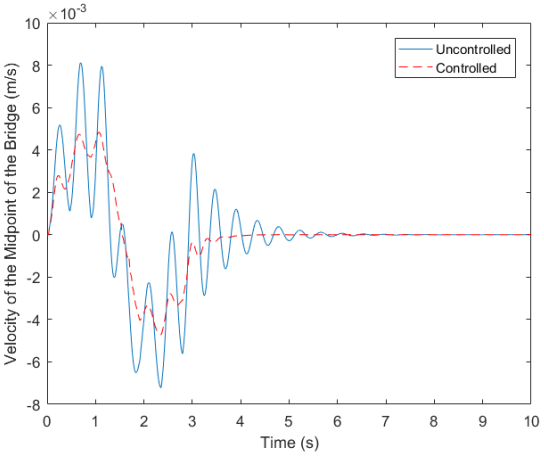

Fig. 4. Velocity of the midpoint of the railway bridge

Fig. 6-7, shows the dynamic MR damper forces and electrical current that supplied the dampers. Blue straight lines and red dashed lines represent 1st and 2nd MR Dampers. After 1.89 seconds, dampers applied same opposite forces to the bridge. Because first wheel on the bridge removed, other forces would be left one by one. It is clearly seen that velocity and MR damper force profiles are similar.

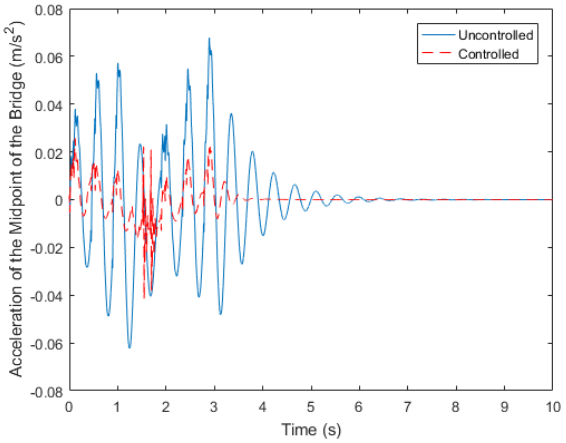

Fig. 5. Acceleration of the midpoint of the railway bridge

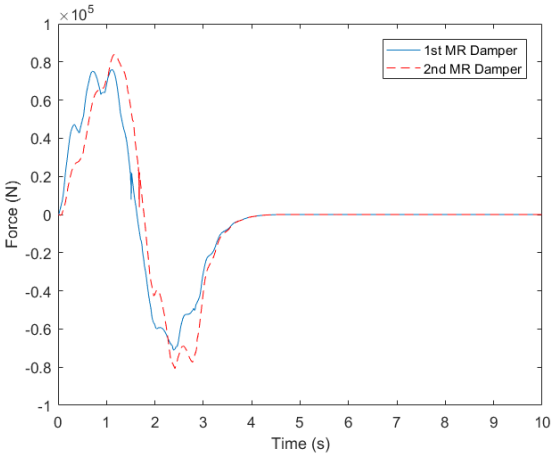

Fig. 6. Two MR Dampers' Forces

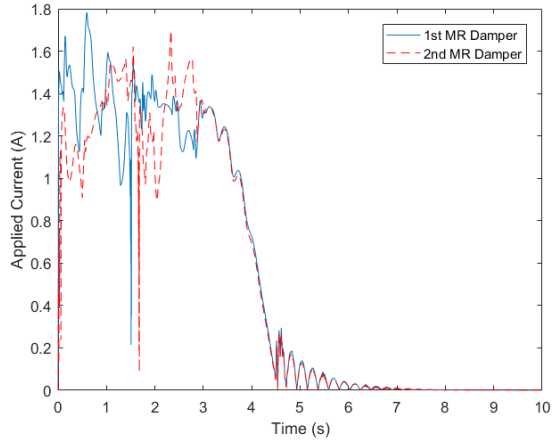

Fig. 7. Applied Current on the MR Dampers

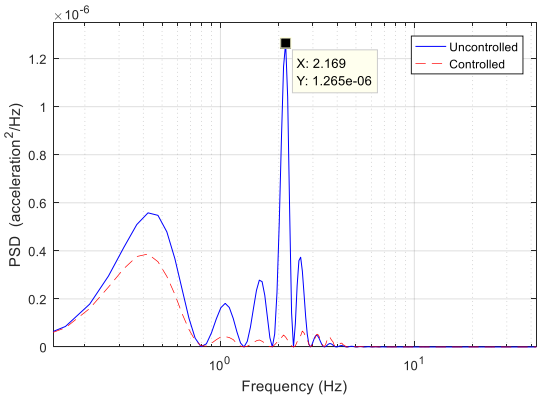

Fig. 8. Power spectral density of acceleration data of the railway bridge

Power spectral density (PSD) of bridge vertical acceleration is shown on Figure 8. When we analyze the Figure 8 it can be seen that the Fuzzy Logic Controller reduced the magnitude of the bridge vertical acceleration in all frequencies significantly.

Natural frequencies are calculated as 2.29, 9.17, 20.63, 36.69, 57.32 Hz, by using Eq. 13. It is widely known that, the most dangerous frequency is the first natural frequency in the structures. In this regard, the first natural frequency is well suppressed via Fuzzy Logic controlled MR dampers.

$$W_n = \left(\frac{i\pi}{L}\right)^2 \sqrt{\frac{EI}{m}} \quad i = 1,..5 \tag{13}$$

6. Conclusions

In this study the railway bridge vibrations are controlled through Magnetorheological (MR) damper by using Fuzzy Logic Control algorithms.

Firstly, the railway bridge is modeled as Euler-Bernoulli beam. Equations of the bridge are achieved according to Galerkin Method. To suppress the railway bridge vertical vibrations, two MR dampers positioned at the bridge ends. In the mathematical model of the bridge, MR damper is considered as friction based Modified Bouc-Wen model. The damping force of MR damper which changes with applied electrical current is controlled by the use of Fuzzy Logic Controller. In simulations, railway vertical vibrations are analyzed for active and passive MR damper situations, while 6 axle railway vehicle is passing through the bridge. When the simulation results are examined, the vibration reduction performance of Fuzzy Logic controller in time and frequency domain can be seen.

It is supposed that, extension of bridge life, mitigation of negative effect of vibrations on human bodies and rail vehicles and increasing of passenger comfort can be provided by reduction of bridge vibration values. For the future works, different control algorithms can be compared and it can be applied on the real bridge systems.

7. References

[1] Luu M, Martinez-Rodrigo M D, Zabel V and Könke C, "Semi-active magnetorheological dampers for reducing response of high-speed railway bridges", Control Eng. Pract. 32 147–60, 2014.

[2] Ray W. Clough and Joseph Penzien, "Dynamics of structures 2nd edition", McGraw-Hill, New York, 1993.

[3] Jiang, Z. and Christenson, R., "Experimental Verification of an MR Damper Controlled Highway Bridge", 19th Analysis & Computation Specialty Conference, ASCE,2010, pp. 347-358.

[4] Sadiku, S. and Leipholz, H. H. E.," On the dynamics of elastic systems with moving concentrated masses", Ingenieur-Archiv, 57,223-242, 1987.

[5] Akin, J. E., and Mofid, M., "Numerical solution for response of beams with moving mass", J. Struct. Eng., ASCE, 115 (1), 120-131, 1989.

[6] Pisal, A., Y. and Jangid, R., S., "Vibration control of bridge subjected to multi-axle vehicle using multiple tuned mass friction dampers", Int. J. Adv. Struct. Eng., 8:213-227, 2016.

[7] Metin, M., and Guclu, R., "Rail Vehicle Vibrations Control Using Parameters Adaptive PID Controller", Mathematical Problems in Engineering, Vol. 2014, 2014.

[8] Metin, M., Yücel, M.E., Paksoy, M., and Çetin, Ş., "Controlling Rail Vehicle Vibrations Using Magnetorheological Damper," 3rd International Symposium on Railway Systems Engineering (ISERSE'16), October 13-15, 2016, Karabuk, Turkey.

[9] Zong, L., Gong, X., Xuan, S., Guo, C., "Semi-active H∞ control of high-speed railway vehicle suspension with magnetorheological dampers", Vehicle System Dynamics: International Journal of Vehicle Mechanics and Mobility, 51:5, 600-626, 2013.

[10] W.H. Liao and D.H. Wang, Semiactive vibration control of train suspension systems via magnetorheological dampers, J. Intell. Mater. Syst. Struct. 14(3) (2003), pp. 161–172.

[11] Radeström, S., "Application of fluid viscous dampers to mitigate vibrations of high-speed railway bridges", International Journal of Rail Transportation, 5(1):47-62 ,2017.

[12] Yang, M., "Longitudinal vibration control for a suspension bridge subjected to vehicle braking forces and earthquake excitations based on magnetorheological dampers", Journal of Vibration and Control, 22(17): 3659-3678, 2015.

[13] Metin, M., "Raylı sistem araçlarının modellenmesi ve titreşimlerinin kontrolü", M.S. thesis , YTU, Istanbul, 2007.

Automatic Control of Half Barrier Level Crossing Systems and the Risk Model

Oğuz Kırbıyık[1], M.Turan Söylemez[2]

[1,2] Control and Automation Engineering Department
Istanbul Technical University
oguzkirbiyik@gmail.com, soylemezm@itu.edu.tr

Abstract

Level crossing systems are very important in rail transportation. A level crossing system exists at the intersection of a road and a railway. Therefore, there are many associated risks which cause accidents. Especially, safety has gained more importance in rail transport system. In this paper, risk analysis for an automatic half-barriered level crossing system is done. First, the risk index in a level crossing system is specified. Possible failure scenarios for level crossing system and failure rates are then defined using FMEA and FTA risk analysis methods. Especially, precautions for blocking zigzag manuvours of drivers at automatic half-barrier level crossing system are specified. SIL safety system analysis is done for a half-barrier level crossing system. System requirements for an automatic half-barriered level crossing system is specified and lastly an automatic half-barrier level crossing system is designed.

1. Introduction

A level crossing is defined as the intersection of railway and road. Precautions must be taken to prevent accidents in a level crossing area. Level crossing systems are used in different types of structures in the world such as barriers and gated crossing, open crossings and pedestrian only crossings [1].

Almost all automatic level crossing systems have railway vehicle detection devices. These can be track circuits or axle counters for continuous train detection, or short track circuits, vehicle loops, wheel sensors or balises for spot detection. The location of the detection devices for a train approach depend on the length of level crossing and the use of barriers. The devices for detecting outgoing trains should be near to the level crossing [2].

An automatic level crossing system usually comes with an automatic train protection system (ATP). When the train approaches to the level crossing area, the speed of the train is supervised by the ATP. The aim of using ATP is to minimize possible accidents [2].

2. Risk Analysis

Risk is the combination of two elements. The first is the probability of occurrence of an event or combination of events leading to a hazard. The second is the consequence of the hazard [3]. Risk analysis considers various phases of the system life cycle and it shall be well documented. The documentation shall contain an analysis methodology, assumptions, limitations and justification of the methodology, hazard identification results, risk estimation results and their confidence levels, results of trade-off studies, data, their sources and confidence levels and references [3].

Table 1 provides typical categories of probability or frequenecy of occurrence of a hazardous event and a description of each category for a railway system [3].

Table 1. Frequency of occurrence of hazardous events

Category	Description
Frequent	Likely to occur frequently. The hazard will be continually experienced.
Probable	Will occur several times. The hazard can be expected to occur often.
Occasional	Likely to occur several times. The hazard can be expected to occur several times.
Remote	Likely to occur sometime in the system life cycle. The hazard can reasonably expected to occur.
Improbable	Unlikely to occur but possible. It can be assumed that the hazard may exceptionally occur.
Incredible	Extremely unlikely to occur. It can be assumed that the hazard may not occur.

Tablo 2 describes typical hazard severity level. Hazard severity level used to estimate the likely impact [3].

Table 2. Hazard severity level

Severity Level	Consequence to Persons or Environment	Consequence to Service
Catastrophic	Fatalities and/or multiple severe injuries and/or major damage to the environment.	
Critical	Single fatality and/or severe injury and/or significant damage to the environment	Loss of a major system
Marginal	Minor injury and/or significant threat to the environment	Severe system(s) damage
Insignificant	Possible minor injury	Minor system damage

The frequency – consequence matrix is used for the evaluation of the result of risk analysis, risk categorization, risk reduction or elimination of intolerable risks and risk acceptance [3]. A frequency – consequence matrix is shown in Table 3 [3].

Qualitative categories of risk contains risk category and actions to be applied against each category. Some qualitive risk categories are shown in Table 4 [3].

Table 3. Frequency – consequence matrix

Frequency of occurrence of a hazardous event	Risk Levels			
Frequent				
Probable				
Occasional				
Remote				
Improbable				
Incredible				
	Insignificant	Marginal	Critical	Catastrophic
	Severity Levels of Hazard Consequence			

Table 4. Qualitative risk categories

Risk Category	Actions to be applied against each category
Intolerable	Shall be eliminated
Critical	Shall only be accepted when risk reduction is impracticable and with the agreement of the Railway Authority or the Safety Regulatory Authority
Marginal	Acceptable with adequate control and with the agreement of the Railway Authority
Insignificant	Acceptable with/without the agreement of the Railway Authority

Typical example of risk evaluation and acceptance shown in Table 5 [3].

Table 5. Frequency – consequence matrix

Frequency of occurrence of a hazardous event	Risk Levels			
Frequent	Condition 3	Condition 4	Condition 4	Condition 4
Probable	Condition 2	Condition 3	Condition 4	Condition 4
Occasional	Condition 2	Condition 3	Condition 3	Condition 4
Remote	Condition 1	Condition 2	Condition 3	Condition 3
Improbable	Condition 1	Condition 1	Condition 2	Condition 2
Incredible	Condition 1	Condition 1	Condition 1	Condition 1
	Insignificant	Marginal	Critical	Catastrophic
	Severity Levels of Hazard Consequence			

Conditions are defined as follow:

- Condition 1: Negligible
- Condition 2: Tolerable
- Condition 3: Undesirable
- Condition 4: Intolerable

Failure Modes and Effect Analysis (FMEA) is a product development management procedure that classifies a system by its probabilities and similarities to analyze the types of potential faults. A successful failure type analysis helps identify fault types based on past experiences of similar products or processes. The FMEA is also an iterative process that is updated as the design develops. Design changes will require that relevant parts of the FMEA be reviewed and updated.

FMEA is conducted by a team that has a product experts. This team recognize and evaluate consequences of different kind of failures. This kind of team work can provide required expertise on topic.

FMEA provides a list of failure modes and the effect of these failure modes on the system.

In industry and product design FMEA is commonly used technique. FMEA has application special worksheet design. FMEA table design can be change with the type of application. Example of FMEA worksheet shown in Table 6 [4].

Table 6. Example of FMEA worksheet

No	Failure	Effects	Components	Risk Evaluation WITHOUT Mitigation			Mitigation Measures	Risk Evaluation WITH Mitigation		
				Severity	Frequency	Risk Level		Severity	Frequency	Risk Level
1										
2										
3										

Fault tree analysis (FTA) is a common method of interacting with the system. Fault tree analysis can be used qualitatively for each system. Fault tree analysis accounts for the error quantitatively. Qualitative and quantitative definitions made are systematically analyzed by FMEA analysis [4].

Fault tree analysis is a method in which the logic relationships between the faults, components, and other conditions in the subsystem are formed. Example of a fault tree analysis shown in Figure 1 [4].

Safety integrity level (SIL) is an important safety step for railway systems. According to the SIL level calculation, the possibility of error of the functional units can be calculated in detail.

The safety integrity level is based on the European functional safety standard IEC 61508. The IEC 61508 standard defines 4 SIL levels. SIL 1 is the lowest safety level and SIL 4 is the highest safety level. SIL 0 can be considered as no safety requirements for the system.

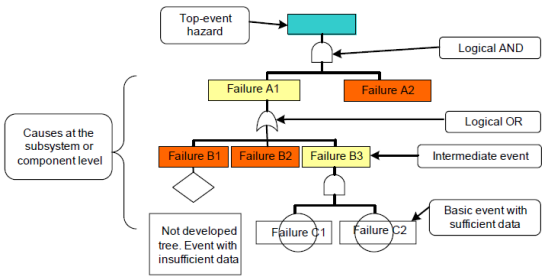

Fig. 1. Example of fault tree analysis

Tolerable hazardous rates (THR) have been determined for each railway equipment in railway systems.

The composition of two independent items in an AND gate the basic formula for THR for highly available systems can be used. The simple formula for THR equation with the AND gate of two independent parts is shown below.

$$THR_S \approx \frac{FR_A}{SDR_A} x \frac{FR_B}{SDR_B} x(SDR_A + SDR_B)$$
$$SDR_S \approx (SDR_A + SDR_B) \quad (1)$$

Where THR is the tolerable hazardous rates; FR stands for potential hazardous failure rates and SDR is expressed as equivalent safe down rate [5].

The SIL table is shown in Table 7 [5].

Table 7. SIL Table

THR (h^{-1})	SIL
$10^{-9} \leq$ THR < 10^{-8}	4
$10^{-8} \leq$ THR < 10^{-7}	3
$10^{-7} \leq$ THR < 10^{-6}	2
$10^{-6} \leq$ THR < 10^{-5}	1

3. Application of Automatic Control of Half Barrier Level Crossing System

FMEA should be done first when performing the safety analysis of automatic control of half barrier level crossing system. First of all, possible accidents that may occur for the level crossing system should be indicated. The calculation of the safety level crossing system should be made using the fault tree analysis in the FMEA analysis table. After fault tree analysis is performed, the SIL level of automatic control of half barrier level crossing system should be calculated. FMEA analysis carried out again if any error occurs after the level crossing system is installed. Risk evaluation with mitigation is done in the FMEA table. The SIL is recalculated. With the SIL account, the optimum level of safety of the system is determined.

Possible error scenarios for the automatic half level crossing system should be defined. Possible error scenarios are:

- Error 1: Poor visibility
- Error 2: Sunlight
- Error 3: No pay attention to the next train
- Error 4: Ground
- Error 5: Car and train collision
- Error 6: Car malfunction
- Error 7: Behind the car and train collision
- Error 8: Using of the road unsafety
- Error 9: Occurrence of an error during manuel control of level crossing system
- Error 10: Signal failure
- Error 11: Machinist failure
- Error 12: Barrier failure
- Error 13: Fracture of the barrier arm

All error probabilities were generated as a result of FMEA analysis. The error rates for errors in the automatic half level crossing systems are shown in Table 8. The numerical values shown in Table 8 are based on the opinions of railway personnel who are experienced in the level crossing systems.

Table 8. Automatic half level crossing system failure rates

Fault No	Fault	Frequency	Probability of fault (1 year = 8760 hour)	Tolerable Hazardous Rate (λd) (THR)
1	Poor visibility	1	4.00	2.85388E-05
2	Sunlight	1	4.00	2.85388E-05
3	No pay attention to the next train	1	20.00	5.70776E-06
4	Ground	1	20.00	5.70776E-06
5	Car and train collision	1	4.00	2.85388E-05
6	Car malfunction	1	20.00	5.70776E-06
7	Behind the car and train collision	1	20.00	5.70776E-06
8	Using of the road unsafety	1	0.75	0.000152207
9	Occurrence of an error during manuel control of level crossing system	1	20.00	5.70776E-06
10	Signal failure	1	4.00	2.85388E-05
11	Machinist failure	1	4.00	2.85388E-05
12	Barrier failure	1	4.00	2.85388E-05
13	Fracture of the barrier arm	1	0.75	0.000152207

The possible failure rate equation that can occur as a result of the vehicle drive fault in the level crossing zone is shown is equation 2 and the vehicle drive failure rate in equation 3.

$$\lambda_{Ddrive\_failure} = (\lambda_{Dh1} \times \lambda_{Dh2}) + (\lambda_{Dh4} \times \lambda_{Dh5}) + (\lambda_{Dh3} \times \lambda_{Dh6} + \lambda_{Dh7}) \quad (2)$$

$$\lambda_{Ddrive\_failure} = 9.7736 \times 10^{-10} \quad (3)$$

The possible failure rate that can result in misuse of the road by driver in the level crossing area is given equation 4.

$$\lambda_{Dusing\_of\_the\_road\_unsafety} = 0.00015 \quad (4)$$

The possible failure rate equation that can be the result of railway personnel's failure in the level crossing area is given equation 5 and the personnel failure rate in equation 6.

$$\lambda_{Dpersonnel\_failure} = \lambda_{Dh9} + \lambda_{Dh10} + \lambda_{Dh11} \quad (5)$$

$$\lambda_{Dpersonnel\_failure} = 6.2785 \times 10^{-5} \quad (6)$$

The possible failure rate equation, which may be result of equipment failure in the level crossing system in the level crossing area, is given in equation 7 and the driver failure rate in equation 8.

$$\lambda_{Dequipment\_failure} = \lambda_{Dh12} + \lambda_{Dh13} \quad (7)$$

$$\lambda_{Dequipment\_failure} = 4.3438 \times 10^{-9} \quad (8)$$

The probability of collision of the car with the train in the level crossing area is given in equation 9.

$$\lambda_{Dcollision} = \lambda_{Ddrive\_failure} + \lambda_{Dusing\_of\_the\_road\_unsafety} + \lambda_{Dpersonnel\_failure} + \lambda_{Dequipment\_failure}$$
$$\lambda_{Dcollision} = 2.15 \times 10^{-4} \quad (9)$$

When the whole level crossing system is examined, it seems that the level crossing system does not satisfy any of the SIL levels.

- It must provide the SIL level required for the drive failure.
- It is necessary to improve precautions agains the zigzag maneuvers in order to abuse the level crossing road.
- The manuel control should be removed to reduce the railway personnel fault, the equipment should be upgraded for signal / protective fault and the level crossing system should be rectified so that there is no fault of the train driver.
- It must provide the SIL level required for the level crossing equipment failure.

The SIL level needs to be upgraded to improve the railway system. Using of the road unsafety, signal failure and machinist failure must be regulated in FMEA analysis. Besides, manuel control system will be removed in the level crossing system. Instead, an automatic control system will be created in the level crossing system.

With the updated FMEA analysis, possible failure rates in the level crossing system were determined. FTA analysis was performed again. Manual control in the level crossing system was removed in the updated FMEA analysis.

One of the most important accident factors for automatic level crossing system is that the vehicle drivers zigzag in the level crossing zone. In order to prevent this situation, the fault situation in the FTA analysis has been examined in more detail.

FTA analysis with mitigation is required to raise the SIL level. The failure rates for the FTA analysis with mitigation are shown in Table 9.

Table 9. Failure rates with mitigation

Fault No	Fault	Frequency	Probability of fault (1 year = 8760 hour)	Tolerable Hazardous Rate (λd) (THR)
1	Poor visibility	1	4.00	2.85388E-05
2	Sunlight	1	4.00	2.85388E-05
3	No pay attention to the next train	1	20.00	5.70776E-06
4	Ground	1	20.00	5.70776E-06
5	Car and train collision	1	4.00	2.85388E-05
6	Car malfunction	1	20.00	5.70776E-06
7	Behind the car and train collision	1	20.00	5.70776E-06
8	Using of the road unsafety	1	300	3.80518E-07
9	Signal failure	1	300	3.80518E-07
10	Machinist failure	1	300	3.80518E-07
11	Barrier failure	1	4.00	2.85388E-05
12	Fracture of the barrier arm	1	0.75	0.000152207

As a result of probability of fault increase, tolerable hazardous rate (THR) has decreased considerably. As a result of THR reduction, safety integrity level (SIL) increases in level crossing system.

In order to be able to get ahead of the zigzag situation, it is necessary to comply with the specified rules, especially the car driver. These rules;

- According to the signs on the road, the car must stop.
- The car must stop at the position where the train will not crash.
- There should be no trains in level crossing zone. However, the train may approach the level crossing zone. If there is a train in level crossing zone, the car driver must stop in front of the level crossing zone [8].

In order to minimize the personnel fault on the railway, the manuel control on the level crossing system has been removed. The flow chart diagram of automatic control of half barrier level crossing system is shown in Figure 2.

$$\lambda_{Dpersonnel\_failure} = \lambda_{Dh9} + \lambda_{Dh10} \quad (10)$$

$$\lambda_{Dpersonnel\_failure} = 7.6104 \times 10^{-7} \quad (11)$$

The probability of collision between the car and the train in the level crossing zone is given in Equation 12.

$$\lambda_{Dcollision} = \lambda_{Ddrive\_failure} + \lambda_{Dusing\_of\_the\_road\_unsafety} + \lambda_{Dpersonnel\_failure} + \lambda_{Dequipment\_failure}$$
$$\lambda_{Dcollision} = 1.1469 \times 10^{-6} \quad (12)$$

When all calculations are made it appears that the level crossing system is at SIL 2 safety level.

A schematic representation of the automatic control of half barrier level crossing system is shown in Figure 3.

The barrier closure times must be optimally adjusted to prevent zigzag maneuvers of the vehicle. The train will stop before danger zone if a car is in danger zone after the barriers are closed.

The barriers will close when the train arrives at the activation zone. The signal will be green when the barrier closed and the train will travel safely in danger zone. The barriers will be opened when the train leaves the danger zone.

If the barriers do not close when the train arrives at the activation zone or there is an error in the danger zone, the signal will be red. If the train is in the approach zone, automatic train protection (ATP) will be enable and the train will be stop.

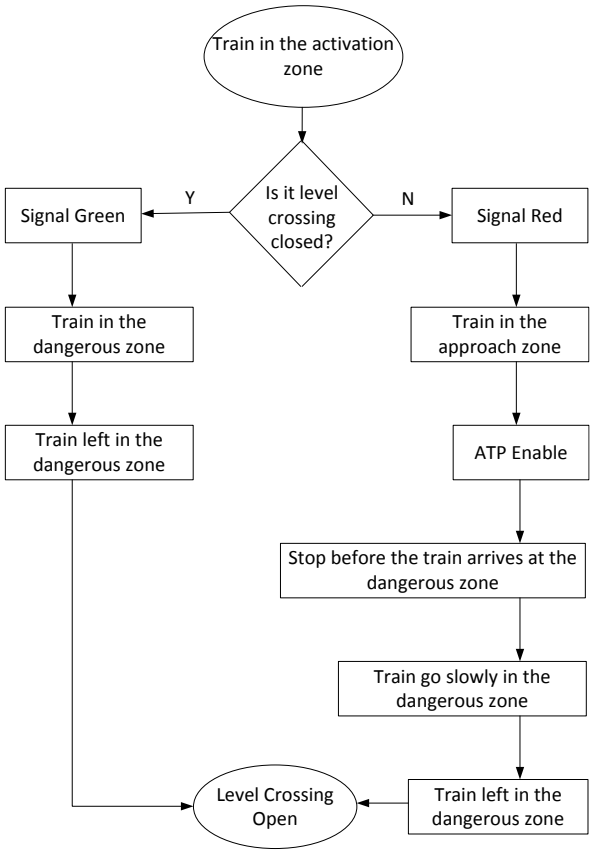

Fig. 2. Flow chart of automatic control of half barrier level crossing system

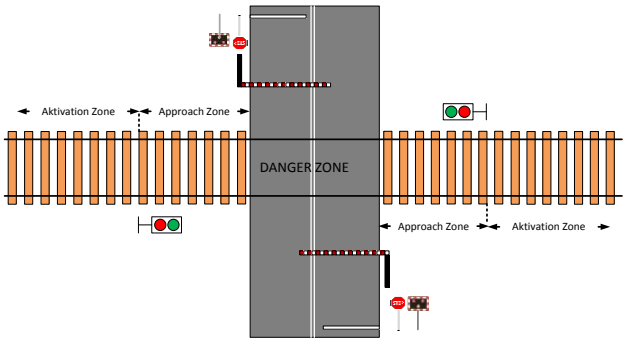

Fig. 3. A schematic of automatic control of half barrier level crossing system

4. Conclusions

In this study, it is focus on level crossing systems. The definitions of the level crossing systems have been made and their varieties are emphasized. The control steps for the level crossing system have been expressed in detail.

The automatic half barrier level crossing system, which is a subset of the level crossing system, has been dealt with in detail. Risk analysis has been carried out for the automatic half barrier level crossing system and the possible accident scenarious have been expressed in detail. The safety analysis of the automatic half barrier level crossing system was performed using the FMEA and FTA methods from risk analysis evaluation methods.

The final SIL level for the level crossing system was found by carrying out a risk analysis of the automatic half barrier level crossing system.

5. References

[1] <https://tr.scribd.com/document/262768343/10692-Level-Crossing-User-Guide>, erişim tarihi 18.10.2016.

[2] UIC 761 (2004). International Union of Railways: Guidance on the automatic operation of level crossigns.

[3] BS EN 50126-1 (1999). Railway Applications – The Specification and Demonstration Reliability, Availability, Maintainability and Safety (RAMS) – Part 1: Basic Requirements and Generic Process. London: British Standards Institution (BSI).

[4] BS EN 50126-2 (2007). Railway Applications – The Specification and Demonstration Reliability, Availability, Maintainability and Safety (RAMS) – Part 2: Guide to the Application of EN 50126-1 for Safety. London: British Standards Institution (BSI).

[5] BS EN 50129 (1999). Railway Applications – Communication, Signalling and Processing Systems – Safety related Electronic Systems for Signalling. London: British Standards Institution (BSI).

[6] BS EN 60812 (2006). Analysis Techniques for System Reliability – Procedure for Failure Mode and Effects Analysis (FMEA). London: British Standards Institution (BSI).

[7] BS EN 61025 (2007). Fault tree analysis (FTA). London: British Standards Institution (BSI).

[8] SELCAT (2006). Safer European Level Crossing Appraisal and Technology, D3 – Report on risk modeling techniques for level crossing risk and system safety evaluation.

[9] An, M. (2005). A review of design and maintenance for railway safety – the current status and future aspects in the UK railway industry. World Journal of Engineering, Vol.2(3), pp.10-22.

[10] An, M. Lin ve W., Huang, S (2013). An Intelligent Railway Safety Risk Assessment Support System for Railway Operation and Maintenance Analysis. The Open Transportation Journal, Vol.7, pp.27-42.

[11] Boulanger, J. L. (2005). Brail – Requirement Analysis, IADIS Virtula Multi Conference on Computer Science and Information System 2005. Proceedings of the Third International Conference on GeoComputation, (pp.343-348). France : Universite de Technologie de Compiegne.

[12] Ghazel, M. & Koursi, E. M. E. (2007). Automatic level crossings: from informal functional requirements' specifications to the control model design, *IEEE International Conference on System of Systems Engineering*, (pp. 1-6). Villeneuve d'Ascq, France, April.

[13] Gofuku, A., Koide, S. & Shimada, N. (2006). Fault tree analysis and failure more effects analysis based on multi-level modeling and causality estimation. *In:* SICE-ICASE, 2006. International Joint Conferencei 2006. IEEE, 497-500.

[14] Kohda, T., & Fujihara, H. (2008). Risk analysis of level crossing accidents based on systems control for safety.*Proceedings of the Institution of Mechanical*

Engineers, Part O: Journal of Risk and Reliability, (pp.419-429).

[15] Medikonda, B. B. S., Ramaiah, P. S. & Gokhale, A.. (2011). FMEA and Fault Tree based Software Safety Analysis of a Railroad Crossing Critical System, *Global Journal of Computer Science and Technology.*

[16] Ortmeier, F. & Schellhorn, G. (2007). Formal Fault Tree Analysis: Practical Experiences. *Electronic Notes in Theoretical Computer Science*, (pp.139-151). July 13.

Increasing The Electrical Energy Efficiency In Urban Rail Systems

Ahmet YILDIZ[1], Oktay ARIKAN[2]

[1]Metro Istanbul, Yenikapı Campus, Turkey
Ahmetyldz91@gmail.com
[2] Yıldız Technical University, Davutpasa Campus, Turkey
oarikan@yildiz.edu.tr

Abstract

Energy conservation plays a big role in all systems where electricity energy is used and it is important to work on energy conservation as it requires great power in Railway Mass Transit systems as well. International Association of Public Transport (UITP) and International Railways Association (UIC) have recently made these work a current issue and aimed at creating a standardization. However, in a context characterized by increasing capacity demands and rising energy costs, and where other transport modes are considerably improving their environmental performance, urban rail must minimize its energy use without affecting its service quality. Istanbul urban rail public transport system, which is approximately 149 kilometers long, consumes nearly 300 million kWh annually. Urban rail energy consumption is defined by a wide range of interdependent factors. Therefore a system wide perspective is required, rather than focusing on energy savings at subsystem level. In this study, a brief summary of the current efforts to reduce the total energy consumption of urban rail transport systems is given. In addition, simulations were carried out with the help of the Rail-Sim program to demonstrate the effects of train weight changes and jumpered of catenary lines for the selected sample area between Yenikapı-Bayrampaşa stations.

1. Introduction

Transport and energy politics have a direct impact on human life. Regardless of age and activity, energy and mobility play a fundamental role in human life. Mobility is the key of the quality of life and is the backbone of the economy [1]. However, transport is currently one of the most energy-consuming and polluting sectors in both developing and developed countries. In the European Union (EU), for instance, it causes approximately 31% of total greenhouse gas (GHG) emissions [2]. Within this sector, metropolitan transportation is responsible for about 25% of total CO_2 emissions [3]. Additionally, high levels of air pollution and congestion are major issues related to transport in urban areas. Therefore in a worldwide context of growing urbanisation, the implementation of efficient, reliable and environmentally friendly transport systems becomes imperative not only to meet the international agreements on GHG emissions reduction [4,5], but to guarantee livable conditions in urban areas. In this vein, the EU aims at halve the use of oil-fuelled vehicles in urban transport by 2030 and eventually phase them out in urban centres by 2050 [3]. Instead, cleaner metropolitan public transport systems are being strongly promoted.

Urban rail is regarded as an ideal solution to reduce the impact of urban mobility because of its great capacity, safety, reliability and excellent environmental performance. Urban rail systems have been gaining increasing appeal as effective and sustainable methods of mass-transport fort he last decade in Istanbul, as shown in Fig.1.

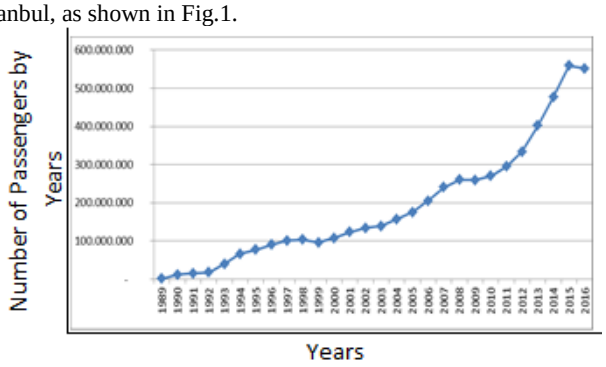

Fig. 1. Evolution of Urban Rail Transport Demand in Istanbul

Istanbul urban rail public transport system, which is approximately 149 kilometers long, consumes nearly 300 million kWh annually. Consumed energy distributions vary on tram and subway lines. For example, 55% of the energy consumed on subway lines is used for trains to move, while 45% is used for internal needs. For rail systems such as trams, this ratio is used as 95% for trains and 5% for internal requirements. Along with the railed systems that continue to be constructed rapidly, Istanbul is planning to complete many new lines at the final destination after 2023. However, the length of the line is expected to be 1000 km. Thus, energy saving studies are very important in rail systems.

International Railways Association (UIC – www.uic.asso.fr) had established a committee to investigate approaches and technologies which are applicable to rail transportation systems. This committee published its report in March 2003, and identified various technology and approaches that have been put into practice so far and that have potential benefits [6]. Similarly, International Association of Public Transport (UITP – www.uitp.com) has been working on measures to reduce energy consumption in urban public transport systems through its members [7].

Urban rail systems consist of different sub-systems where energy consumption is linked such as rail network, trains, signaling, electrification and communication. Since the interactions of these subsystems are complex, the effects on energy consumption are also complex. Therefore, what is

needed is a global perspective ensuring that the introduction of new measures reduces the energy consumption at system-level, rather than concentrating on individual energy efficiency solutions that may compromise other aspects of the system performance.

Energy efficiency studies in urban rail systems are generally based on; braking energy recovery, energy storage systems, energy-saving driving methods, energy-efficient traction systems, energy-optimised timetables, smart energy management in fixed facilities etc. Some of the studies made on this subject are summarized below.

In a study by Hansang Lee and et al in 2013, it had been proved that the peak power reduction and energy efficiency improvement can be achieved by using 100 kWh superconducting flywheel energy storage systems (SFESs) with the optimally controlled charging or discharging operations. FESSs are projected to be used in the Daejeon Metro system, which has 7 transformer centers and 22 stations. As a result of the study, peak power decreased from 9334 kW to 5959 kW by 36.7% with 360 s headway time. This means that the cost of energy is reduced by 36.7%. [8].

In Yuuki Lino et al.'s work, the performance results of a storage system built using Lithium-Ion batteries at Haijima and Okegawa transformer centers are shared. The annual amount of the discharged energy from the energy storage system at Haijima SS (SS: Substation) is 400 MWh/year. And it is approximately 4% of the total traction energy over the year at Haijima SS. In addition, the annual amount of the discharged energy from the energy storage system at Okegawa SS is 750 MWH/year. And it is approximately 8% of the total traction energy over the year at Okegawa SS [9].

In a study by Shuqi Liu and his colleagues, a more accurate model of the train energy consumption is presented by considering the control strategy of Automatic Train Operation (ATO). Two modifications of Tabu Search (TS) algorithm, which are named as Acceleration Rate Decided Modification (ARDM) and Distance Decided Modification (DDM), are proposed to optimize train recommended speed curve based on the presented model. To verify the effectiveness of the proposed approach, case studies are conducted based on Beijing Subway. The train operation is optimized for the section between Jinghailu and Ciqunan stations. The percentage of traction energy reduction optimized by the TS algorithm with DDM is %8,93 and the percentage of traction energy reduction optimized by the ARDM is %2,54 [10].

In another study by Gerben M. and Rob M. P, they investigated the effect of a decrease in headway time from 300 seconds to 270 seconds. In this case, compared to mechanical braking, regenerative braking has increased from 18% to 25% but overall energy consumption has increased. [11].

In order to demonstrate the effect of vehicle weight on energy consumption, the number of passengers in the train was increased by 50 from empty car to full load and tested. In the simulations the passenger weight has been taken as 71 kg. As a result of the simulation, the vehicle weight increased by 60% from empty to full load, while the increase in energy consumption was found to be 42%. For person*km, it is observed that the energy consumption was about 10 Wh/person*km in the case of 250 passengers and it decreased to 3.30 Wh/person*km in case of 1000 passengers [12].

In the study carried out by Açıkbaş, using the SimuX program, feeding systems of 750 VDC and 1500 VDC were compared by considering various parameters. Tests has been carried out by taking into account 2 different headway time (TH) as 150 s and 300 s, and two different load conditions, fully loaded (FL = 271 tonnes) and half loaded (HL = 219 tonnes). As a result, it has been indicated that the 1500 VDC system has many advantages over the 750 VDC system. In this study, which was made with the data about Üsküdar-Ümraniye Metro line planned to be made Anatolian side of Istanbul, it was determined that the saving to be obtained 10% when the feeding system is selected as 1500 VDC instead of 750 VDC. Similarly, in the study conducted with the data concerning the Kadıköy-Kartal line, it is estimated that annual savings will be realized as 12.5 million kWh in operating conditions of 2025. [13].

In an application for auxiliary systems, the application of the frequency converter for 85 escalators in Taksim-4.Levent metro has been started and thus, the escalators can be operated at double speed and it can be moved at 0.16 m/s when there is no passenger. Some measurements show that the escalators save 40% on energy consumption.

In terms of energy saving, it is important that railway vehicles are made with materials that reduce their tare mass during the production phase. Some examples of mass reductiton projects using lightweight materials in urban rail include the following: development of composite grab rails (50% lighter than existing stainless steel bars) [14], replacement of current floor planes by 40% lighter sandwich constructions [15], development of a crashworthy driver's cab using advanced composite sandwich materials up to %40 lighter [16]. These measures should be primarily implemented at design stages, although retrofitting may be also viable in some cases.

This paper has introduced energy efficiency enhancement methods used in urban rail systems. Simulations were performed using Rail-Sim software for the Yenikapı-Bayrampaşa line selected as a sample. The results obtained by examining the effect of train weight changes and jumpered of catenary lines on the power consumption and the voltage level are presented.

2. Methods of Increasing Energy Efficiency In Railway Systems

Many applications are being made to improve energy saving in urban rail transportation systems. Commonly used methods are presented below.

Recovering of Braking Energy: Trains that capable of regenerative braking can return a large portion of the energy taken during braking phase into the supply line.

Energy Storage Systems: The energy released during braking phase can be used by another train in the same electric section or stored and used as needed.

Energy-Saving Driving Methods: It refers to the group of techniques intended to operate rail vehicles as efficiently as possible while ensuring the safety and punctuality of services.

Adjusting the Headway Time: Adjusting the headway time ensures that the regenerative energy generated by trains during braking can be used more efficiently.

Optimized Train Speed management: Taking into account all the relevant parameters, ensuring that the train travels at optimum speed during its movement.

Energy Transmission with Superconducting Cable: Superconducting transmission lines have a tremendous size advantage and lower total electrical losses for high capacity transmission plus a number of technological advantages compared to solutions based on standard conductors.

Energy Saving Approaches on Auxiliary Facilities: More efficient usage of such systems elevator, escalator, heating, cooling, ventilation, lighting etc. provides great energy savings.

Energy transmission with high voltage: In terms of reducing line losses, high voltage energy transmission provide an advantage.

3. System Overview

In this study, the part between Yenikapı-Bayrampaşa stations is taken as an example system. The total line length at which the simulation is performed is 4206 meters. A schematic representation of the system structure is given in Fig.2. It is also seen in the Fig.2. that two catenary system are jumpered in every 1000 m.

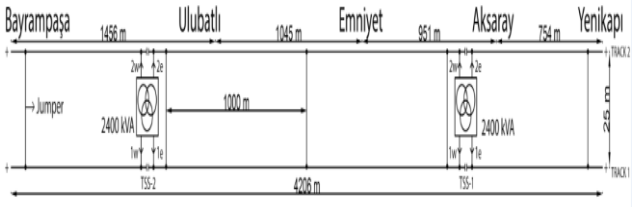

Fig. 2. System Structure Overview (in case of jumpered in every 1000 m)

Since the simulations were carried out for a single train, the actual number of transformers in the system has been changed. The line is fed with 2 transformers at 34,5 kV/2x580 V and 2400 kVA power.

In the model, 4x(4x1x240) mm^2, 2x(5x240) mm^2 and 1x240 mm^2 conductors have been used as the feeder line, return line and jumper, respectively. For 1 km of 1x240 mm^2 copper cable, the resistance value was taken as 87.3 mΩ. The resistances of the conductors were calculated based on this value.

As the train, 4-car Alstom vehicle was selected.

4. Modelling

In the simulation study between Yenikapı-Bayrampaşa stations, all line data were entered with their real values and the results were analyzed by running the Alstom vehicle between these stations with the help of Rail-Sim program.

The line model fed by 2 transformers in Aksaray and Ulubatlı stations is shown in Fig.3.

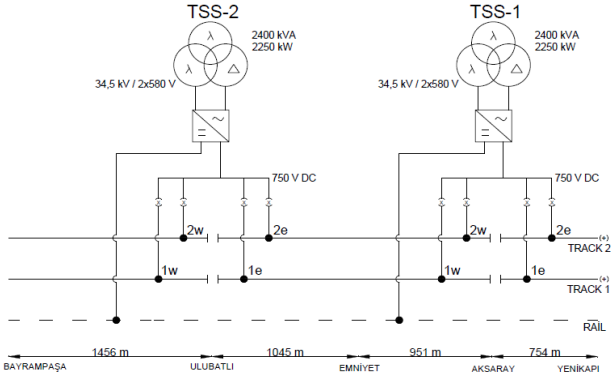

Fig. 3. General Line Structure

Figure 3 shows that the model of the feed structure of the line in which the simulation is performed. The total line length is 4206 meters.

4.1. Jumpering of Catenery Lines

In a double line systems fed by DC voltage, the catenary systems of both lines can be jumpered by insulated cables. Along with the visual advantage, jumpering also provides energy saving. Jumpering of the two catenary systems have the advantages of such increasing the current distribution, reducing the load on the system and reducing energy losses.

The values shown in Tables 1 and 2 are the results of the simulation carried out with the Railsim program between the Yenikapı-Bayrampaşa stations of Istanbul Metro M1 Line. In this simulation all line and train parameters are modeled with their real values. As the train, 4-car Alstom vehicle was selected. The transformer selection and its positioning was done specifically for the work being performed in such a way that it feeds the system in a suitable manner.

An empty train was run between Yenikapı-Bayrampaşa stations and the current, voltage and power values obtained from the output of Aksaray step-down transformer station were presented in Table 1.

Table 1. Values According to Jumper for Aksaray TSS-1

			Without Jumper	2000 m	1000 m	250 m
AKSARAY TSS-1	**Current (I)**	**Min. Value**	200,16	200,14	200,13	200,41
		Max. Value	4309,19	4302,81	4305,87	4283,47
		Averag Value	2401,2	2386,51	2385,4	2377,48
	Voltage (V)	**Min. Value**	762,68	762,73	762,71	762,87
		Max. Value	793,5	793,5	793,5	793,5
		Averag Value	776,99	777,1	777,11	777,17
	Power (kW)	**Min. Value**	158,82	158,81	158,81	159,03
		Maxi. Value	3286,54	3281,88	3284,12	3267,75
		Averag Value	1857,29	1846,27	1845,42	1839,55

According to the results obtained, the average power taken from TSS-1 in normal conditions is 1857.29 kW, while in case of jumpering in every 250 m, it is 1839.55 kW. As seen in the table, the jumpering of DC lines reduced power consumption by 0.95%. Similarly, as the jumpering frequency increases, the average amount of current drawn decreases. Since the parallelism of the lines will reduce the total line resistance, the voltage drop is reduced and the average line voltage is partially increased.

The values values in Table 2 are the results read at the output of Aksaray step-down transformer station during the same simulation. In this case too, the average power and current value decreased as the paralleling frequency increased. 0.69% power savings were achieved in the amount of power drawn.

Table 2. Values According to Jumper for Ulubatlı TSS

			Without Jumper	2000 m	1000 m	250 m
ULUBATLI TSS-2	**Current (A)**	**Minimum Value**	202,65	202,50	202,41	202,63
		Maximum Value	4517,34	4489,61	4486,58	4478,91
		Average Value	2575,57	2559,16	2557,66	2557,11
	Voltage (v)	**Minimum Value**	761,12	761,33	761,35	761,41
		Maximum Value	793,48	793,48	793,48	793,48
		Average Value	775,68	775,81	775,82	775,82
	Power (kW)	**Minimum Value**	160,8	160,68	160,61	160,78
		Maximum Value	3438,24	3418,06	3415,86	3410,28
		Average Value	1991,02	1978,8	1977,69	1977,27

Table 3 shows the lowest voltage levels measured along the line. According to the results, parallelization of the lines reduces the voltage drop. In case of every 250 meters jumpering, the voltage drop was reduced by 6.33%.

Table 3. Minimum Line Voltage

	Without Jumper	2000 m	1000 m	250 m
Minimum Voltage (V)	593,71	628,92	629,55	631,3

4.2. Effect of Increase of Train Mass in Energy Consumption

Lightweight vehicles have lower mechanical resistance than heavyweight ones and require less kinetic energy to achieve the same performance level. Therefore, reducing the total mass of the rail vehicle to the minimum will reduce traction energy consumption. In addition, reducing the mass of the railroad car has less damaging to the road, reducing the wear of the wheels and brakes, thereby reduces operating and maintenance costs of the system.

In order to demonstrate the effect of vehicle weight on energy consumption, the same train was run primarily between Yenikapı-Bayrampaşa stations. Afterwards the train was run at heavy standing (Medium Load) and then full load and the results are given in Table 4.

Table 4. Vehicle Mass Reduction Effect

	Station	**Peak Power**	**Energy Cons.**
		kw	**kwh**
Empty	YENIKAPI-AKSARAY	1972,71	12,21115
	AKSARAY-EMNİYET	1974,32	15,98412
	EMNİYET-ULUBATLI	1973,97	18,44872
	ULUBATLI-BAYRAMPAŞA	1972,98	25,85144
Run Total (With Dwells)		**1974,32**	**75,17543**
Run Total (Without Dwells)		**1974,32**	**72,49543**
Heavy Standing	YENIKAPI-AKSARAY	1968,56	13,23727
	AKSARAY-EMNİYET	1968,73	18,82152
	EMNİYET-ULUBATLI	1968,58	21,84449
	ULUBATLI-BAYRAMPASA	1968,65	31,58588
Run Total (With Dwells)		**1968,73**	**88,16915**
Run Total (Without Dwells)		**1968,73**	**85,48915**
Full Load	YENIKAPI-AKSARAY	1967,25	13,46331
	AKSARAY-EMNİYET	1966,79	19,55884
	EMNİYET-ULUBATLI	1967,11	22,91409
	ULUBATLI-BAYRAMPAŞA	1967,91	33,3916
Run Total (With Dwells)		**1967,91**	**92,00784**
Run Total (Without Dwells)		**1967,91**	**89,32784**

As seen in Table 4, the effect of mass increase on energy consumption is as important as would not be neglected. The total empty weight of the Alstom railroad train is 108,824.00 Kg. The total weight of the train was taken as 157.760,30 Kg and 174.115,10 Kg in the case of heavy standing and in the case of full load, respectively. Based on the energy consumption values of these three different weight states, the full load state was compared with the empty state. In case of the operation With Dwells, approximately 60% increase in mass was increased energy consumption by 22.39%. In the case of Without Dwells, this ratio was calculated as 23.22%.

5. Conclusion

In this study, methods for increasing energy efficiency in urban rail transportation systems, which are becoming increasingly widespread today, have been examined. In addition, with the modeling and simulations for the selected pilot region, effects on energy consumption of catenary jumpering and train weight changes have been demonstrated.

Analyzes have shown that the parallelization of catenary lines reduces the loading of the system and energy losses by increasing the current distribution. In the case of without jumpering of the lines, the average power taken from TSS-1 is 1857.29 kW, while in the case of paralleling in every 250

meters, is 1839.55 kW. The jumpering of the DC lines reduced the power consumption by 0.95%.

According to the test results, parallelization of the lines is reduced the voltage drop. The voltage drop was reduced by 6.33% in case of jumpering in every 250 m.

Simulation results have shown that the increase in train mass is important for energy consumption. Accordingly, in the case of operation With Dwells, approximately 60% increase in mass was increased energy consumption by 22.39%.

The current and voltage values of the dc breaker can be taken with the scada software on the M1 line. Test results can be verified by comparing these values with the simulation data.

As a result of the study carried out, it has been seen that there are many methods used to reduce energy consumption in urban railway systems. For these systems, which are increasing in size and energy consumption, it is revealed that considerable amount of energy saving can be achieved by reflecting the results obtained by calculations and modeling to be done in the design stage.

7. References

[1] "Environmental Guidline for the procurement of new rolling stock, outcome of the UIC project", PROSPE R, Henning Schwatz, DB AG.

[2] IEA and UIC, "Railway handbook 2012 – energy consumption CO_2 emissions", International Energy Agency; 2012. http://www.uic.org/IMG/pdf/iea-uic_energy_consumption_and_co2_emission_of_world_railway_sector.pdf.

[3] European Commission, "Roadmap to a single European transport area – towards a competitive and resource efficient transport system"; 2011. http://eur-lex.europa.eu/LexUriServ/LexUriServ.do?uri=COM:2011:0144:FIN:en:PDF.

[4] Official Journal of the European Union, Decision No 406/2009/EC on the effort of Member States to reduce their greenhouse gas emissions to meet the Community's greenhouse gas emission reduction commitments up to 202; 2009. http://eur-lex.europa.eu/LexUriServ/LexUriServ.do?uri=OJ:L:2009:140:0136:0148:EN:PDF.

[5] European Comission, "A Roadmap for moving to a competitive low carbon economy in 2050" – ref. COM(2011) 112 final; 2011. http://www.eur-lex.europa.eu/LexUriServ/LexUriServ.do?uri=COM:2011:0112:FIN:EN:PDF.

[6] http://www.railway-energy.org/tfee/index.php, Son erişim Ocak 2008.

[7] International Metropolitan Railways Committee, 1997. Public Transport: "The environment and economic efficiency", Part 2, UITP 52. International Congress, Stuttgart.

[8] H.Lee, S. Jung, Y. Cho, D. Yoon, G.Jang, "Peak Power Reduction and Energy Efficiency Improvement With The Superconducting Flywheel Energy Storage In Eelctric Railway System", Physica C 494 (2013) 246-249

[9] Lino Y., Hayashiya H., Hino M., Abe S., Nakao K., Kudo K. "Evaluation of installation effect of the energy storage system in D.C. traction power supply system", 2006. Pages: 280 - 285, DOI: 10.1109/EPEPEMC.2016.7752011.

[10] Liu S., Cao F., Xun J., Wang Y. Energy-Efficient operation of single train based on the control strategy of ATO", 2015. 2015 IEEE 18th International conference on Intelligent transportation systems, 2580 – 2586, DOI: 10.1109/ITSC.2015.415

[11] Hathway R. "Energy efficient train regulation on the Victoria line". In:IMechE Railway Division Seminar ''gaining traction in energy Efficiency'', London, UK; 2012.

[12] Açıkbaş S. "Çok Hatlı Çok Araçlı Raylı Sistemlerde Enerji Tasarrufuna Yönelik Sürüş Kontrolü", Haziran 2008.

[13] Açıkbaş S., Turan Söylemez M. "Energy Loss Comparison Between 750 VDC and 1500 VDC power supply systems using rail power simulation".

[14] Carruthers JJ, Calomfirescu M, Ghys P, Prockat J. "The application of a systematic approach to material selection for the lightweighting of metro vehicles", P I Mech Eng F-J Rai 2009;223:427-37.

[15] Hudson CW, Carruthers JJ, Robinson AM. "Multiple objective optimisation of composite sandwich structures for rail vehicle floor panels". Compos Struct 2010;92:2077-82.

[16] Carruthers J, O'Neill C, Ingleton S, Robinson M, Grasso M, Roberts J, et al. "The design and prototyping of a lightweight crashworthy rail vehicle driver's cab". In: 9th World congress on railway research – WCCR 2011, Lille, France; 2011.

Statistical Analyses and Polynomial Regression for Image Processing based Railway Track Segmentation

M. Alper SELVER[1], Burak BELENLIOGLU[2], Sinan DOGAN[2], and E. Yesim ZORAL[1]

[1] Dokuz Eylül University, Electrical and Electronics Engineering Department, Buca, Izmir, TURKEY
alper.selver@deu.edu.tr, yesim.zoral@deu.edu.tr
[2] Kentkart Research & Development Dept. Kahramanlar Mahallesi Mürselpaşa Bulvarı No: 163, Izmir, Turkey
burak.belenlioglu@kentkart.com.tr, sinan.dogan@kentkart.com.tr

Abstract

Determining the alignment of the rails is a key component of obstacle detection systems, which aim to detect the potential accidents by determining the objects around the tracks. Effective extraction of the rails through a camera faces many challenges due to weather, illumination, and structural conditions. Moreover, the process should be completed almost in real time with minimum dependence to knowledge about the train speed or the camera parameters. Therefore, several methods are developed for track extraction. However, none of these has achieved a perfect result at all challenges. Thus, the extraction should be rectified with an analytic representation of the tracks in order to compensate errors. In this study, a statistical analysis is carried out to model different turns in the same video by using polynomial regression and neural networks. The system is evaluated by concatenating it to an advanced system.

1. Introduction

Camera based condition monitoring through driver support systems is a key component of intelligent railway systems [1, 2]. The extraction of railways is a part of this monitoring and provides useful information for obstacle detection [3], range determination [4], road-sign recognition [5], collision prevention [6], self-localization [7] and offline analysis [8]. In a single video frame of a monocular camera, the rails constitute two stripes, Moreover, the railways have smooth curvatures and their thicknesses get thinner as the distance from the camera increases. Thus the rail extraction is studied with many different approaches such as multi-scale filtering [9], template matching [10], Edge-detection followed by merging via Hough Transform [11]. Unfortunately, in none of these studies, the challenges are completely resolved.

To refine faulty image processing results, modeling approaches are employed such as clothoids [12], recursive estimation of spline curves [13], and high order polynomial fitting [9]. Although these techniques improve the accuracy and reliability of track extraction approaches, they are founded on qualitative descriptions or knowledge about the tracks and empirical assumptions that relies on observations such as the classification of a frame into sub-segments, which would suppose to carry a specific type of track information.

Despite the continuous connected component structure of a track, its visual appearance may be discontinuous due to external effects such as shadows, inverse illumination, level crossings etc. Moreover, the smoothness, limited-curvature and composite structure of the rails enable the use of first and second order functions to model their shape, rather than the use of pixel based classification techniques. Accordingly, this study aims to statistically quantify the curvature of railway tracks by manually delineating several left and right turns during a journey video in order to construct the ground truth. Based on the statistical analysis performed on this ground truth, a polynomial fitting procedure is applied to represent the track with am analytical form. The coefficients of the polynomials are analyzed; conclusions are drawn. Based on these outcomes, a new method is proposed for railway extraction, which exploits the use the coefficients of previously fit polynomial tracks to regularize the initial result of any image processing method by machine learning.

In the rest of this paper, image processing based rail

(a) (b) (c) (d)

Fig. 1. Examples for the challenges of railway extraction: a) raindrop blocking track b) varying birghtness of the track as the distance from the camera increases, c) dirty camera and motion blur, d) crossing railway tracks.

extraction is described in Section 2. Section 3 introduces the results of the statistical analysis and Section 4 presents the application results. Finally, Section 5 draws the conclusions.

2. Image Processing for Railway Extraction

The data set used in this study is a collection of publicly available cabin view videos, details of which are given in [9]. The challenges of image processing based railway extraction can be shortly summarized as non-uniform illumination effects and shadows, which cause causes varying brightness levels for rails; motion blur due to speed and vibrations; weather conditions such as snow or rain, which can cause physical effects blocking the lens view. Furthermore, the turns and level crossings at the railway can appear as blurry and with poor contrast especially at remote corners. These effects are further increased if the tracks are covered by rust or vegetation.

The method used in this study for extracting the railways from video frames include four main parts as; pre-processing, railway extraction, post-processing and model fitting as described in [9]. In this system, the images are pre-processed by separating the video frames into color channels and each image is divided into for sub-regions as as near, far, remote and horizon according to their distance from camera.

After the pre-processing, pre-defined multi-scale and multi-directional Gabor filters are used to obtain the edges in the image (Fig. 2.a). These filters are adjusted to specific angular intervals determined for each sub-region (near, far remote) such that the filters have limited angular selectivity that is specifically designed for track curvature characteristics at the corresponding sub-region. Gabor filters are chose among many ones in wavelet family other due to their superior performance on analyzing non-stationary and inhomogeneous signals via space-frequency analysis.

Finally, the post process is used to obtain the railways in binary form without any discontinuities and missing parts. In order to do that, maximum modulus of filter results is calculated by thresholding (Fig. 2.b). After a careful determination procedure for the threshold value, a binary image is obtained by considering not losing any parts of the tracks or causing discontinuity on rail tracks as well as preventing over-segmentation with unwanted attachments to the rails and/or disconnected objects around the rail tracks. After the thresholding process, small disconnected clusters are eliminated with erosion. Then, detection of the railways from each binary sub-region has been done with a morphological reconstruction algorithm (Fig. 2.c).

Even when such a method is carefully and adequately executed, the nature of some challenges does not allow perfect extraction of the rails. The rails in Fig. 2.d illustrate an example

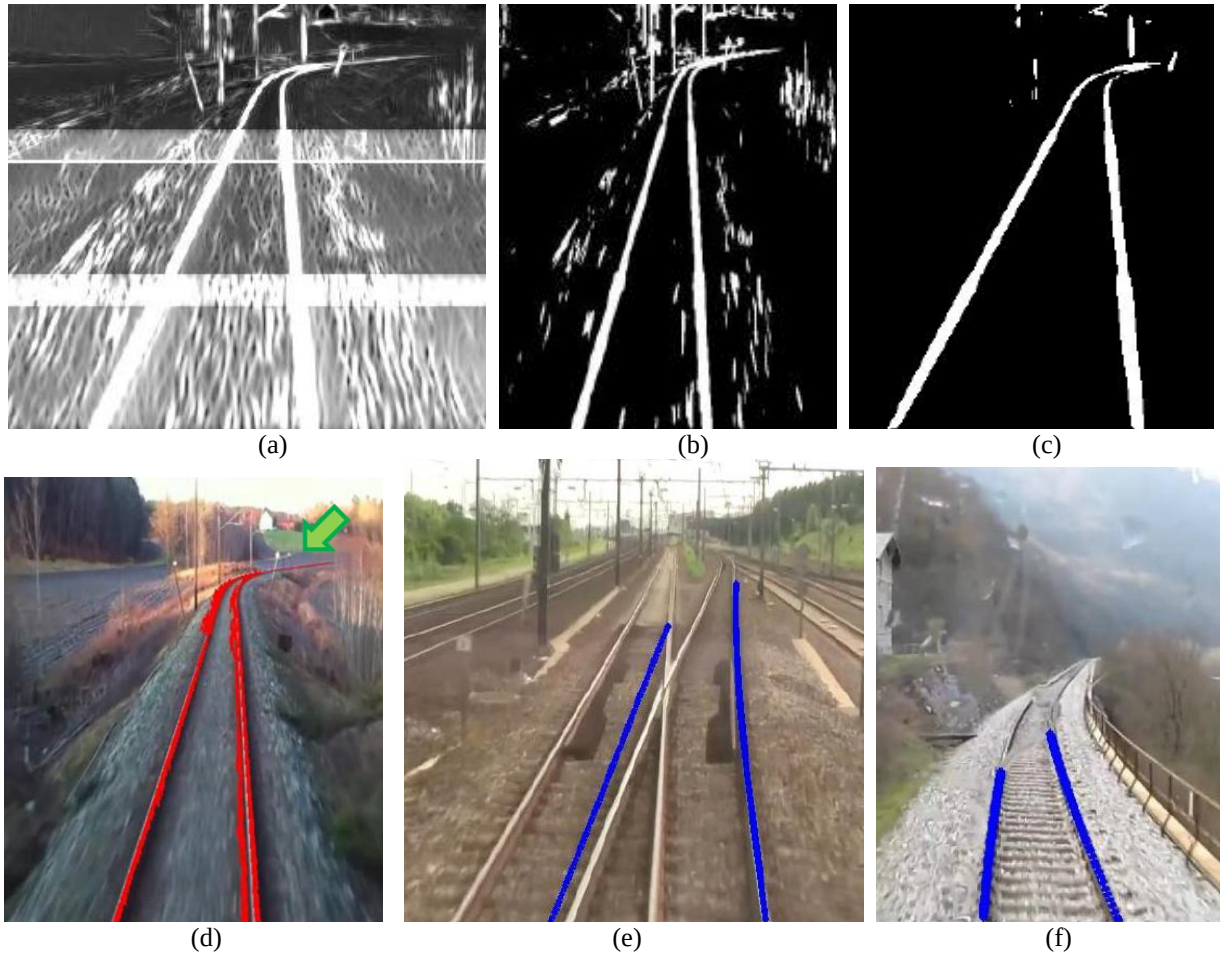

Fig. 2. Image processing steps: a) fitler outputs, b) after thresholding, c) after morphological post-processing. d) Rail track extraction blocked by traffic sign. Faulty image processing results due to e) crossing tracks, f) raindrops.

where railway tracks are almost perfectly segmented, but the traffic sign (indicated by the arrow) prevents continuous extraction of the complete track. Similar challenging cases are given in Fig. 2.e and 2.f.

3. Statistical Analysis of Railway Tracks

The tracks cannot be perfectly extracted at all challenging conditions mentioned above. On the other hand, if appropriate priori knowledge is integrated to the process, then these non-perfect image processing results can be recovered. Thus, by considering the image processing result strategy can be used as the initial model. This allows starting from a partially extracted track and utilizing domain-specific assumptions to generate the final result.

When a single camera is used, the rails appear as a pair of long stripes in video frames, despite being parallel to each other. However, the perspective of the camera makes the image look like they gradually get closer to each other and unify at the horizon. Rails have smooth geometry and slowly changing structure. Considering a standard video camera acquiring 50-60 frames per second, the changes become almost unrecognizable between consecutive frames of a video.

The appearance of the rails in front of the train can be considered as linear [5], but their curvatures vary as the distance from camera increases. Fig. 1.c and 1.d presents two frames, which have the highest variations considered in this study as the rails make a turn followed by another turn such that almost a stretched S shape is formed. It is empirically found that the exact representation of this curve requires a seventh order polynomial. Thus, in the first phase of this study, the manually delineated tracks are fit by finding the coefficients of a polynomial $p(x)=a_7x^7+ a_6x^6+ a_5x^5+ a_4x^4+ a_3x^3+ a_2x^2+ a_1x+b=0$ that fits the data best in a least-squares sense.

Here, it is worth to mention that the ground truth is generated by manual labeling of turns, which usually consists of hundreds of frames. Due to the slow changing characteristics only one of five consecutive frames is labeled (Fig. 3). Although, seventh degree polynomial may seem to be more complex than necessary for most of the cases, it brings no additional complexity to analysis as the coefficients of the higher order terms tend to zero (i.e. having coefficients around 10^{-14}) and can be ignored.

Fig. 4 presents the statistical analysis of linear, quadratic and cubic terms of five railway (right) turns. For each turn, the central (red) line of the boxplot represents the median while top and bottom edges correspond to 75 and 25 percent confidence levels, respectively. The tail lines at the bottom and top correspond to minimum and maximum observations, respectively and the plus (+) shaped data points show the outliers.

Considering the first four turns, the mean and standard deviation of all three terms' coefficients seem to stay in a very narrow range. For instance, the mean values of the coefficients of x1 for turns 2, 3 and 4 are 0.3533, 0.3504, and 0.3422, respectively. When the effective range of this term is analyzed (Fig. 1.h), these variations have almost no visual effect. Although, the fifth turn's statistics seem slightly different than the other four, it can be observed that the coefficients of all terms are doubled, thus they actually correspond to a similar

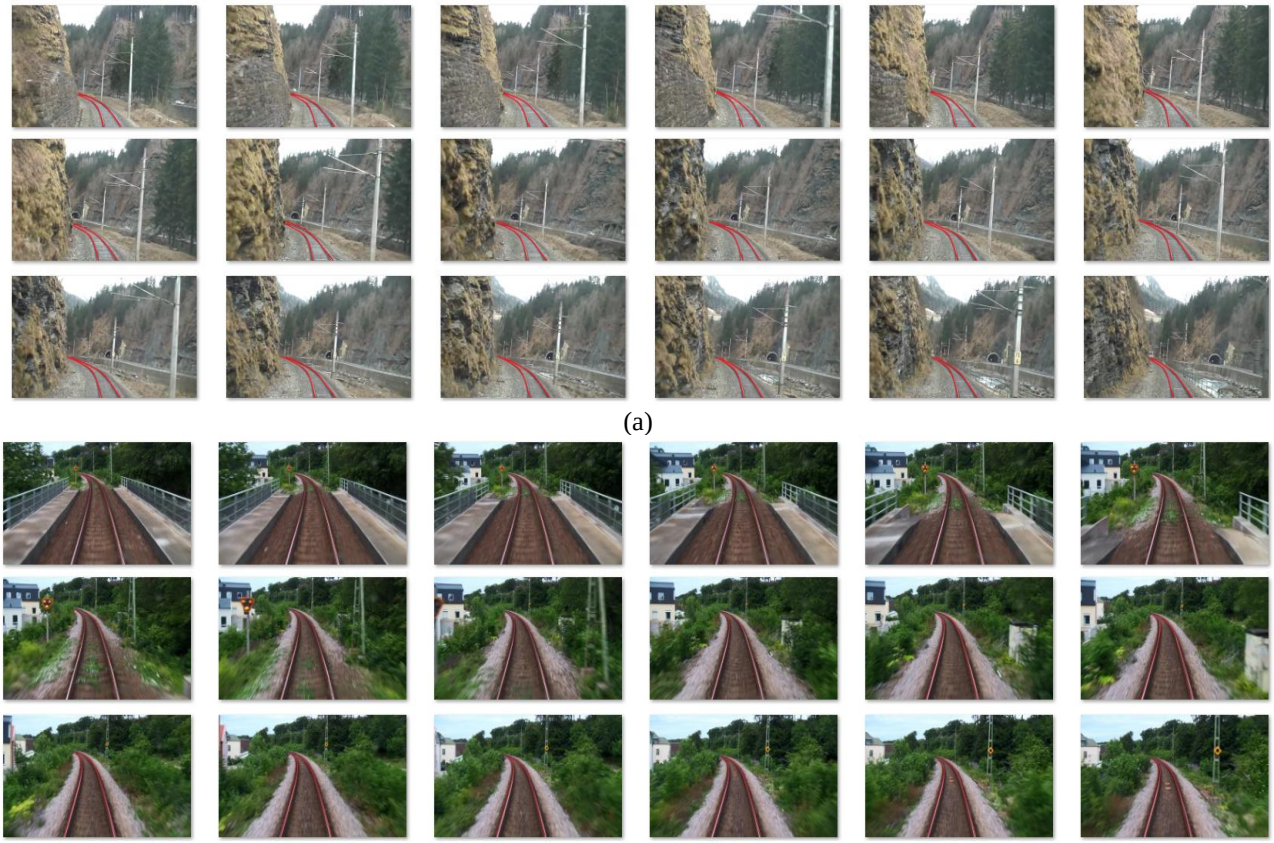

(a)

Fig. 3. Manually delineated railway tracks and examples for the challenges of railway extraction: a) A left turn consisting of 57 labeled images and 18 of which are illustrated. b) Another left turn consisting of 61 labeled images and 18 of which are illustrated.

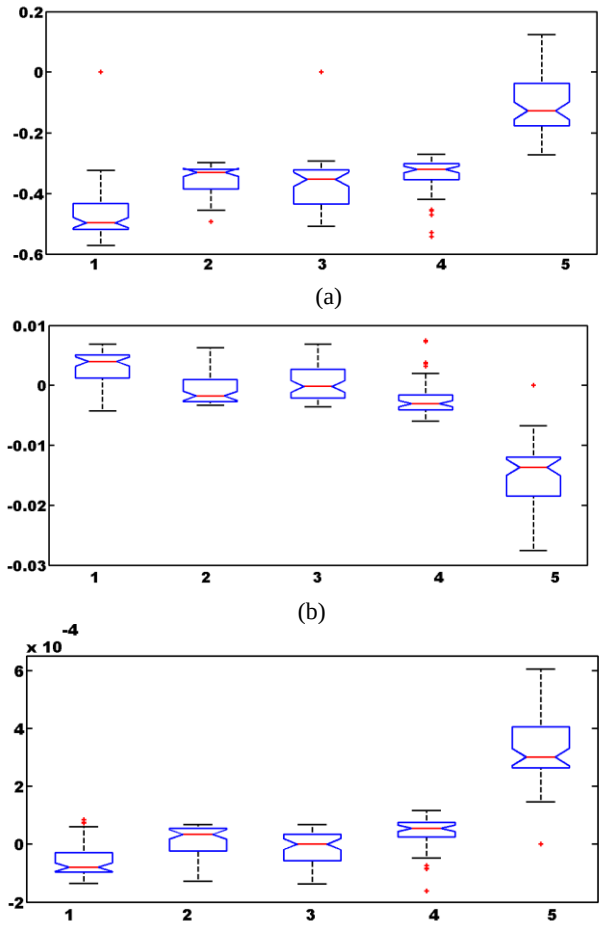

Fig. 4. Statistical analysis for five different turns of the same journey: Coefficient changes for terms (a) x^1, (b) x^2, (c) x^3.

polynomial. Based on these graphics, it can be concluded that the change of coefficients in different turns of a video is limited inside a certain margin and similar polynomial coefficients can be used to represent the railways.

4. Simulations and Results

The similar polynomial coefficients of the turns can be used both to create a ROI, which would limit the search space of the image processing algorithm (Fig. 5.b) and to limit the amount of change in polynomial coefficients at the upcoming frames. Accordingly, a neural network based scheme is proposed in which the coefficients are determined polynomial least-squares approximation followed by MLP networks.

The approach is designed to use the output of any algorithm for a predefined number of frames at least some of which is assumed to provide a reasonably rough approximation of a railway track. The polynomial coefficient range found in the previous section can be used for the training a multi layer perceptron (MLP) network in such a way that the input of the MLP for training is the polynomial coefficients of the previous frames together with the image processing result of the current frame, from which the tracks would be extracted.

During training, the ground truth data for the past frames is fed to the MLP together with the result of algorithm given in Section2. The extracted track profiles of the past frames are weighted to create a distance driven importance scheme such that the closest frame to the current one has the highest weights providing the most important neighborhood information. These inputs are used to learn the relation between the previous and upcoming coefficients by MLP. The desired information is the manually extracted frames, whose coefficients are also calculated by fitting a same order polynomial. During the tests, the connection weights are used to regularize image processing results with predicted coefficients.

Training and test is performed using 2185 manually delineated frames. These are obtained from 29 left and 23 right turns belonging to 14 videos acquired during common public journeys, which include many challenging scenarios stated in the previous sections. As mentioned previously, at least 50 frames are manually delineated for each turn. Several parameters for the use of MLP are tested such as the number of previous frames to fed as input, how to adjust and integrate the importance of the previous frames, the number of hidden layers and the amount of neurons in each.

During the learning phase, the coefficients of five previous frames are used as inputs. Since the effect of each coefficient is analyzed independently in the context of this study, an individual MLP is employed for each coefficient. The output of the MLP has a single neuron, which would indicate the value of the corresponding coefficient.

The results show that the railway tracks can be almost perfectly recovered without any visual difference than the ground truth. This evaluation is conducted by the observers, who compare the manual delineation (i.e. the ground truth) with the MLP based polynomial extraction. In 89% of the cases, the observers report no visual difference between the frames, while 6% of the remaining cases are also just have minor differences. Thus, overall the proposed method can perform 95% percent of the turns in a single video if a turn in the same video is known beforehand. An example is given in Fig. 5.

5. Conclusions and Future Work

This study aims to provide a final step for image processing algorithms that aim to extract railway tracks. In order to do that, first, a statistical analysis is performed on many turns obtained from different videos. As a result of the analysis, it is concluded that if the polynomial characteristics of a turn is known in a journey video, then other turns can be successfully approximated by similar polynomials. This allows to develop a mechanism that can compensate fault image processing results due to various challenges occurred in camera based systems.

Following this conclusion, a universal neural network approximator (i.e. MLP) is employed to predict the upcoming coefficient values of a seventh order polynomial, which would fit the track best in a least square sense. Here, it is assumed that some of the frames (before the frame of interest) are correctly extracted. It is shown that, such a strategy can be adapted to previously developed systems and would be a useful tool for regularizing the results.

Many important improvements are possible as future work. First, the polynomial coefficient changes of the right and left tracks can be analyzed with respect to each other instead of individual analysis as it is done in this paper. Second, this study is focused on individual effects of polynomial coefficients but if they are fed together to a neural network, their combined effect

(a) (b) (c)

Fig. 4. (a) Faulty image processing result due to inverse illumination caused by strong effects of sun, (b) dynamic ROI created by using the knowledge about the previous frames, (c) Regulated rail extraction using polynomial fitting method.

by adjusting them at the same time would benefit from a more diverse set of polynomials and can provide better representation.

6. Acknowledgements

This study is conducted as a part of EUREKA-EURIPIDES project “ADORAS [Advanced Onboard data Recording and Analysis System]” and supported by TUBITAK TEYDEB under grant 9150121, which is conducted by Kentkart.

7. References

[1] Hodge, Victoria J., et al. "Wireless sensor networks for condition monitoring in the railway industry: A survey." Intelligent Transportation Systems, IEEE Transactions on 16.3 (2015): 1088-1106.

[2] Lenior, Dick, et al. "Human-factors engineering for smart transport: Decision support for car drivers and train traffic controllers." Applied ergonomics 37.4 (2006): 479-490.

[3] M. Ruder, N. Mohler, and F. Ahmed, “An obstacle detection system for automated trains,” in Proc. IEEE Intell. Veh. Symp., 2003, pp. 180–185.

[4] F. Maire and A. Bigdeli, “Obstacle-free range determination for rail track maintenance vehicles,” in Control Automation Robotics Vision (ICARCV), 2010 11th Inter. Conf. on, dec. 2010, pp. 2172 –2178.

[5] V. Kastrinaki, M. Zervakis, and K. Kalaitzakis, “A survey of video processing techniques for traffic applications,” Image and Vision Computing, vol. 21, pp. 359–381, 2003.

[6] F. Maire, “Vision based anti-collision system for rail track maintenance vehicles,” in Advanced Video and Signal Based Surveillance, 2007. AVSS 2007. IEEE Conference on, sept. 2007, pp. 170 –175.

[7] J. Wohlfeil, “Vision based rail track and switch recognition for self-localization of trains in a rail network,” in Proc. IEEE Intell. Veh. Symp., 2011, pp. 1023–1028.

[8] S. Aminmansour, “Near-Miss Event Detection at Railway Level Crossings,” Digital Image Computing: Techniques and Applications, 2014 Inter. Conf. on, Wollongong, NSW, 25-27 Nov. 2014, pp1-8.

[9] M. A. Selver et al., "Camera based driver support system for rail extraction using 2-D Gabor wavelet decompositions and morphological analysis" In Intelligent Rail Transportation (ICIRT), IEEE International Conference on, 2016, pp. 270-275.

[10] B. T. Nassu and M. Ukai, "A Vision-Based Approach for Rail Extraction and its Application in a Camera Pan–Tilt Control System," in IEEE Transactions on Intelligent Transportation Systems, vol. 13, no. 4, pp. 1763-1771, Dec. 2012.

[11] F. Kaleli and Y. S. Akgul, “Vision-based railroad track extraction using dynamic programming,” in Proc. IEEE Conf. Intell. Transp. Syst., 2009, pp. 1–6.

[12] S. Fischer, Comparison of railway track transition curves. Pollack Periodica, 4(3), 99-110. 2009.

[13] R. Ross, Track and turnout detection in video-signals using probabilistic spline curves. In Intelligent Transportation Systems (ITSC), 2012 15th International IEEE Conference on (pp. 294-299). 2012.

A Preliminary Study for A Non-Stop Cargo Transportation Concept for the Railroads

Gökhan Dındış[1] and Abdurrahman Karamancıoğlu[1]

[1]Eskişehir Osmangazi Üniversitesi, Eskisehir, Turkey
gdindis@ogu.edu.tr, akaraman@ogu.edu.tr

Abstract

Cargo transportation is a multi-billion dollar market in which the railroad industry has a little share in it. There are many factors causing this outcome. However, most experts agree that, one major factor is the efficiency of the present railroad operating system. It is argued in this manuscript that a significant improvement in the efficiency is possible if certain hardware modifications of the rail vehicles and stations together with a smart management are carried out. In this manuscript, a smart cargo transportation concept is proposed and preliminary discussion is presented. Its implementation uses the current railroad system already in use; therefore, it is apparent that the cost is limited with configuring the smart cargo trains and smart logistic cargo stations.

1. Introduction

Industry 4.0 is not caused simply by industrial requirements alone; it has come into the reality because of the advances in the information and networking knowledge which resulted in the internet technologies. Then the rest has happened inevitably. A smart networking of devices and systems always has the potential for the smart production systems. A consequence is the new industrial revolution concept which is quickly owned by the developed countries. Industry 4.0 is on the door steps now and for the future of the business, everybody must fit in. An incredible amount of people are working on smart communication systems, smart cities, smart transportation, smart factories, smart grids, and so on. Thus, unimaginable breakthroughs have become the realities of the present day. In this manuscript, standard ways of thought and the routines are challenged by a proposal of reconfiguring the current railway system.

The subject of interest in this paper is the railroad transportation system and its place in industry 4.0. Proposed concept seems very unusual or crazy at first look. Biased thinking without any preliminary review may drift the reader to the opposite way of consideration for the discussion. Considering this, some extraordinary successful examples mentioned in Section 2. The authors of this manuscript aim to extend the set of such extraordinary practices which have already become the normal of the present day.

Due to their nature, railroad systems may be considered as robotic or robotic friendly systems themselves. Looking at the factories with advanced robotic systems we notice immediately the assembly lines. Railroads are similar to the assembly lines in the cargo transportation framework of the country. Even though some decision makers are aware of this reality very well, unfortunately some are not. In the case of unawareness, ground transportation never gets a chance of benefiting from this "internet" of cargo transportation network. That is, so much investments on railroad systems may possibly not come with getting best performance out of them. In the reality of industry 4.0, logistic supply chain is more important than ever now. Without a swift and smart logistic supply chain it just does not work. From this point of the view, challenging studies for increasing the efficiency of the matter are quite important.

In Section 2 there are some examples of unusual railroad or transportation ideas realized in the past and also currently being developed. Some examples on the research and development phases are also mentioned. Components and operation of the proposed system are presented in Section 3 and Section 4 respectively. Concluding remarks take place in the last section.

2. Extraordinary Railroad Transportation Examples

Conventional train moves on a two parallel steel rails and its wheels contact these rails. The main differences in the conventional trains are in the traction mechanisms where some use diesel engines and some other use electrical motors for it. However, there are extraordinary rail configurations and traction systems, which may be considered unrealistic in the past but have become reality for few decades. Below we review three examples briefly: the monorail, magnetic levitation, and the hyperloop systems.

In a monorail system train moves on a single rail [1]. This rail supports and guides the train. Train wagons interact with the rail using a set of tires so that they move smoothly and derailment is avoided. The monorail is constructed several meters above the ground level, consequently it does not occupy space allocated to the ground level vehicles. Besides, the train and rail interaction also results in a low environmental noise.

Magnetic levitation trains are powered by electricity and they use no traction engine. These type of trains do not touch the railroad; they float over it. This is achieved by using the most basic principle of magnets: like poles repel each other. The electrical energy is used for creation of the like poles, one end on the train and the other end is on the road. The basic principles of electromagnetics are used for the traction as well as the floating of the trains. The current day technology allows 600 km/h speed [2], which makes the magnetic levitation transportation an alternative to the airlines. Besides its speed, it is also advantageous in noise sense.

Hyperloop is a new train system invented by Elon Musk. It combines the magnetic levitation and propulsion idea and a low pressure tube. The magnetic levitation and propulsion part eliminates the need for a traction engine, and the low pressure tube (or tunnel) lowers the friction that opposes the train motion. "For propulsion, magnetic accelerators will be planted along the length of the tube, propelling the pods forward. The tubes

would house a low pressure environment, surrounding the pod with a cushion of air that permits the pod to move safely at such high speeds, like a puck gliding over an air hockey table" [3]. It is reported that 700 km/h speeds are possible in a hyperloop system.

There are other unusual rail transportation systems not mentioned above are in pilot use or in development phase. The main idea in this section is that the innovations do never stop coming out; their common characteristics is that they had not been "feasible" or "logical" before they became realities.

3. Proposed Logistic Cargo Transportation

The transportation system proposed below aims to minimize the overall transportation time of the cargo trains. In the conventional cargo handling systems, when the maximum travel distance is long and number of cargo drop-off and pick-up stations is high, average cargo-per-hour rate drops drastically. To compete with the alternative transportation systems, and even to make it better, proposed concept may result a significant improvement. However, not all the components are off the shelf, unfortunately, some vital ones have to be designed or redesigned accordingly, or the available versions of these components are used with the cost of compromising some efficiency. Below, these vital components of the proposed system are described.

3.1. Automatic Train Couplers

Train coupling and de-coupling is very simple with automatic coupling units. Air, hydrolic and electric ones with suitable electronics assure a reliable coupling operation. There are companies world-wide for producing such couplers [4]. The system proposed in this manuscript requires reliable coupling and de-coupling timing.

3.2. Fully Controllable Brake Systems for the Cars

Air brakes for commercial freight and passenger trains are highly advanced today. In addition to distributed air or vacuum brakes, dynamic braking of the locomotives are also commonly in use. The proposed system requires fully controllable brakes for desired deceleration rates for each car. It should be noted that a quality braking alone allows implementation of fairly complicated control algorithms. Such systems are available in the market and getting more affordable every day.

3.3. Fast Railroad Switches

Rail road switches are important components to allow route control of the trains. There are numerous places still in rural stations using manual switches. However, modern railroad systems, including the ones used in metro systems require fast, reliable, and fully remote controllable switches. The ones satisfying the speed requirements of the proposed system, if not off the shelf, then must designed and manufactured.

If a designer does not mind the quality, the components described above are available in the market. However, a satisfactory level of feasibility of the proposed cargo transportation system requires having their improved and affordable versions.

4. Operation of the System

As a setting, consider a locomotive and N-1 wagons moving in the positive x direction towards the drop-off station. This station has a switching point where each wagon's course is changed in the case of need. Let us remove the wagon connecting hooks at a certain location before the braking operation starts. Following this, it is intended to form a gap between every two successive wagons before the wagon of interest reaches the switch. If the gap is long enough then the switch becomes capable of letting any individual wagon to change its course while preserving the course of the remaining wagons. Forming the gap is achieved by applying a controlled braking to each wagon independently. Thus, the goal for each wagon is, in a harmony, to start deceleration when its time comes and use its own appropriately calculated deceleration rate to reach down to the switch speed right before the switch, at the switch-distance proximity of the next wagon. Therefore, the train operating system must make decisions on the brake timings for each wagon. The braking rate of the first wagon must not exceed the max operational braking rate acc_{max}. However, deceleration or braking rate will be reduced down toward the trailing wagons. Below, a braking process for the wagons is presented.

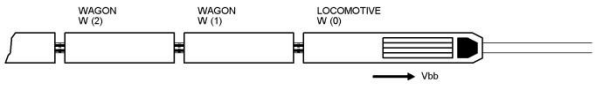

(a) Coupled train cars

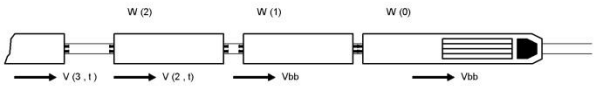

(b) Decoupled cars, at the time third car just starts braking.

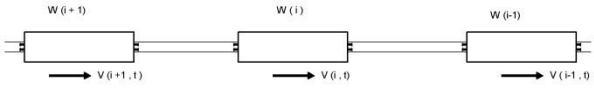

(c) Forming precise gaps among the wagons

Fig. 1. Total decoupling process of the train, prior to the station switch.

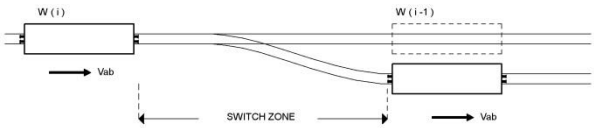

Fig. 2. Switch zone, a zone which needs to be clear for the safe switching operation of approaching wagon.

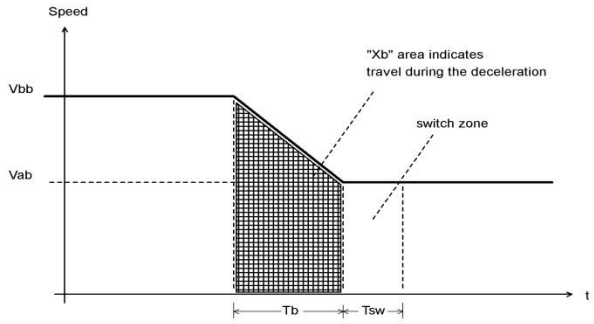

Fig. 3. Generalized speed/time graph for any wagon W_i entering the switch zone

Let us denote the locomotive and wagons, from leading end to the trailing end of the train, by W_0, W_1, …, W_n. Let us also denote speed of the train before braking by V_{bb} and prespecified speed after braking by V_{ab}. The terms X_{b0} and T_{b0} denote braking distance, namely the distance from first wagon to the switch, and time frame to complete this operation respectively. They are calculated as follows:

$$X_{b0} = \frac{(V_{ab} + V_{bb})}{2} T_{b0}$$

$$T_{b0} = \frac{(V_{ab} - V_{bb})}{acc_{max}}$$

Above expressions lead to:

$$X_{b0} = \frac{V^2{}_{ab} - V^2{}_{bb}}{acc_{\max}}$$

In the worst case scenario, all the alternating wagons would be leaving the train for heading the station. For the simplicity in presentation we do particular calculations for the second and third wagons before the generalization of calculations to N wagons. Let us consider W_1, the second wagon. For this wagon, braking event will start T_1 seconds earlier than the first wagon, and will reach the switching zone T_{sw} seconds after first wagon:

$$T_{b1} = T_{b0} + T_1 + T_{sw}$$

During the braking of second wagon, travel distance will be X_{b1} meters and calculated simply as below:

$$X_{b1} = \frac{(V_{bb} + V_{ab})}{2} T_{b1}$$

Same distance is calculated from the first wagon's motion of equations:

$$X_{b1} = X_{b0} + V_{bb} T_1 + L_{w0}$$

where, L_{w0} is the length of the first wagon.

Thus, third wagon starts braking T_2 seconds earlier than the second wagon, or equivalently $T_1 + T_2$ seconds earlier than the first wagon. Obviously, it will reach the switching zone T_{sw} seconds after the second wagon. So the equations will be:

$$T_{b2} = T_{b0} + T_1 + T_2 + 2T_{sw}$$

and

$$X_{b2} = \frac{(V_{bb} + V_{ab})}{2} T_{b2}$$

$$X_{b2} = X_{b0} + V_{bb}(T_1 + T_2) + L_{w0} + L_{w1}$$

respectively. In generalized form equations can be expressed as:

$$T_{bi} = T_{b0} + \sum_{k=1}^{i} T_k + iT_{sw}, \qquad i = 1,2,\dots,n-1$$

and

$$X_{bi} = \frac{(V_{bb} + V_{ab})}{2} T_{bi} = \frac{(V_{bb} + V_{ab})}{2} \left(T_{b0} + \sum_{k=1}^{i} T_k + iT_{sw} \right)$$

$$X_{bi} = X_{b0} + V_{bb} \sum_{k=1}^{i} T_k + \sum_{k=0}^{i-1} L_{wk}$$

The solution for i=1 is:

$$T_1 = \frac{V_{avg}(T_{b0} + T_{sw}) - X_{b0} - L_{w0}}{(V_{bb} - V_{avg})}$$

and for the higher indices i>1 we have :

$$\sum_{k=1}^{i} T_k = \frac{V_{avg}(T_{b0} + iT_{sw}) - X_{b0} - \sum_{k=0}^{i-1} L_{wk}}{(V_{bb} - V_{avg})}$$

$$T_i = \frac{V_{avg}(T_{b0} + iT_{sw}) - X_{b0} - \sum_{k=0}^{i-1} L_{wk}}{\sum_{k=1}^{i-1} T_k \, (V_{bb} - V_{avg})}$$

where, $V_{avg} = \frac{(V_{bb} + V_{ab})}{2}$.

Acceleration rates for each wagon calculated simply as:

$$acc_i = \frac{V^2{}_{ab} - V^2{}_{bb}}{X_{bi}}$$

Braking operation of the train starts as soon as the distance from the last wagon to the switching zone becomes X_{bn-1} meters. It can be reflected to the front edge of the first wagon as:

$$train\ braking\ zone\ distance = X_{bn-1} - \sum_{i=0}^{n-2} L_{Wi}$$

where, L_{Wi} is the length of i_{th} wagon, end to end.

When the first wagon reached the switching zone is considered as t=0, braking time for any wagon W_i is:

$$t_i = -T_{b0} - \sum_{k=1}^{i} T_k$$

This means operation starts as soon as the train enters the braking zone and clock is set for all the wagons as t_{n-1} , which is described as:

$$t_{n-1} = -T_{b0} - \sum_{k=1}^{n-1} T_k$$

Following the first wagon, all others will reach the switch T_{sw} seconds apart from each other.

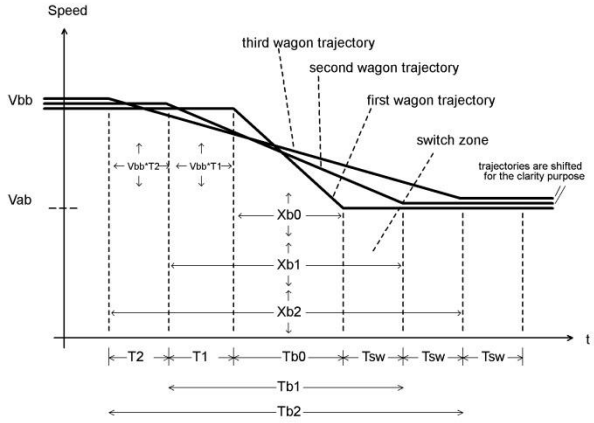

Fig. 4. Motion trajectories for the wagons

If desired, as a control strategy, smoother S-curves or spline curves can be used as reference trajectories, which allow a very smooth operation of the motion, but its complexity is no help to explain the general concept here. For the sake of simplicity, a straightforward trapezoidal waveform is used for the braking trajectories as in Fig. 4.

In the paragraphs above leaving wagons at a switching point is described conceptually. After a certain distance from the switching location the process above is reversed with the wagons not left at the station. Even though there are similarities between the phases of leaving and collecting back the wagons, the latter is simpler. To avoid repeating the straightforward reversing process we omit its presentation.

5. Conclusions

An efficient train cargo operation is proposed. The proposed system needs the use of automatic train couplers, fully controllable brake systems for the cars, and reliable fast switches. As mentioned in the introduction that the proposal presented is unusual in today's terms. However, the technology needed for a start is available; all we need is an initial step. The above presentation is on a single train's role in the cargo delivery system. Future research may consider a network of such trains and their routings as well as improving an individual train's role.

6. References

[1] K. A. Pedersen, Monorails: Trains of the Future-Now Arriving, The monorail Society Publication, 2015

[2] Japan's maglev train breaks world speed record with 600km/h test run, url= https://www.theguardian.com/world/2015/apr/21/japans-maglev-train-notches-up-new-world-speed-record-in-test-run, 21 April 2015.

[3] W. Nicol, "As hyperloop progress glides forward, here is what you need to know", url=https://www.digitaltrends.com/cool-tech/hyperloop news/, 31 May 2017.

[4] Automatic train couplers, url= https://www.youtube.com/watch?v=kpf2f5dPIFg, date accessed: 24 August 2017.

The Influence of the Track Roughness Parameter on the Actively Controlled Railway Vehicle

Aslı Soyiç Leblebici[1], Semiha Türkay[2]

[1]Eskisehir Osmangazi University, Eskisehir, Turkey
aleblebici@ogu.edu.tr
[2]Anadolu University, Eskisehir, Turkey
semihaturkay@anadolu.edu.tr

Abstract

In this paper, the effect of random rail profile roughness parameter on the railway vehicle is studied. As a disturbance input, a power-spectral-density (PSD) function taken from Federal-Railroad-Administration (FRA) international standard is used. First, a coupled vertical vehicle-track system is formed as an affine-parameter-dependent function of the track roughness parameter and its influence on the vehicle dynamics is discussed in frequency domain. Then, for a range of track roughness parameters, a multi-objective controller is designed to improve the ride comfort without permitting any critical breakdowns on the safety performance of the vehicle. Later, a controller with fixed roughness parameter values is synthesized and the results are compared by using the frequency response plots and the root-mean-square values of the carbody accelerations and the wheel-rail forces.

1. Introduction

Nowadays, in order to compete with other transportation systems, reliable, eco friendly railway vehicles are designed with high speed demands and large freight or passenger capacity. Upsurge at the travel speeds, increase the axle loads which in turn will decrease the passenger comfort and safety level of the vehicle.

The main vibration source for the railway vehicles is the uneveness of the rail track [10] and can be modelled either as deterministic or random process. In the literature, the random track irregularity is ussually assumed to be a stationary, ergodic Gaussian process which can be characterized by a single power-spectral-density (PSD) function [7],[1]. An international standard defined by Federal Railroad Administration (FRA) is used to classify the rail tracks into eight different categories ranging from extremly poor to very good quality tracks defined under maximum allowable speed limits [5]. Large batches of measurement data collected from various field sections are used to characterize the geographical variations and curve fitting methods are used to obtain the best fitting PSD functions to the empirical data represented as a rational function of a single surface roughness parameter and multiple break frequencies.

Modelling of track geometry has a large spaces in the industry and academia and is widely used for offline simulations and design purposes. In [6] both deterministic and stochastic track inputs are applied to study the output responses of a half-bogie railway vehicle represented as an elastic beam. Noise reduction properties by suppressing the rail irregularities are discussed in [8] and some experimental results are presented to support the achievable performance in practice. All these studies point to discomfort analyses which are basically caused by severe track irregularity inputs. In the international standard organization (ISO) directive it is pointed out that humans are mainly sensitive to the low frequency excitations ranging especially in the $1-15\ Hz$ frequency band [4]. Klasztorny and his coworkers in [7] studied the effects of random vertical track inputs on the bridge-track structure-high speed train systems by using the finite element methods to model the the rail track as an elastic structure. Although it gives a good notion about the system dynamics, the analysis itself is not applicable for linear control design methodologies.

In this work, the primary objective is to design controllers for a high speed railway vehicle which can minimize the vertical carbody accelerations and keep the wheel-rail holding forces below their passive values simultaneously. It is assumed that the vehicle travels on a straight rough surface line where the quality of line can possiblly differ during driving. The study is organized as follows: Section 2 presents a mathematical model for the railway vehicle and the stochastic rail profile is modelled by a fourth-order power spectral density function. In Section 3, an affine-parameter-dependent system is formulated in terms of the track roughness parameter and an optimization problem is proposed to solve the conflict between the trade-off curves of the carbody accelelerations and wheel-rail-holding forces. The study is ended by Conclusions part in Section 4.

2. System Modelling

Fig. 1 shows a six-degrees-of-freedom mathematical model of a typical high speed passenger railway vehicle. The carbody m_c is assumed to perform the bounce and pitch motions z_c, θ_c, simultaneously. The suspension part between the carbody and bogie frames is called the secondary suspension and consists of the passive elements k_2, c_2 and active forces u_1, u_2. The primary suspension is the part betweeen the bogie frames and the wheelsets and is constituted of the linear spring damper set k_1, c_1 and bogie mass m_t

which can oscillate in vertical and pitch directions for the front and rear displacemets $z_{t1},\ z_{t2},\ \theta_{t1},\ \theta_{t2}$, respectively. The random rail excitations are represented with displacements z_{wi} for $i = 1, ..., 4$ and only vertical vibrations of the vehicle are considered.

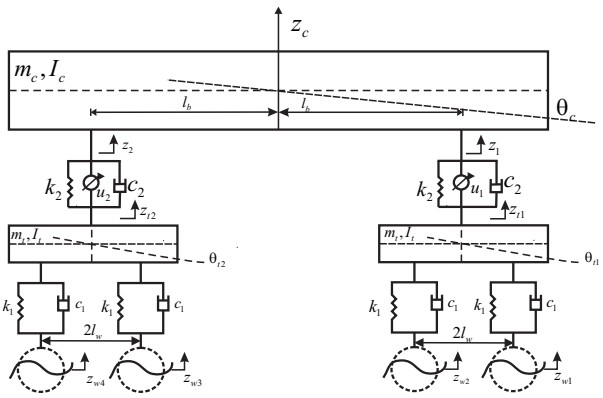

Fig. 1. Railway vehicle 6 DOF half car model.

In this work, the parameter values of a Bombardier I11 passenger coach running in Belgian Railways [3] are going to be used for the simulation studies and are presented in Table 1. This vehicle has a typical high speed passenger railway vehicle structure and has a 200 km/h speed limit.

Table 1. 6DOF vehicle model dynamic parameters [3].

Variable	Description	Value
m_c	Half of carbody mass	13420 kg
I_c	Car body pitch moment of inertia	0.67 $\times$ 10^6 kgm^2
m_t	Half of bogie mass	6800 kg
I_t	Bogie pitch moment of inertia	1.475 $\times$ 10^3 kgm^2
c_1	Primary suspension damping coeff.	3.750 kNs/m
c_2	Secondary suspension damping coeff.	11.3 kNs/m
k_1	Primary suspension spring stiffness	0.475 MN/m
k_2	Secondary suspension spring stiffness	0.12 MN/m
l_b	Half distance between bogie centers	9.2 m
l_w	Half of the wheel base	1.28m

A general notation for the state-space representaion can be given as,

$$\frac{d}{dt}x = Ax + B_1\frac{d}{dt}z_w + B_2u \tag{1}$$

where x shows the state vector, $z_w = [z_{w1}\ z_{w2}\ z_{w3}\ z_{w4}]^T$ is the exogeneous input and $u = [u_1\ \ u_2]^T$ is the control force. The description of the state-space matrices for the half-car model in Fig. 1 are omitted for the sake of brevity. The reader is reffered to [4].

The main goal of this study is to evaluate the performance trade-off of the actively controlled suspension system by minimizing the carbody vertical accelerations as an indication of a better ride comfort and keeping the wheel-rail forces below a limit as an indication of good rail holding on safety. Hence,

$$\begin{aligned} z_2 &= C_2x + D_{22}u \\ z_\infty &= C_\infty x + D_{\infty 1}\frac{d}{dt}z_w. \end{aligned} \tag{2}$$

where $z_2 = [\ddot{z}_c\ \ddot{\theta}_c]^T$ is the exogeneous output and $z_\infty = z_\infty^1 - z_w$ is the regulated output with,

$$z_\infty^1 = \begin{bmatrix} 1 & l_w & 0 & 0 \\ 1 & -l_w & 0 & 0 \\ 0 & 0 & 1 & l_w \\ 0 & 0 & 1 & -l_w \end{bmatrix} \begin{bmatrix} z_{t1} \\ \theta_{t1} \\ z_{t2} \\ \theta_{t2} \end{bmatrix},$$

and

$$Y = \begin{bmatrix} -\frac{1}{m_c} & -\frac{1}{m_c} \\ -\frac{l_b}{I_c} & \frac{l_b}{I_c} \end{bmatrix}, \quad K_l = \begin{bmatrix} k_2Y & 0_{2\times 4} \end{bmatrix}$$

$$C_l = c_2Y \begin{bmatrix} 1 & 0 & -0.5 & 0.5 & 0 & 0 \\ 0 & 1 & 0 & 0 & -0.5 & 0.5 \end{bmatrix},$$

$$F_l = \begin{bmatrix} 0_{4\times 2} & I_4 \end{bmatrix},$$

$$C_2 = \begin{bmatrix} K_l & C_l \end{bmatrix}, \quad D_{22} = Y,$$

$$C_\infty = \begin{bmatrix} k_1F_l & c_1F_l \end{bmatrix}, \quad D_{\infty 1} = -c_1I_4.$$

2.1. Stochastic Rail Road Modelling

The railway vehicle is assumed to travel on a random rail profile with a constant speed V. The Federal Railroad Administration classified the random track irregularities into eight classes (the last three are only hypothetical) with corresponding track roughness values and maximum allowable speed limits as in Table 2. The class 1 refers to a track with extremly poor quality where class 8 represents a hypothetically good quality with maximum travelling speed of $250km/h$ [1, 5]. In the FRA standard directive the power spectral density function used to characterize the rail track profiles is represented with a rational function

$$S_{\text{FRA}}(\Omega) = \rho_r \frac{\Omega_c^2}{(\Omega^2 + \Omega_c^2)(\Omega^2 + \Omega_r^2)}, \tag{3}$$

where ρ_r is the roughness constant and Ω_r, Ω_c show the cut-off frequencies in $cycle/m$. The cut-off frequencies are independent of the track classes and are fixed as $\Omega_r = 0.146\ rad/m$, $\Omega_c = 0.825\ rad/m$. The track roughness parameter ρ_r is frequently changing during travelling and remains in the interval: $0 \leq \rho_r^{min} \leq \rho_r \leq \rho_r^{max}$, where $\rho_r^{max},\ \rho_r^{min}$ are corresponding to a very poor and excellent quality track profiles, respectively.

Let S_{FRA} be decomposed into its spectral factor as $S_{\text{FRA}}(\Omega) = G_{\text{FRA}}(j\Omega)G_{\text{FRA}}(-j\Omega)$, where

$$z_{wi} = G_{\text{FRA}}\eta \tag{4}$$

[1]Hypotetical track classes

Table 2. FRA Track Roughness Classification [5].

Track classes	ρ_r $(10^{-6}\ m)$	**Velocity Limit** (km/h)
Class-4	0.1566	120
Class-5	0.1058	145
Class-6	0.0719	177
Class-7 [1]	0.04234	201
Class-8[1]	0.0254	257

and η is a zero mean white noise process and $j = \sqrt{-1}$. Since G_{FRA} will linearly scale the Eqs. (1-2) the system with no control $(u = 0)$ is strongly influenced by the track roughness parameter and the dominant system modes will be badly damped on rough territories. Fig. 2 shows the effect of ρ_r on the on wheel-rail forces. It can be seen that, the magnitude of wheel-rail forces are amplified for the whole frequency range when the track roughness parameter is increased. This remark is practically crucial, since the effect is distinctly visiable also in Figs. (2)–(5) by numerical simulations. Then, the track irregularity effects can be analyzed by tunning the roughness parameter in a range.

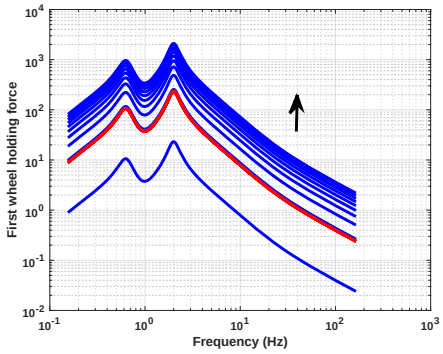

Fig. 2. The effect of ρ_r on the the wheel-rail force frequency response for $V = 160\ km/h$.

When the train is running with changing velocities on different track profiles the ride comfort and safety considerations will be strongly influenced. The vertical carbody acceleration $\ddot{z}_c$ respond to rail irregularities between $0-20Hz$, which corresponds the acceleration felt by the passengers, while wheel-rail forces z_∞ counteract between $0 - 30Hz$, representing the ability of the wheels to stay in contact with the rail surface. Since it will messy to show the effect on different rail profiles in frequency domain, the root-mean-square (RMS) responses are used in Figs. (3)-(4) to quantify the vibrational effect in more compact form. From the figures, it can be seen that even travelling on smooth tracks with considerable high speeds will substantially increase the dynamic wheel-rail forces, endangering the safety handling and leading to high levels of discomfort for passengers experiencing it.

In [2], it was shown that the vehicle forward speed V and the track roughness parameter linearly multiply the RMS response of the vehicle. If the track roughness is fixed, or likewise if the train is travelling on a prescribed rail profile for a certain time period, *e.g*

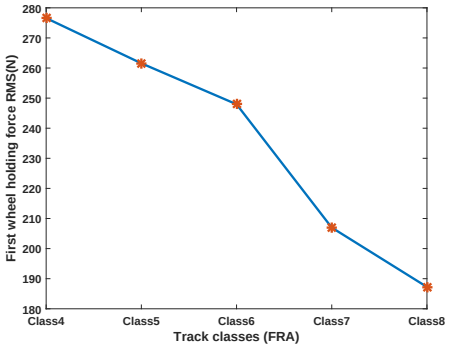

Fig. 3. Wheel-rail RMS response on the FRA track classes .

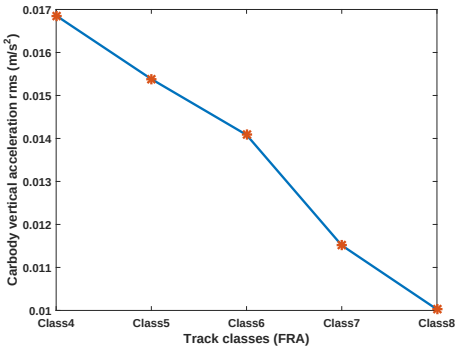

Fig. 4. Carbody vertical acceleration RMS response on the FRA track classes.

for a varying forward speed from 50 km/h to 210 km/h and on a rail profile with uneveness $\rho = 0.042 \times 10^{-6}$, the increased levels of vibration will be more prominent at high speed values. This is demonstrated in Figs. (5)-(6) where the latter shows that speeds $V \geq 170km/h$ have negative impact on the carbody accelerations where the carbody resonance frequencies are more pronounced. In summary, it is desirable to avoid extreme values both for roughness parameter and speed, both lowest and highest.

The main motivation of this paper is to search for an optimal performance of an active controller in the secondary suspension, by evaluating the cost in ride comfort and handling properties of the vehicle on the tracks with different qualities. Then the problem should be defined as an affine system in terms of track roughness parameter.

3. The Effect of Track Roughness Parameter

Let's define a parameter-dependent-systems with the parameter vector $\beta = [\beta_1 \ \ \beta_2]$ for any state-space quadruplet (A, B, C, D). Then, the parameter-dependent system $P(\beta) = P^0 + \beta_1 P^1$ is as:

$$P(\beta) = \left(\begin{array}{c|c} A(\beta) + jE(\beta) & B(\beta) \\ \hline C(\beta) & D(\beta) \end{array}\right), \ P^1 = \left(\begin{array}{c|c} A^1 + jE^1 & B^1 \\ \hline C^1 & D^1 \end{array}\right)$$

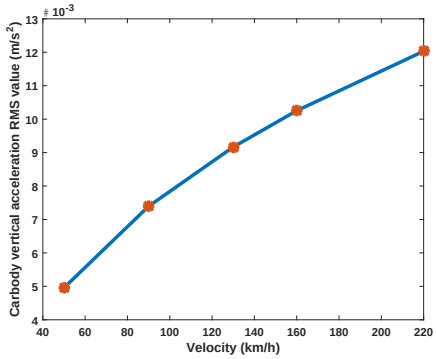

Fig. 5. The effect of V on carbody vertical acceleration for $\rho_r = 0.042 \times 10^{-6}$.

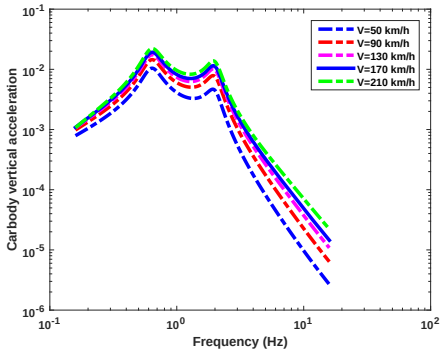

Fig. 6. The effect of V on carbody vertical acceleration frequency response for $\rho_r = 0.042 \times 10^{-6}$.

where

$$\begin{aligned} A(\beta) &= A^0 + \beta_1 A^1, \quad B(\beta) = B^0 + \beta_1 B^1, \\ C(\beta) &= C^0 + \beta_1 C^1, \quad D(\beta) = D^0 + \beta_1 D^1, \\ E(\beta) &= E^0 + \beta_1 E^1. \end{aligned} \tag{5}$$

In this study the effect of the track roughness parameter ρ_r on the railway vehicle defined in Eqs. (1),(2) will be studied. Then, the parameter-dependent representation of the vehicle system can be shown as follows:

$$P(\rho_r) = P^0 + \rho_r P^1, \tag{6}$$

with

$$P^0 = \left(\begin{array}{c|cc} \tilde{A}^0 & \tilde{B}_1^0 & \tilde{B}_2^0 \\ \hline \tilde{C}_\infty^0 & \tilde{D}_{\infty 1}^0 & \tilde{D}_{\infty 2}^0 \\ \tilde{C}_2^0 & \tilde{D}_{21}^0 & \tilde{D}_{22}^0 \end{array}\right), P^1 = \left(\begin{array}{c|cc} \tilde{A}^1 & \tilde{B}_1^1 & \tilde{B}_2^1 \\ \hline \tilde{C}_\infty^1 & \tilde{D}_{\infty 1}^1 & \tilde{D}_{\infty 2}^1 \\ \tilde{C}_2^1 & \tilde{D}_{21}^1 & \tilde{D}_{22}^1 \end{array}\right) \tag{7}$$

where the quadruplet

$$\left(\tilde{A}, \quad [\tilde{B}_1 \quad \tilde{B}_2], \quad [\tilde{C}_2 \quad \tilde{C}_\infty]^T, \quad \begin{bmatrix} \tilde{D}_{\infty 1} & \tilde{D}_{\infty 2} \\ \tilde{D}_{21} & \tilde{D}_{22} \end{bmatrix} \right)$$

is the state-space realization of the augmented *"track-vehicle"* model obtained by using Eqs. (1),(2)-(4) for the transfer function matrix from the inputs $[\eta \;\; u]^T$ to outputs $[z_2 \;\; z_\infty]^T$ as,

$$\begin{bmatrix} z_2 \\ z_\infty \end{bmatrix} = \begin{bmatrix} C_2(sI-A)^{-1}B_1 s G_{\text{FRA}} & C_2(sI-A)^{-1}B_2 \\ C_\infty(sI-A)^{-1}B_1 s G_{\text{FRA}} & C_\infty(sI-A)^{-1}B_2 \end{bmatrix} \begin{bmatrix} \eta \\ u \end{bmatrix}.$$

Recall that, the aim of an active suspension system is to filter the track disturbances to the carbody, without deteriorating the wheel-rail forces. Let's define the following cost functions through L_2 and L_∞ metrics:

Design: A state feedback controller $K(s)$ that will stabilize the closed-loop system and

$$\begin{aligned} \min_{u} \quad & J_k \\ \text{s.t} \quad & ||\Lambda_k||_\infty < \gamma_k. \end{aligned} \tag{8}$$

Let's $k = 1$ and $J_1 = \Phi||T_{z_2\eta}||_2^2$ be the criteria to be minimized over the closed-loop transfer function $T_{z_2\eta}$ for the carbody vertical and pitch accelerations with penalty matrix $\Phi > 0$, and $\Lambda_1 = T_{z_\infty \eta}$ be the inequality constraint to be satisfied for the wheel-rail forces. This optimisation problem is going to be solved by using LMI Toolbox in MATLAB software. All the closed loop poles are restricted to lie on the rectangular region $D \in \mathcal{R}^2$ defined by $D = \{z = x + iy, -40 < x < -0.001, |y| < 70\}$ to prevent the controller blow up. To explore the active suspension performance two different controller are going to be synthesized:

i) K_f with fixed $\rho_r = 0.0719 \times 10^{-6}$ representing FRA track Class-6;

ii) K_p with $\rho_r \in (\sqrt{0.0254 \times 10^{-6}}, \sqrt{0.1566 \times 10^{-6}})$ representing any track roughness in the FRA track Classes 4-8;

The train is assumed to travel over the track profiles with a constant speed of $V = 160\ km/h$. Table 3 lists the RMS responses for passive and actively controlled systems with both K_f and K_p, respectively. Their percentage improvements are also shown underneath. From the table it is seen that preknowledge of the track roughness parameter will increase the controller performance up to 24% for the ride comfort while keeping the handling safety within limits (slightly improving $\approx 2.81\%$). A typical unworn rail profile with a common speed limit is usualy represented with the track model in FRA Class-6. In this study this model is taken as a reference, and is compared with controllers where the roughness is confined in an interval. Figs. 7-8 show that the performance improvements in Table 3, are expectedly obtained in the low frequency range where the human body is very sensitive to vibrations. It is seen that the first dominant mode is very well damped, both for the carbody and wheel-rail forces, while the second mode is kept within the passive limits. Similar frequency responses are obtained with the controller K_p where the track roughness is varying. This is a very motivating result and may suggest designing polytopic controllers when its is hard to know the precise value of the track roughness or when it changes frequently during driving because of the geographical variations.

Table 3. Passive and active RMS responses for (J_1, Λ_1).

RMS	**Passive**	K_f	K_p
$\ddot{z}_c$	0.0134	0.0102 **(24.04%)**	0.0114 **(14.94%)**
$\ddot{\theta}_c$	0.0023	0.0019 **(17.82%)**	0.0021 **(7.98%)**
z_∞	231.32	224.82 **(2.81%)**	213.71 **(7.62%)**

The controllers K_f and K_p are also tested on different rail profiles with changing track roughnesses for $V = 160km/h$ as reported in Figs. (9)-(10). From the figures it seen that the RMS responses are increasing on rough surfaces for any kind of controller but K_p copes better for wheel-rail forces on harsh conditions, while K_f performs much better for carbody vertical accelerations.

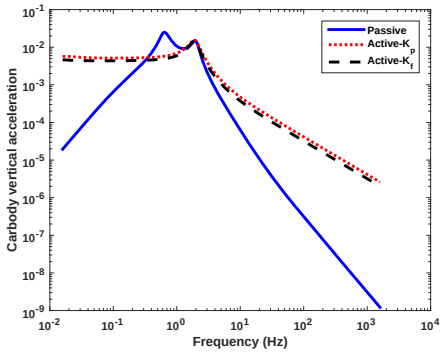

Fig. 7. $\ddot{z}_c$ frequency responses: $(-)$: Passive; $(--)$: Active design with K_f controller; $(...)$: Active design with K_p controller.

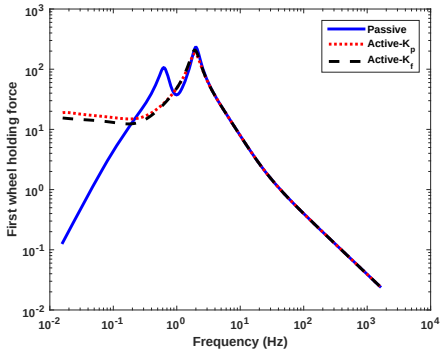

Fig. 8. z_∞ frequency responses: $(-)$: Passive; $(--)$: Active design with K_f controller; $(...)$: Active design with K_p controller.

The safety handling counterpart of this optimization problem should also be elaborated, for conditions when safety requirements are of utmost priority. Then, the handling cost function is defined as $J_2 = \Pi||T_{z_{\infty\eta}}||_2^2$ for any weighting matrix $\Pi > 0$ and the constraint function is $\Lambda_2 = T_{z_2\eta}$ in Eq. (8) for $k = 2$. Here it is intended to minimize the dynamic forces transmitted from the track to the wheels or vice versa for environmental vibration isolation without any allowed degradation in passenger comfort. Note that the

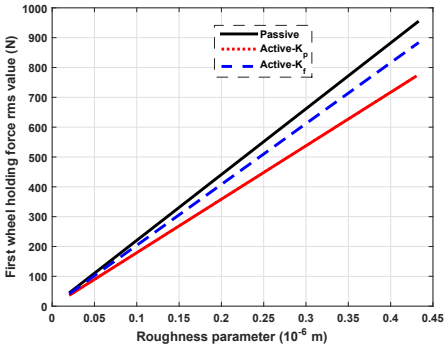

Fig. 9. z_∞ RMS responses for ρ_r increasing: $(-)$: Passive; $(--)$: Active design with K_f controller; $(...)$: Active design with K_p controller.

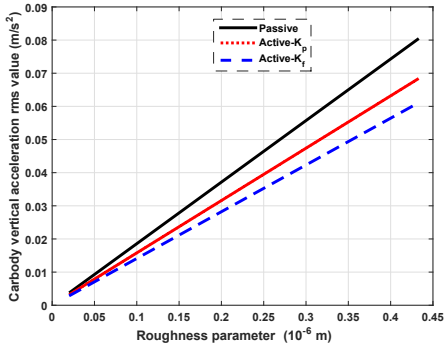

Fig. 10. $\ddot{z}_c$ RMS responses for ρ_r increasing: $(-)$: Passive; $(--)$: Active design with K_f controller; $(...)$: Active design with K_p controller.

comfort and the handling criteria have switched places in the optimization problem in Eq. (8) and the handling oriented cost function J_2 also guarantees any impervious force transmission from the train to the environmental buildings at high speeds.

This problem is solved for the same LMI region D and ρ_r confined in $(\rho_r^{min},\ \rho_r^{max})$ for FRA track classes in Table 2. Let $\widetilde{K}_f$ shows the state feedback controller designed with a fixed ρ_r, and $\widetilde{K}_p$ represents a controller designed for system with polytopic uncertainity ρ_r. The numerical computation for the RMS responses are repoorted in Table 4. The frequency response plots are shown in Figs.(11)-(12). From the figures it can be concluded as follows:

- The handling control provides the best results in terms of passenger comfort without a degradation ($\approx 0.6\%$ improvement) of the performances in safety handling. Note that the best ride comfort performances are obtained by the minimization of the handling criteria.
- The optimal handling response outperforms the passive setting at the low and mid frequencies. Interestingly, the active controllers slightly attenuate the magnitude around the wheel (second) dominant mode where a probable invariant point is located.
- At high frequencies, *e.g* above $15Hz$, the carbody vertical accelaration appears to be not so well attenuated, even

markedly increased. But this won't be of concern, since the human body is insensitive to amplifications above these frequencies.

Table 4. Passive and active RMS responses for (J_2, Λ_2).

RMS	Passive	$\widetilde{K}_f$	$\widetilde{K}_p$
z_∞	231.32	229.80 $(\mathbf{0.6}\%)$	223.17 $(\mathbf{3.47}\%)$
$\ddot{z}_c$	0.0134	0.0110 $(\mathbf{17.64}\%)$	0.0117 $(\mathbf{12.35}\%)$
$\ddot{\theta}_c$	0.0023	0.0016 $(\mathbf{27.60}\%)$	0.0017 $(\mathbf{23.86}\%)$

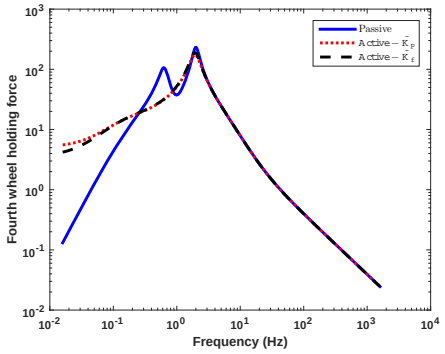

Fig. 11. z_∞ frequency responses: $(-)$: Passive; $(--)$: Active design with $\widetilde{K}_f$ controller; $(...)$: Active design with $\widetilde{K}_p$ controller.

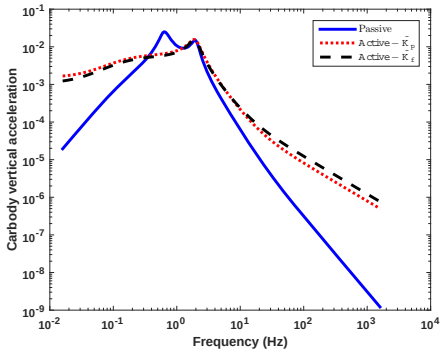

Fig. 12. $\ddot{z}_c$ frequency responses: $(-)$: Passive; $(--)$: Active design with $\widetilde{K}_f$ controller; $(...)$: Active design with $\widetilde{K}_p$ controller.

4. Conclusion

In this paper, a 6 DOF half-car model for a high speed railway vehicle is considered. The vehicle is assumed to travel on the random track profiles classified by international FRA directive. The effect of the track roughness parameter on the performance trade-off for the ride comfort and safety handling is discussed in detail. The influence of forward speed on different track conditions is also discussed. A polytopic system representation is adapted to cope up with track roughness uncertainities during driving. A cost function, representing the performance objective, either comfort or handling to be minimized and the norm bounded dynamical inequality constraints are defined for two different active applications. The performance limitations both for the handling and ride comfort criteria are discussed for two different types of controllers designed: (i) when the track roughness parameter is precisely known; (ii) when is confined in an interval. The optimisation problems are solved by using LMI Toolbox in MATLAB software. The solutions obtained provide sucessfull improvements in the carbody vertical and pitch accelerations for active suspensions without deteriorating the dynamic wheel-rail forces. This is quite motivating to carry on a futher study that will concentrate on detailed modelling of the wheel-rail contact to eloborate the influence of wheel-rail forces on the suspension system or environmental surroundings.

5. References

[1] V. K. Garg and R.V. Dukkipati, *Dynamics of Railway Vehicle Systems*, Academic Press, 1984.

[2] A.S. Leblebici and S. Türkay, "The influence of passive suspension parameters on the ride performance of high speed passenger railway vehicle ", *Turkish National Meeting on Automatic Control (TOK'16)*, Turkey, 2016.

[3] G. Kouroussis, D.P.Connoly, O.Verlinden, "Railway induced ground vibrations-a review of vehicle effects", *International Journal of Rail Transportation*, Vol. 2, No. 2, pp: 69–110, 2014.

[4] S. Türkay and A.S. Leblebici, "Effect of multi-objective control on ride quality in high speed railway vehicle" *14-th IFAC Symposium on Control in Transportation Systems*, Istanbul, Turkey, 2015.

[5] A. Hamid, K. Rasmussen, M. Baluja, T.L. Yang,"Analytical descriptions of track geometry variations Volume I - Main Text", *National Technical Information Service*, U.S. Department of Commerce, Springfield, 1983.

[6] S.M. Zadeh, S.A. Mosayebi, R. Moosapoor, "Investigating on the Effects of Random Irregularities of Railway Track by Half-Bogie Model", *Advances in Railway Engineering, An International Journal*, Vol. 1, No. 1, pp:61-75, 2013.

[7] M. Klasztorny, M. Podworna, "Influence of random track irregularities on dynamic response of bridge/track structure/high-speed train systems",*Proc 9th International Conference on Structural Dynamics (EURDYN 2014)*, 2014.

[8] S.L. Grassie, "Rail irregulairities, corrugation and acoustic roughness: characteristics, significance and effects of reprofiling", *Proc IMechE Part F: J Rail and Rapid Transit*, Vol. 226, No. 5, pp:542-557, 2012.

[9] X. Lei, *High Speed Railway Track Dynamics: Models, Algorithms and Applications*, Springer, 2016.

[10] A.S. Leblebici, S. Türkay, "Track Modelling and Control of a Railway Vehicle", *Proc 7th IFAC Symposium on Mechatronic Systems (Mechatronics 2016)*, September 2016, U.K.

[11] Bombardier, *Railway vehicle parameters*, May 2017 URL: http://www.bombardier.com/en/transportation/projects.

AUTHORS

V

Z

TMMOB
ELEKTRİK MÜHENDİSLERİ ODASI
ESKİŞEHİR ŞUBESİ

ESKİŞEHİR OSMANGAZİ
ÜNİVERSİTESİ

ULUSLARARASI

ERUSİS 2017

ELEKTRİKLİ RAYLI ULAŞIM SİSTEMLERİ SEMPOZYUMU

ESKİŞEHİR OSMANGAZİ ÜNİVERSİTESİ KONGRE VE KÜLTÜR MERKEZİ **27-28 Ekim 2017**

SPONSORS

Savronik

RAILWAY NEWS
RAILWAY MARKET and NEWS WORLDWIDE

ÇözümTR Bilgi Sistemleri

PITON Ar-Ge ve Yazılım Evi

STM

PENTAIR
Schroff

www.erusis.org
erusis2017@emo.org.tr

İLETİŞİM
Adres: İSTİKLAL MAH. ŞAİR FUZULİ CADDESİ ÖZKAL İŞMERKEZİ
NO:36 K:2 D:1 ODUNPAZARI - ESKİŞEHİR
Telefon: +90 222 2319447 Faks: +90 222 2319447 E-posta: erusis2017@emo.org.tr